School of Mechanical, Materials and

Manufacturing Engineering

Modelling and Active Control of the Vacuum Infusion Process for Composites Manufacture

by

Dhiren Modi (B.E., M.S.)

Thesis submitted to The University of Nottingham

for the degree of Doctor of Philosophy

January 2008

Abstract

Vacuum infusion technology, even though first reported more than 50 years ago, was not popular for mainstream fibre reinforced polymer composites manufacturing until recently. Its present-day popularity is due to the increasing emphasis on the manufacturing cost as well as environmental and health concerns. As a result, novel processes such as Vacuum Infusion (VI) and Seemans' Composite Resin Injection Moulding Process (SCRIMP^{TM}), employing the same basic technology, have been developed. As latecomers, these processes have not been investigated in detail and there exists a lack of understanding that can undermine the potential improvements in composites manufacturing offered by them. The present work is focused on (i) enhancing the fundamental understanding, and (ii) advancing the processing technology to fully exploit their potential.

Limitations of the existing analytical models for fluid flow in VI are explored. Then, improvising upon and extending these models, analytical formulations for the pressure profile and fill-times in rectilinear and radial flow VI processes are developed. An important result from this study is that with increasing reinforcement compliance, the analytical VI pressure profile diverges from the RTM pressure profile. It is found that for rectilinear as well as radial flow processes, the fill-time ratio between equivalent RTM and VI remains constant. Experimental validation for these formulations show that the pressure profile varies with flow progression in both rectilinear and radial flow VI. This leads

to a dynamically changing fill-times ratio between RTM and VI. This dynamic behaviour, which is contrary to analytical predictions, is explained by hypothesising that the compliance characterisation experiments do not replicate the actual events in VI.

The issue of process control is also investigated for the VI process. A novel approach, using non-intrusive sensors and real-time flow simulations, is designed and implemented. The study gives important insights about the controllability of this process. It is found that in VI, due to low driving pressure, an optimum window of opportunity exists for process control. Reinforcements with high permeability give higher flow velocity, while low permeability reinforcements lead to lower flow velocity. Both of these cases lead to a marginal window of opportunity and poor process controllability. For reinforcements that offer good controllability, the control system is able to identify flow deviations and correct them, increasing the process efficiency.

Jay Shree Ganeshay Namah

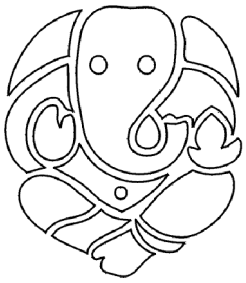

Acknowledgements

I am thankful to the almighty god for giving me strength. Unreserved appreciation is due to Prof. Andrew Long, who has been a major guiding force throughout this endeavour. I am also thankful to Prof. Christopher Rudd, Dr. Francois Robitaille and Dr. Michael Johnson for their support and guidance. The financial support provided by EPSRC-NIMRC, international office and the school of M3 is much appreciated.

Appreciation is due to my wife - Tejal, who has supported me in all circumstances, despite having to overcome many personal challanges while settling in a new country and adapting to a new culture. I also wish to thank my parents, my brother, my in-laws and other family members, who have supported me during this journey. In addition, my grandparents are heartfully thanked for their blessings.

In addition, my collegues, especially Phil, Sophie, James and Nuno, who were more like friends, deserve appreciation for all their help and support. Technicians Roger, Paul and Jeoff, as well as the staff of "School of M3", are also thanked for their help. In addition, I wish to thank my teachers and professors, in India and US, who have made this learning experience much enjoyable. Finally, all those whom I may not have remembered here, but were helpful in many direct and indirect ways, are also thanked.

જય શ્રી ગણેશાય નમઃ

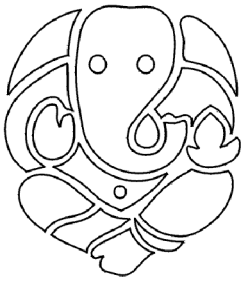

આભાર-અભિવ્યક્તિ

હું ભગવાનનો ખુબ જ આભારી છું કે તેમણે મને મારો અભ્યાસ પુરો કરવાની શક્તિ આપી. હું પ્રોફેસર એન્દ્રુ લોંગનો ખુબ આભારી છું, જેમણે મને મારા આ પ્રયાસ દરમ્યાન ખુબ જ સહાય, માર્ગદર્શન અને પ્રોત્સાહન આપ્યું છે. પ્રોફેસર ક્રિસ્ટોફર રડ, ડો. માઈકલ જોહ્નસન અને ડો. ફ્રાંસવા રોબિટેલનો પણ તેમની સહાયતા અને માર્ગદર્શન માટે આભાર માનું છું. આ ઉપરાંત, ઈ.પી.એસ.આર.સી.-એન.આઈ.એમ.આર.સી., ઈન્ટરનેશનલ ઓફીસ અને સ્કૂલ ઓફ એમ.થ્રી. તરફથી આપવામાં આવેલી આર્થિક સહાય માટે તેમનો આભાર માનું છું.

મારી પત્ની- તેજલ, જે નવા દેશમાં, નવી સંસ્કુતીમાં રહેવા જેવી મુશ્કેલીઓમાં પણ, દરેક સંજોગોમાં મને પ્રોત્સાહિત કરતી, તેનો હું આભારી છું. મારા માતા-પિતા, ભાઈ અને સગા-સંબધિઓનો પણ તેમની સહાય બદલ આભારી છું. આ ઉપરાંત, મારા દાદા-દાદી, જેમનાં આશિર્વાદથી હું આ ઉચ્ચ-શિક્ષણ પામી શક્યો, તેમનો હું આભારી છું.

મારા સહકાર્યકર્તાઓ, ફિલ, સોફિ, જેમ્સ, અને નુનો, જે મારા મિત્રો જેવા છે, તેમનો પણ તેમની મદદ માટે આભાર માનું છું. ટેક્નિશિયનો- રોજર, પૉલ અને જેફ, અને સ્કૂલ ઓફ એમ.થ્રી.ના કાર્યકર્તાઓ તરફથી આપવામાં આવેલી સહાય માટે તેમનો આભારી છું. આ ઉપરાંત, મારા ભારત અને અમેરિકાના શિક્ષકો અને પ્રોફેસરોનો ખુબ આભાર માનું છું. અંતમાં, હું એ બધાનો આભારી છું, જેમણે જાણે-અજાણે પણ મને મારા આ પ્રયાસને સફળ બનાવવામાં મદદ કરી છે, અને જેમને મેં અહીં આભાર વ્યક્ત નથી કર્યો.

Contents

List of Figures

List of Tables

Nomenclature

$A = \frac{\left[\frac{K}{\phi}\right]_{|\alpha=1}}{\frac{K}{\phi}} = \left[\frac{(1-\phi)}{\phi}\right]^2 \left[\frac{\phi}{(1-\phi)}\right]^2_{|\alpha=1}$

B - Curve fitting parameter for reinforcement compliance behaviour

D - Complete Derivative

h - Reinforcement thickness (m)

h^* - Normalised thickness of reinforcement $\left[= \frac{h}{h_{\alpha=1}}\right]$

$I = \frac{dP}{d\alpha}$

$\overline{F}$ - Body force vector (Kg^{-1})

$\overline{\overline{K}}$ - Reinforcement permeability tensor (m^2)

K - Reinforcement permeability (m^2)

k - Empirical permeability coefficient (Kozeny constant) (m^2)

n - Number of reinforcement layers

P - Resin pressure (Pa)

P_{atm} - Atmospheric pressure (Pa)

P_{comp} - Compaction pressure $[= P_{atm} - P](Pa)$

P_{inj} - Injection pressure (Pa)

P_{vent} - Vent pressure (Pa)

S - Fluid Source

S_d - Reinforcement surface density ($kg\,m^{-2}$)

t - Fill-time (s)

t_{RTM} - Fill-time in RTM process (s)

t_{VI} - Fill-time in VI process (s)

$\overline{u}$ - Fluid superficial velocity vector ($m\ s^{-1}$)

u - Fluid superficial velocity ($m\ s^{-1}$)

$\overline{u}_{filter}$ - Fluid filter velocity ($m\ s^{-1}$)

V_f - Fibre volume fraction

V_{fo} - Curve fitting parameter for reinforcement compliance behaviour

Rectilinear Flow

C_t^1 - Fill-time ratio for rectilinear (1D) flow processes $\left[= \frac{t_{RTM}}{t_{VI}}\right]$

D_1- Constant of proportionality for pressure gradient at the flow front in the rectilinear flow VI and RTM processes

L - Flow front position in rectilinear flow processes (m)

u_x - Flow velocity in the rectilinear (i.e. x) direction ($m\ s^{-1}$)

x - Any position in mould (between injection gate and flow front) in rectilinear flow processes(m)

Radial Flow

C_t^2 - Fill-time ratio for radial (2D) flow processes $\left[= \frac{t_{RTM}}{t_{VI}}\right]$

D_2 - Constant of proportionality for pressure gradient at the flow front in the radial flow VI and RTM processes

r - Any position in mould (between injection gate and flow front) in radial flow processes(m)

r_{inj} - Injection gate radius (m)

R - Flow front radius in radial flow processes(m)

u_r - Flow velocity in the radial (i.e. r) direction ($m\,s^{-1}$)

Greek Symbols

α- Non-dimensional distance [$(= x/L)$ - for rectilinear flow]

[$= \left(\frac{r-r_{inj}}{R-r_{inj}}\right)$ - for radial flow]

μ- Resin viscosity ($Pa\ s$)

ϕ - Reinforcement porosity [$= 1 - V_f$]

ρ - Fibre density ($kg\,m^{-3}$)

$\bigtriangledown\cdot$ - Divergence

σ - Cauchy stress tensor

Chapter 1

Introduction

1.1 Polymer Matrix Composites (PMC)

Technological advancements have stimulated a demand for materials that can perform under challenging conditions. Whether natural or man-made, these high-performance materials are required to offer superior mechanical properties, design flexibility, lower weight and reduced costs as compared to conventional materials such as metals. These advanced materials are made by combining two or more dissimilar materials at macro, micro or atomic levels. Polymer Matrix Composite (PMC) is one such advanced material. It consists of a polymer matrix reinforced by a fibrous material. The polymer matrix binds the reinforcement together and provides surface finish and durability to the composite. The reinforcement is the main load-bearing constituent and provides strength and stiffness to the composite. During process set-up, one can easily alter the arrangement of the reinforcement to orient the fibres in a required direction and thus, tailor properties of a composite to suit its performance requirements. This is a major advantage from a design perspective and allows one to replace homogeneous metals, alloys and other conventional materials in many applications.

1.2 Materials for PMC

The main constituents of PMC materials are the polymeric matrix or resin and fibrous reinforcements.

1.2.1 Polymer Matrix

The polymer matrix contains polymeric chains. Each chain is made up of 10^3 to 10^6 monomer units, assembled through chemical reactions. Depending on the type of bond formed between these chains, the polymer matrix can be categorised as either a thermoplastic or a thermoset. Thermosets, in general, offer ease of processing, better mechanical properties and better thermal stability compared to thermoplastsics; hence, they are used widely in the composites industry. However, they undergo chemical reactions during curing, an irreversible process in which the matrix is thermally and chemically activated to form strong covalent bonds and cross-links between polymer chains. During this process, unreacted matrix components, or Volatile Organic Compounds (VOCs) such as styrene, are released.

1.2.2 Fibrous Reinforcement

In PMCs, fibrous reinforcement is the basic load-bearing component. There are numerous varieties of reinforcements available, mainly differing in their architecture and material type. The difference in the reinforcement architecture stems from various methods used to manufacture them such as weaving, knitting, stitching etc. In addition, different patterns and arrangements can be made in each of these processes, creating further variations in the reinforcement architecture. Fibrous reinforcements can be made from man-made (e.g. glass, carbon, boron, aramid fibres etc.) or natural materials (e.g. hemp, coconut, sisal fibres etc.).

1.3 PMC Manufacturing Processes

Numerous composite manufacturing processes have been invented to process different matrices (thermoset or thermoplastic) and reinforcements (continuous or discontinuous). Each process has advantages that make it the most suitable for a particular application.

Depending on the type of matrix and reinforcement used, these manufacturing processes can be broadly categorised into three main groups (Advani and Sozer, 2003). For short or discountinuous fiber reinforcements, Compression Moulding, Extrusion and Injection Moulding are the main processes. In these processes, either a thermoset or a thermoplastic matrix can be used. For a thermoplastic matrix and long fibre reinforcements, Composite Sheet Forming and Pultrusion are the main processes. Hand Lay-up, Autoclave Moulding, Liquid Composite Moulding (LCM), and Filament Winding are the main processes for long fibre reinforcements using a thermoset matrix. In addition, based on the moulding arrangement, the last category of processes can also be categorised as either open (e.g. Hand Lay-up) or closed (e.g. LCM) mould processes.

LCM is a general moulding philosophy, where a dry reinforcement is placed inside a rigid, semi-rigid or flexible mould. Uncured thermoset resin, in liquid form, is injected from a source and infiltrates the reinforcement. After complete infusion of the reinforcement, the resin is allowed to cure. Once the resin is cured, a finished part is extracted (Rudd et al., 1997). Resin Transfer Moulding (RTM), Structural Reaction Injection Moulding (SRIM), Injection-Compression (I/C) Moulding, Vacuum Infusion (VI) etc. are some of the main LCM processes (Gutowski, 1997).

In the past, the majority of thermoset matrix composite parts were manufactured using open mould processes. However, recently introduced regulations for mandatory reduction of styrene emission in workplaces (HSE, 2002a,b)

have prompted manufacturers to look for suitable alternatives to open mould processes. Styrene is a naturally occurring monomer and is used in the production of variety of polymers. Its adverse effects on health range from short-term irritation, drowsiness, headaches and nausea to long-term neurotoxic and genetic effects. In the fibre reinforced plastics industry, the styrene exposure rate has been found to vary from 102 $mg\ m^{-3}$ to 350 $mg\ m^{-3}$, which results in an estimated average daily intake of 2 grams per operator. This is one of the highest styrene exposure rates, compared to other industries such as paint, adhesives etc (WHO, 2000). Because of a closed mould set-up, RTM and VI allow one to capture VOC emissions at source, and thus offer a cost-effective way to ensure safe-working conditions and meet legal obligations without significant financial investments (Williams et al., 1996). Furthermore, materials and processing-related advancements in the last two decades have exhibited significant advantages of using LCM processes, particulary RTM and VI, for composites manufacture. These processes can also use the same, readily available, cheaper raw-materials that hand lay-up manufacturers are more familiar with. This lowers their anxiety when implementing any production changes. It is noteworthy that while the capital investment required in RTM and VI is generally higher than processes such as hand lay-up, it is considerably lower than many other closed-mould processes such as SRIM and I/C moulding. Nevertheless, the higher investment is often offset by higher production rates. Hence, RTM and VI are becoming increasingly popular in industries such as boat-building and wind energy.

Figure 1.1 shows general steps of the VI process. First, porous reinforcement is laid on top of a rigid mould bottom half (Step-I). A sealant tape is laid around the periphery of the reinforcement, while injection and vent lines are positioned on top of it. The injection and vent lines pass through the sealant tape to connect to a resin source and a vacuum pump, respectively. Additionally, a resin trap can be added between the vent line and the vacuum pump to

prevent resin from entering the vacuum pump and causing damage. Then, the mould is covered with a flexible plastic sheet. This plastic sheet attaches to the sealant tape to seal the mould and acts as the top half of the mould (Step-II). In addition, if required, the injection and vent lines can also be passed through the plastic sheet provided sufficient sealing is maintained. The vacuum pump evacuates air from inside the mould, thus creating a negative pressure gradient. This negative pressure gradient drives resin from its source through the injection line into the porous reinforcement (Step-III). Once the reinforcement is completely infused, resin injection is stopped while the vent is kept open and resin is allowed to cure before extracting the finished part (Step-IV).

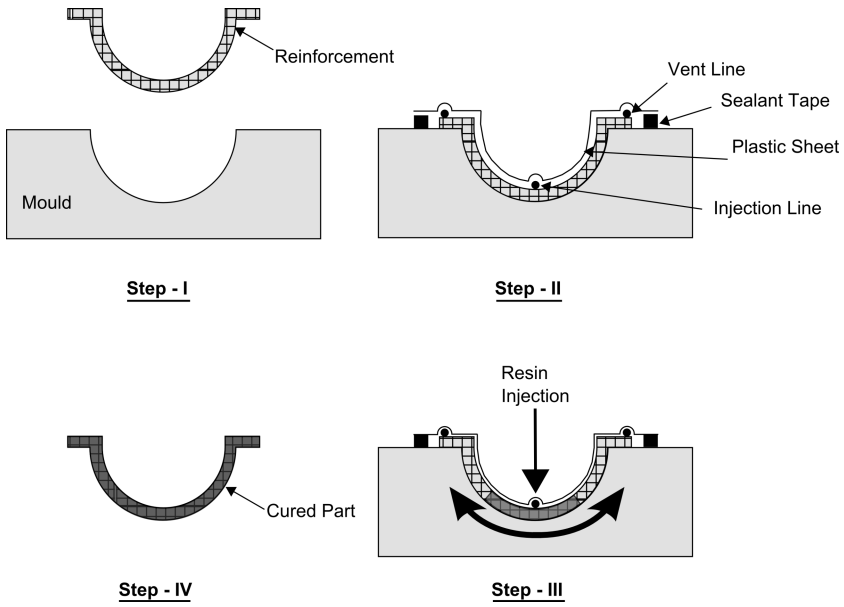

Figure 1.1: General steps of the Vacuum Infusion (VI) process.

The VI process is limited by the maximum achievable vacuum pressure and, in general, gives longer infusion times as compared to resin cure times. Variants of the process employ different means to spread resin faster and thus, speed up the process. In Seemans' Resin Injection Moulding Process (SCRIMP^{TM}) (Seamann, 1990), a patented and one of the most popular variant of the VI process, a layer of fluid pervious peel-ply and high permeability material (or

Distribution Media (DM)) are placed on top of the reinforcement. Resin injected from an inlet immediately spreads in the DM in the planar direction before infiltrating the reinforcement in the thickness direction. This leads to a difference in the flow front position at the top and the bottom side of the reinforcement, also known as lead-lag distance. Peel-ply facilitates easy removal of DM and the mould top half, once resin has cured. In another variant of VI, channels are used in place of DM to facilitate faster resin spreading in the in-plane direction (Lang and Rydin, 2002, 2005). VI is particularly suitable for low volume production of large parts. Typical VI parts can be 25-30 metres in length and several metres in width.

In the RTM process, resin is injected under positive pressure, while the vent can be either open to atmosphere or connected to a vacuum pump. The positive injection pressure necessitates proper clamping of the mould and use of rigid tooling (Figure 1.2). In addition, to prevent the porous reinforcement from being washed away due to the high injection pressure, it needs to be compacted to many times the atmospheric pressure. Composite parts of up to 4 metre length and 5 metre width have been manufactured successfully by RTM (Jacob, 2006). However, high tooling and equipment costs limit the suitability of RTM for large parts.

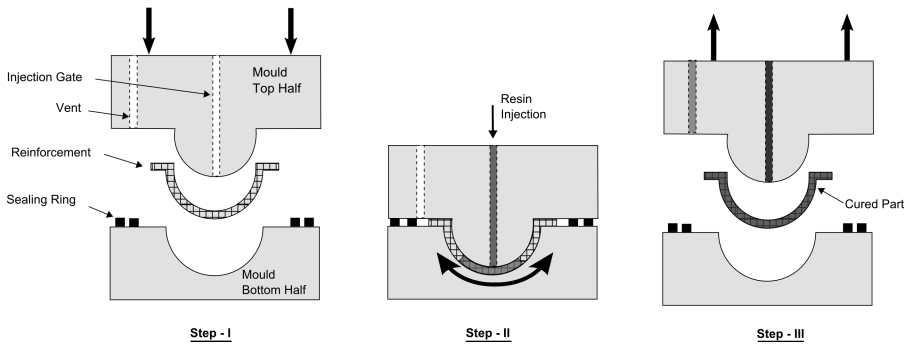

Figure 1.2: General steps of the Resin Transfer Moulding (RTM) process.

1.4 Processing Science and Technology

In LCM processes, manufacturing quality, signified by the degree of reinforcement infusion, is a critical factor determining the mechanical properties of the final part (Gutowski, 1997). Ideally, resin should completely infuse the porous reinforcement before reaching a vent or starting to cure. Various processing parameters such as clamping pressure, injection pressure, reinforcement thickness, fill-time, cure-cycle etc. affect the degree of reinforcement infusion. Hence, it is extremely important to develop a fundamental understanding of the processing science, particularly of the infusion process, to improve the process reliability and cost-effectiveness (Advani and Sozer, 2003).

1.4.1 Flow through Porous Media Theory

In general, fluid flow in a Eulerian space is modelled using mass and momentum conservation laws (Equations 1.1 and 1.2).

$$\frac{\partial \rho}{\partial t} + \nabla \cdot (\rho \overline{u}) + S = 0 \tag{1.1}$$

$$\rho \frac{D\overline{u}}{\partial t} = \nabla \cdot (\sigma) + \rho \overline{F} \tag{1.2}$$

For low Reynolds number, incompressible flow and no gravity effects, the momentum equation reduces to Darcy's law (Equation 1.3) (Scheidegger, 1974).

$$\overline{u} = -\frac{\overline{\overline{K}}}{\mu} \nabla P \tag{1.3}$$

Darcy's law was originally derived for water flow across a stationary sand bed. Pillai (1997) validated the extension of Darcy's law to describe flow of viscous, polymeric resin through a stationary fibre bed. Here, $\overline{u}$ is the volume-averaged or superficial fluid velocity vector, μ is the fluid dynamic viscosity and ∇P is the fluid pressure gradient across the porous medium. The constant of

proportionality ($\overline{\overline{K}}$), also known as permeability, is a second order symmetric tensor and characterises the resistance offered by the porous medium to the fluid flow through it. Note that the superficial ($\overline{u}$) fluid velocity is related to the microscopic (or filter) fluid velocity ($\overline{u}_{filter}$) by Equation 1.4.

$$\overline{u} = \overline{u}_{filter}\,\phi \tag{1.4}$$

Here, porosity (ϕ) is a measure of empty space in a unit volume. It is generally characterised by fibre volume fration (V_f), which is its complementary parameter and is a measure of space occupied by reinforcement fibres in a unit volume i.e. $\phi\,(= 1 - V_f)$.

Then, assuming no fluid source and substituting Equation 1.3 into 1.1,

$$\nabla \cdot \left(-\frac{\overline{\overline{K}}}{\mu} \nabla P \right) = 0 \tag{1.5}$$

Equation 1.5 is solved using the following boundary conditions for constant pressure injection,

$$\begin{aligned} P &= P_{inj} \text{ at injection gate} \\ \nabla P &= 0 \text{ at mould boundaries} \\ P &= 0 \text{ at Vent} \end{aligned} \tag{1.6}$$

For accurate description and design of the infusion process, characterization of reinforcement permeability is very important. Various characterisation efforts (Phelan and Wise, 1996; DeParseval et al., 1997; Nedanov and Advani, 2002) have used either constant flow rate or constant pressure injection in rectilinear or radial flow systems. These methods have their distinct advantages and disadvantages. For example, in the rectilinear flow process, fiber pull-out can

lead to accelerated fluid flow near the mould boundaries compared to the majority flow inside the mould, which is also known as race-tracking. This significantly affects the accuracy of the results. On the other hand, in the radial flow processes, mathematical calculations can be more involved. A detailed comparison of various methods is reported by Weitzenbock et al. (2002).

1.4.2 Numerical Methods

Because of moving boundaries, analytical treatment of the fluid flow problem is difficult except for a few simple geometries and numerical treatment is necessary. Also, numerical treatment allows one to investigate variety of flow problems faster and in a cost-effective way. Various numerical solution methods such as the Finite Difference Method, Finite Element Method, Boundary Element Method, Finite Element Control Volume (FE/CV) Method etc. have been developed (Chen et al., 1997; Lin et al., 1998; Mohan et al., 1999; Kuan and Gizawy, 2000). All of these methods use Equation (1.3) in either derivative or integral form and need information about permeability ($\overline{\overline{K}}$). In addition, the high viscosity of polymeric resins gives dominant viscous forces, which allows one to assume a creeping flow i.e. the solution procedure can be simplified by formulating the problem as a quasi-steady state problem.

Amongst all the numerical methods, the FE/CV method has been shown to be efficient as long as one is solving a linear set of equations with a direct solver (Simacek and Advani, 2004). As the method is widely reported and discussed in the literature (Fracchia et al., 1989; Bruschke and Advani, 1990), it is only discussed briefly here. In the FE/CV method, the solution domain is discretized using a fixed mesh. Nodal control volumes are defined using the mid-side points of the element edges and element centroids such that each node is situated at the centre of an associated control volume. Figure 1.3 shows such a mesh with the solid and dotted lines representing FE and control volume boundaries, respectively. At the beginning of a solution, all nodes are

assigned a fill factor of zero. This nodal fill factor, with its value ranging from zero to one, denotes resin volume as a fraction of the porous volume in the associated control volume. In any control volume, a fill factor of zero implies a completely empty porous volume, while a fill factor of one denotes that the porous volume is completely filled with resin. Nodes with a fill factor value higher than a pre-defined value (usually greater than 0.999) are considered fully filled and are employed in the pressure solution, while nodes with a fill factor value between zero and the pre-defined limit are considered near the flow front. Typically, the Galerkin residual method based finite element approximation is used to compute the pressure distribution in the filled region using Equation 1.5. This pressure is used within Darcy's law (Equation 1.3) to determine the resin velocity at each node. Using surface area of control volumes, flow rates are calculated for all nodal control volumes. From this flow rate and the present values of nodal fill factors, a suitable time-step is chosen to advance the flow such that at least one control volume is completely filled. Then, the fill factors for all other nodes are updated. The solution procedure is repeated until all the nodes in the solution domain are filled.

It is important to note that although several authors have attempted to apply this technique to the VI process (Kang et al., 2001; Correia, 2004), none of these studies have been validated thoroughly. This method has only been tested for the constant thickness RTM process. It is well-known that the thickness (Williams et al., 1998; Andersson et al., 2003b) and hence, the porosity and permeability of reinforcement change in VI, for which the validity of the method has not been tested rigorously.

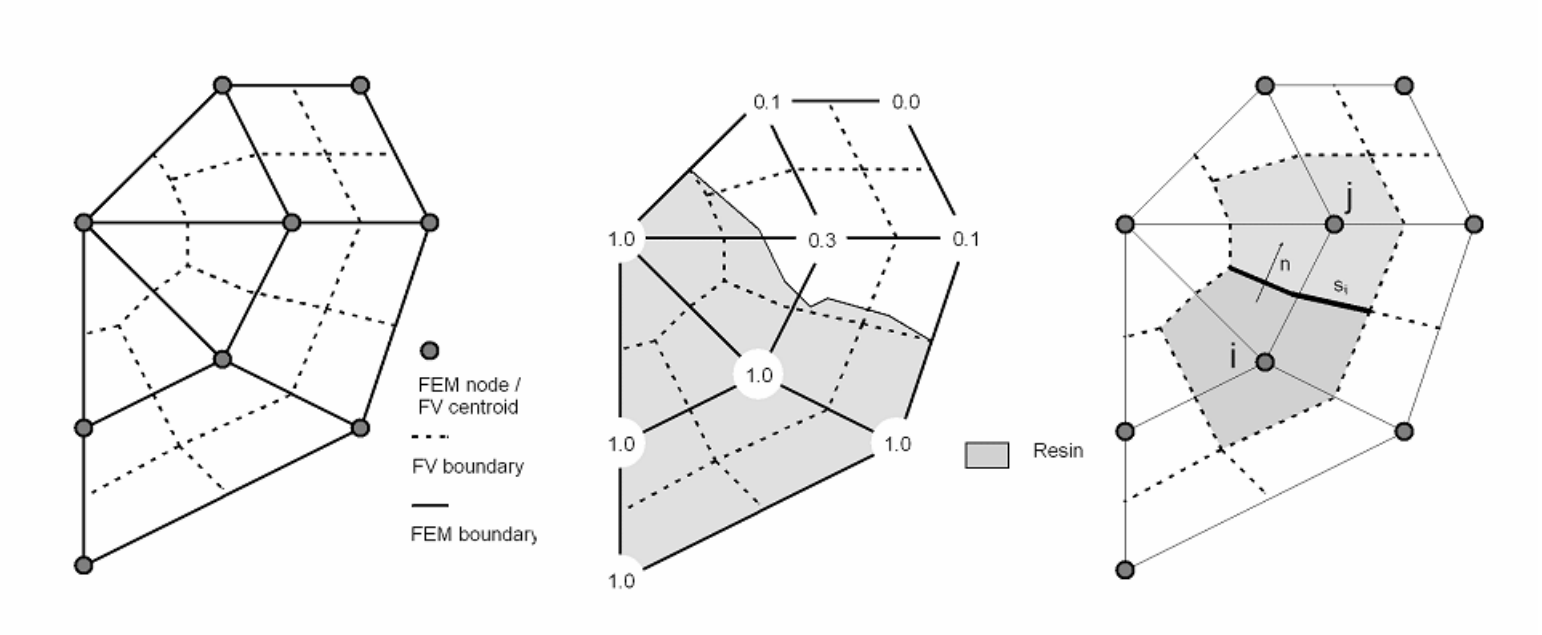

Figure 1.3: Modeling the problem of flow through a porous media using the Finite Element Control Volume (FE/CV) method (Simacek and Advani, 2004).

1.4.3 Process Variability and Control

Both analytical and numerical treatments of closed moulding processes require accurate knowledge of permeability. It is widely known that exact and consistent characterisation of permeability is difficult due to its dependence on a multitude of reinforcement related parameters such as fibre architecture, heterogeneity etc. as well as process related parameters such as nesting, dual-scale flow etc. The exact effect of any of these parameters is difficult to predict using simulation tools and it is not uncommon to find differences between the actual and predicted flow patterns. Often, this difference in flow patterns can lead to incomplete or poor quality infusion and part rejection. To an extent, the issue of incomplete infusion can be addressed by resin bleeding, an additional processing step in which resin injection is continued even after resin has reached the vent. However, most of the resin thus injected flows out of the vent and increases process waste and costs. Another solution is process control, which offers maximum probability of reducing or avoiding these problems.

1.5 Aims and Objectives

Most of the current knowledge, related to analytical and numerical modelling of infusion through closed mould processes as well as process control, is derived from RTM. Although closely related, there are unique differences between the RTM and VI processes. For example, in the VI process, the maximum driving pressure is limited to 1 bar, while in RTM, it is limited only by the available injection equipement and the associated tooing. Also, the flexible mould top half in VI results in more complex and dynamic process physics compared to RTM. The added challenges of VI make it difficult to either investigate the process seperately or extend the current vast knowledge-base available for RTM.

The main objective of this work is to study the VI process in detail. Var-

ious aspects of the process, including mathematical formulation, numerical modelling, experimental analysis, and finally, active control will be explored. The main focus is on developing an understanding of the: (i) pressure profile, and (ii) flow progression, during the infusion stage. The extension of a previously reported pressure and fill-time formulation for a rectilinear flow process (Correia, 2004) to model a radial flow process will be investigated. This new formulation will be validated against experimental results to gain important insights into the process physics. Finally, an active flow control system for VI will be designed, developed and tested.

The current academic understanding of the VI process is limited to one dimensional (1D) or the rectilinear flow process only. The aim of the present study is to extend this understanging to two dimensional (2D) or radial flow processes. It is intended that the analytical and numerical developments, backed up with experimental investigations, will lead to validation and verification of the theory used in modelling of the VI process. The development and implementation of a flow control system for VI, which is believed to be the first in this field, is intended to verify advanced concepts proposed in the literature. It is hoped that the wide spectrum of areas covered in this work will lead to improved modelling tools, increased process reliability, repeatability and reduced costs. At the same time, it is also hoped that such a study will highlight the shortcomings in the present knowledge base, covering various areas such as material compliance, process physics and process controllability.

1.6 Outline

The thesis consists of four subsequent chapters that deal with the specific areas of analytical formulation, experimental investigation and implementation of an active flow control system for VI. The second and the fourth chapters have already been published as journal papers (Appendix 1.A). Appendix 1.B lists

additional conference publications stemming from the current work.

In the second chapter, a previously reported analytical formulation for the pressure field in a rectilinear flow process is modified to obey the law of conservation of mass. For the radial flow process, a new formulation for the pressure field is also developed. The issues with modelling the VI process using an existing Finite Element/ Control Volume (FE/CV) method based simulation tool are discussed. Suitability of other methods to find solutions of these coupled formualtions is investigated, using convegence studies and finally, the numerical results are presented. Using a previously reported approach and the new pressure solution, a fill-time solution for the rectilinear flow process is derived. The issue of direct extension of this approach for a radial flow process is discussed and a novel technique is developed to find the fill-time solution. From the results, important and useful conclusions regarding the similarity of RTM and VI processes are drawn.

In the third chapter, new mould set-ups are presented to measure the pressure profile in the rectilinear and the radial flow VI processes. Pressure field and fill-time studies are performed and the experimental results are used to investigate the validity of the analytical formulations reported in the second chapter.

In the fourth chapter, an active flow control system to address the issue of reinforcement/flow heterogeneity is designed. The development of various stages of this control system and the experimental validation are described in detail. The test results are presented for three different reinforcement lay-ups to draw conclusions regarding process controllability i.e. the ability of process control.

Finally, in the fifth chapter, the work carried out during this project is summarised and the knowledge gained is discussed to draw some important conclusions. In addition, various topics that need to be explored in future are discussed.

Chapter 2

Analytical Investigation of Pressure Profile and Flow Progression in the Vacuum Infusion (VI) Process

2.1 Introduction

The top half of a mould in the VI process is made from a flexible or semi-flexible bag. Also, mould clamping as well as reinforcement compaction is purely due to the outside atmospheric pressure and the injection pressure is limited to one atmosphere. During the infusion stage, the fluid pressure of the flowing resin balances against some of the compaction pressure. This leads to varying part thickness, in both space and time (Figure 2.1).

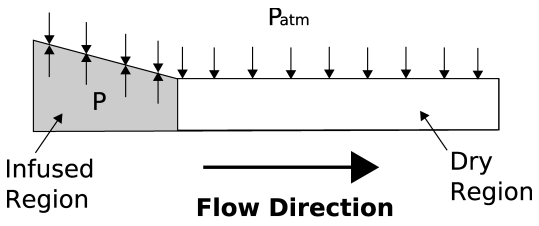

Figure 2.1: Flow progression induced dynamic variation of the reinforcement thickness in VI.

This has major implications for the process such as:

1. The final cured part may also contain undesired thickness gradients.

2. The reinforcement fibre volume fraction and permeability, which govern the pressure and velocity of the flowing resin, are affected. Due to this coupling between fluid pressure-thickness-fibre volume fraction-permeability, the fill-time is also affected and straightforward use of simple formulations developed for the RTM process may not be possible.

3. In the absence of analytical formulations, one cannot develop flow simulation tools, which are essential for process optimisation.

To address these issues, it is necessary to develop a fundamental understanding of the process physics. The main areas of development include characterisation of reinforcement compliance behaviour under various conditions, porosity-permeability dependence as well as new and improved formulations for pressure and fill-time. Then, the added knowledge about thickness gradients may enable the design of corrective measures such as resin bleeding or lay-up changes to minimise these potential problems.

2.1.1 Previous Work: Reinforcement Compliance Characterisation

In general, reinforcement compliance characterisation should take into account several factors such as reinforcement architecture, number of layers, stacking sequence, reinforcement condition (dry/wet), initial load, loading direction (compacting or expanding), loading rate, maximum load, number of cycles etc. Two main approaches are used for reinforcement compliance characterisation. The first approach involves use of micro-mechanics to model compaction of reinforcements. These theoretical models, nonetheless, require experimental data to calculate values of various empirical parameters. The second approach involves curve-fitting experimental results to an empirical model, without any theoretical basis.

Initial reinforcement compliance characterisation efforts were focused on the autoclave process. In this process, pre-infused reinforcements or prepregs are placed in a pressure chamber and consolidated by applying heat and pressure. The applied pressure can be many times the atmospheric pressure and the majority of the fluid flow is through percolation. From the compliance point of view, only wet compaction is relevant for this process (Hubert and Poursartip, 1998) (Table 2.1). Cai and Gutowski (1992), Toll (1998) etc. proposed micro-mechanics based analytical models, while Robitaille and Gauvin (1998b), Saunders et al. (1999), Kelly et al. (2006) investigated compaction of saturated reinforcements experimentally.

Increased popularity of RTM led to a realisation that in this process also, the reinforcement compliance behaviour affects its permeability and fibre volume fraction. Thus, many researchers considered reinforcement compliance behaviour an important process parameter and investigated it in detail. In the RTM process, the applied compaction pressure can be many times atmospheric pressure and the majority of fluid flow is through infiltration. As the

mould thickness remains constant during the process cycle, compaction of dry reinforcements is the governing phenomenon. Rudd et al. (1996) and Liu et al. (2004) investigated compaction of dry reinforcements experimentally, while Chen et al. (2001) proposed a micro-mechanics based analytical model. Robitaille and Gauvin (1998a) reviewed the state of the art to date.

It is important to note that results from wet (or saturated) compaction experiments suggest a different compliance behaviour compared to dry compaction. Generally, wet reinforcements exhibit lower initial thickness or higher initial fibre volume fraction(Kim et al., 1991). In addition, the presence of resin (or other lubricant) promotes sliding at contact points. Hence, one needs lower compaction pressure in the infused network, as compared to the dry network, to achieve any fibre volume fraction (Hammami and Gebart, 1998, 2000; Toll, 1998; Kim et al., 1991).

As shown earlier, in the VI process, the applied compaction pressure is limited to one atmosphere. In addition, the flexible nature of the mould top half leads to a dynamically increasing thickness in the saturated region that also affects the pressure profile. Measurements of this thickness variation in the VI process show that the reinforcement thickness is minimum at or just behind the flow front. The fluid pressure starts to rise behind the flow front leading to increasing thickness (Williams et al., 1998; Andersson et al., 2003b). Hence, as shown in Figure 2.1, saturated expansion behaviour is more relevant for the infusion stage (Table 2.1).

Previously, wet expansion characterisation of reinforcement has received extremely limited attention. Correia (2004) characterised unsaturated and saturated, compaction and expansion behaviour of four reinforcements with different architectures. The compliance results were curve-fitted to a power law model reported by (Robitaille and Gauvin, 1998a,b). His results showed that in each case, reinforcement compliance characterisation parameters have different values. Also, the values of these parameters varied with the reinforcement

architecture. Thus, for the VI process, use of compliance data from the appropriate compliance experiments, i.e. saturated expansion experiments, is crucial.

Table 2.1: Process vs. relevant compliance properties

Process	**Phase**	**Fabric Condition**	**Compliance**	**Flow Process**
Autoclave	Consolidation	Saturated	Saturated compaction	Percolation, through-thickness and/or in-plane
RTM	Infusion	Unsaturated	Unsaturated compaction (including relaxation in the 1^{st} cycle)	Impregnation, through-thickness and in-plane
VI	Debulking	Unsaturated	Unsaturated compaction (including relaxation in more than one cycles)	N/A
	Infusion- behind the flow front	Saturated	Saturated expansion	N/A
	Bleeding & consolidation	Saturated	Saturated compaction	Percolation, through-thickness and/or in-plane

2.1.2 Previous Work: Vacuum Infusion (VI) Modelling

Many researchers have reported the development of VI process models. These include Hammami and Gebart (1998; 2000), Han et al. (2000), Kang et al. (2001), Andersson et al. (2003a) and Correia (2004).

To model a rectilinear (or 1D) VI process, Hammami and Gebart (1998; 2000) modified the continuity equation and set the rate of change of mass equal to the rate of change of thickness, within a unit volume. The fluid velocity, in this modified continuity equation, was replaced with Darcy's law. The authors noted that this equation can be solved numerically, provided conservation of mass is ensured. However, they made a simplifying assumption of quasi-stationary flow, i.e. they assumed that the cavity height will have time to approach its static equilibrium value at every instant in time during the infusion process. It was argued that this assumption corresponds to neglecting the thickness variation (i.e. $\frac{\partial h}{\partial t} = 0$) in the modified continuity equation. The authors solved the resulting formulation using a finite volume method. The numerical solution for the pressure profile was not presented, but the numerical fill time solution was reported to exhibit a power law behaviour, with the power and the multiplication factor having different values from that of the RTM process. It is important to note that the validity of the simplifying assumption of quasi-stationary flow was not assessed. Experimental results (Williams et al., 1998; Andersson et al., 2003b) reported for dynamic thickness variations in the VI process suggest that it is not negligible.

Han et al. (2000) reported an approach to model the SCRIMP^{TM} process numerically. In their model, they explicitly modelled the fibre mat compressibility induced porosity and permeability changes under a quasi-static flow assumption. Note that the authors did not assume the thickness variation to be negligible as done by Hammami and Gebart (1998; 2000). The authors did not present validatation for their formulation.

Using a unified model developed by Dave (1990), Kang et al. (2001) derived another formulation for the VI process. This formulation was solved explicitly using the finite element/control volume (FE/CV) method. Again, no validation or verification of the results was presented.

Andersson et al. (2003a) used Hammami and Gebart's (1998; 2000) analytical model in a commercially available computational fluid dynamics package (CFX-4) to model the VI process. They also assumed quasi-stationary flow and modelled the fluid flow using the finite volume method (FVM). The reinforcement compliance behaviour was modelled using the relationship proposed by Toll (1998). The authors noted that impregnation of fibres with resin leads to lubrication induced reduction in their compaction stiffness, which should be accounted for to accurately model the process. However, in the absence of any supplementary work to correctly modify the characterisation relation, they chose to use the relation for compaction of dry reinforcements. Then, after every computational cycle, the new mould thickness was calculated using this modified formulation and the corresponding values of the reinforcement permeability were calculated using Gebart's formulation (Gebart, 1992). Even though the results captured the variable reinforcement height, no quantitative data were presented to validate the model.

Correia (2004) developed a coupled formulation for the pressure distribution in a rectilinear (or 1D) VI process, which was shown to be a consolidation of several of the previously reported models. The solution of this formulation was found using a central finite difference method and a Gauss elimination algorithm. The VI process was also modelled using LIMS-VI, a custom implementation of the LIMS software. LIMS is a FE/CV method based flow modelling tool developed at Center for Composite Materials, University of Delaware (Simacek and Advani, 2004). To model the VI process, at the start of each time step, the pressure profile was calculated. From the local pressure values, new values of local reinforcement properties (i.e. V_f, K, h) were calcu-

lated, from which the pressure profile was recalculated. This iterative process was repeated until the successive change in the pressure profile resulted in convergence to a predefined tolerance. Then, the fill-factors were updated to advance the flow front and the process was repeated. The results from both analytical and FE/CV approaches matched closely. For rectilinear flow, the VI pressure profile was shown to be nonlinear as compared to the linear pressure profile of the RTM process. In addition, at all locations inside the infused region, the fluid pressure values were shown to be higher in the VI process than in an identical constant pressure injection RTM process. For fill-time analysis, the author pointed out that the normalised pressure gradient in the rectilinear flow VI process remains constant with flow progression. Hence, one can calculate a scaling factor, which will allow the RTM fill-time to be scaled to find the corresponding VI fill-time. In this way, one can easily use the modelling tools developed for the RTM process to model the VI process. It is important to note that the values of reinforcement compliance parameters, used in the calculation of pressure profiles, were derived from dry compaction experiments. As discussed in Section 2.2.4, wet expansion is more relevant for VI and hence, these pressure profile results may be inaccurate. In addition, very limited experimental evidence supporting the analysis was presented. Also, the concept of using a scaling factor for fill-times was only proven for rectilinear (1D) flow.

2.1.3 Outline of the Chapter

In the present work, the same reinforcements as used by (Correia, 2004) were planned to be used. As the compliance behaviour of these reinforcements, particularly the saturated expansion behaviour, had already been characterised, it was decided to use these results and not to perform any additional experiments. It is also clear that if accurate solutions for pressure and fill-time can be found by using appropriate charactersiation data and formulations, then the thickness profile can be accurately estimated. Hence, the issue of control

over the final part thickness also was not explored.

However, so far, there has not been a comprehensive effort to develop a VI model, in terms of important process parameters, and then fully validate it with experiments. This is the main aim of the present investigation, i.e. to develop accurate formulations for the VI process that are based on fundamental understanding and are validated experimentally. This chapter deals with the first part of this aim i.e. development of pressure and fill-time formulations for the VI process. The experimental validation is presented in the next chapter. The understanding of process physics thus developed can help one form a basis for the use, modification or extension of simulation tools, developed for the constant thickness RTM process, to model the VI process. In addition, it can also be useful for investigation of variants of the VI process such as SCRIMP^{TM}, which employ multiple reinforcement lay-ups including a high permeability infusion medium.

The objectives are to develop and extend the pressure and fill-time formulations for the VI process involving lay-ups of a single reinforcement type. In the next section, an improvement to Correia's (2004) formulation, for the rectilinear VI process, is presented. Also, using the same approach, the derivation of the analytical pressure formulation for a radial flow VI process is presented. As these pressure formulations are nonlinear, their solutions are found using an iterative procedure. The pressure profile predictions, for four different reinforcements, are reported in Section 2.3. In Section 2.4, fill-time formulations for the rectilinear and radial flow VI processes are presented. Through a fill-time investigation, the equivalence of the RTM and VI processes is investigated in Section 2.5 and finally, some important implications of the study, relating to the modelling of the VI process, are discussed.

2.2 Pressure Profile Formulation

2.2.1 Rectilinear (1D) Flow

As shown in Appendix 2.A, starting with a modified continuity equation that accounted for the variable thickness, Correia (2004) derived a pressure formulation for rectilinear flow VI process (Equation 2.1).

$$\frac{d^2P}{d\alpha^2} + \left[\frac{1}{K}\frac{dK}{dP} + \left(\frac{1-h^*\alpha}{h}\right)\frac{\partial h}{\partial P}\right]\left(\frac{dP}{d\alpha}\right)^2 = 0 \tag{2.1}$$

During derivation, the author argued that flow rate remains constant in a rectilinear flow process. However, the assumption of constant flow rate is valid only for the constant thickness RTM process. In the VI process, as shown in Figure 2.2, the dynamic variation of the reinforcement thickness leads to a dynamically changing flow rate.

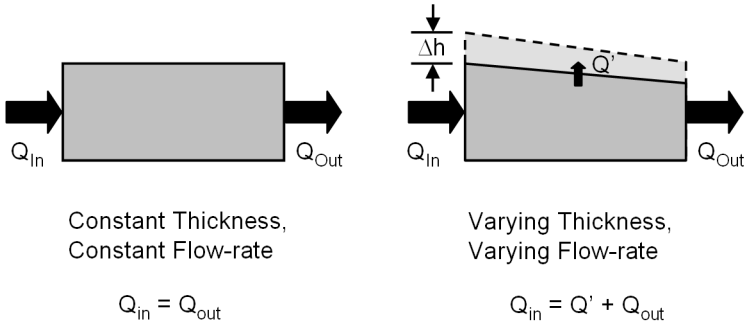

Figure 2.2: Conservation of mass in the constant thickness (RTM) and varying thickness (VI) processes.

To address this drawback, a new formulation needs to be derived. Assuming that the reinforcement permeability is constant and using Darcy's law in the conservation of mass law leads to,

$$\frac{\partial h}{\partial t} = -\frac{\partial}{\partial x}\left(-\frac{Kh}{\mu}\nabla P\right) \tag{2.2}$$

then,

$$\frac{\partial h}{\partial t} = \frac{1}{\mu}\frac{\partial}{\partial x}\left(Kh\frac{\partial P}{\partial x}\right) \tag{2.3}$$

or,

$$\frac{\partial h}{\partial t} = \frac{1}{\mu}\left[(Kh)\frac{\partial^2 P}{\partial x^2} + \left(h\frac{\partial K}{\partial x}\right)\frac{\partial P}{\partial x} + \left(K\frac{\partial h}{\partial x}\right)\frac{\partial P}{\partial x}\right] \tag{2.4}$$

which, after simplifying can be written as:

$$\frac{\partial h}{\partial t} = \frac{Kh}{\mu}\left[\frac{\partial^2 P}{\partial x^2} + \left(\frac{1}{h}\frac{\partial h}{\partial P} + \frac{1}{K}\frac{\partial K}{\partial P}\right)\left(\frac{\partial P}{\partial x}\right)^2\right] \tag{2.5}$$

Normalising with $\alpha = x/L$,

$$\frac{\partial \alpha}{\partial x} = \frac{1}{L} \quad \text{and} \quad \frac{\partial \alpha}{\partial L} = -\frac{\alpha}{L} \tag{2.6}$$

Also,

$$\frac{\partial P}{\partial x} = \frac{\partial P}{\partial \alpha}\frac{\partial \alpha}{\partial x}; \quad \frac{\partial h}{\partial x} = \frac{\partial h}{\partial P}\frac{\partial P}{\partial \alpha}\frac{\partial \alpha}{\partial x} \quad \text{and} \quad \frac{\partial K}{\partial x} = \frac{\partial K}{\partial P}\frac{\partial P}{\partial \alpha}\frac{\partial \alpha}{\partial x} \tag{2.7}$$

Then, Equation (2.5) can be written as:

$$\frac{\partial h}{\partial t} = \frac{Kh}{\mu L^2}\left[\left(\frac{1}{h}\frac{\partial h}{\partial P} + \frac{1}{K}\frac{\partial K}{\partial P}\right)\left(\frac{\partial P}{\partial \alpha}\right)^2 + \frac{\partial^2 P}{\partial \alpha^2}\right] \tag{2.8}$$

Also, simplifying the left hand term in Equation (2.8),

$$\begin{aligned}
\frac{\partial h}{\partial t} &= \frac{\partial h}{\partial P}\frac{\partial P}{\partial \alpha}\frac{\partial \alpha}{\partial L}\frac{\partial L}{\partial t} \\
&= \frac{\partial h}{\partial P}\frac{\partial P}{\partial \alpha}\frac{\partial \alpha}{\partial L}\left(-\frac{K}{\mu\,\phi}\frac{\partial P}{\partial \alpha}\frac{\partial \alpha}{\partial L}\right) \\
&= -\frac{K\alpha^2}{\mu\phi L^2}\frac{\partial h}{\partial P}\left(\frac{\partial P}{\partial \alpha}\right)^2
\end{aligned} \tag{2.9}$$

Hence, from Equations (2.8 & 2.9), the pressure formulation for the rectilinear

flow in the VI process can be written as:

$$\frac{d^2P}{d\alpha^2} + \left[\frac{1}{K}\frac{dK}{dP} + \left(\frac{\phi + \alpha^2}{h\phi}\right)\frac{dh}{dP}\right]\left(\frac{dP}{d\alpha}\right)^2 = 0 \tag{2.10}$$

It is clear from Equations (2.1 & 2.10) that accounting for a variable flow rate in the 1D flow VI process leads to a slightly different formulation.

2.2.2 Radial (2D) Flow

For a unit volume taken from a saturated reinforcement (Figure 2.3), the thickness will be a function of time as well as position. For such a volume, one can write the conservation of mass law in the radial direction as:

$$\frac{\partial h}{\partial t} = -\frac{1}{r}\frac{\partial}{\partial r}\left(rhu_r\right) \tag{2.11}$$

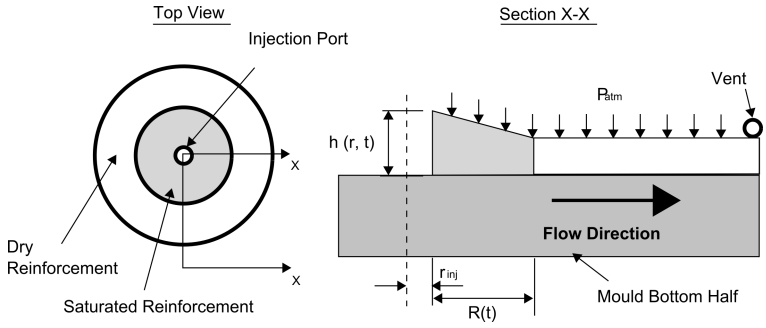

Figure 2.3: Schematic of the radial flow VI process.

Then, using Darcy's law in radial form Delleur (1998),

$$\frac{\partial h}{\partial t} = \frac{1}{r}\frac{\partial}{\partial r}\left(\frac{rhK}{\mu}\frac{\partial P}{\partial r}\right) \tag{2.12}$$

Note that here, the reinforcement permeability is assumed to be constant. Then,

$$\frac{\partial h}{\partial t} = \frac{1}{r\mu}\frac{\partial}{\partial r}\left(rhK\frac{\partial P}{\partial r}\right) \tag{2.13}$$

Operating partials on the right-side and simplifying,

$$\frac{\partial h}{\partial t} = \frac{1}{r\mu}\left[rhK\frac{\partial^2 P}{\partial r^2} + r\left(K\frac{\partial h}{\partial P} + h\frac{\partial K}{\partial P}\right)\left(\frac{\partial P}{\partial r}\right)^2 + hK\frac{\partial P}{\partial r}\right] \tag{2.14}$$

Let,

$$\alpha = \frac{r - r_{inj}}{R - r_{inj}} \tag{2.15}$$

Then,

$$\frac{\partial \alpha}{\partial r} = \left(\frac{1}{R - r_{inj}}\right) \quad \text{and} \quad \frac{\partial \alpha}{\partial R} = \left(-\frac{\alpha}{R - r_{inj}}\right) \tag{2.16}$$

Also,

$$\frac{\partial P}{\partial r} = \frac{\partial P}{\partial \alpha}\frac{\partial \alpha}{\partial r}; \quad \frac{\partial h}{\partial r} = \frac{\partial h}{\partial P}\frac{\partial P}{\partial \alpha}\frac{\partial \alpha}{\partial r} \quad \text{and} \quad \frac{\partial K}{\partial r} = \frac{\partial K}{\partial P}\frac{\partial P}{\partial \alpha}\frac{\partial \alpha}{\partial r} \tag{2.17}$$

Hence, Equation (2.14) can be written as:

$$\frac{\partial h}{\partial t} = \frac{hK}{\mu\ (R - r_{inj})^2}\left[\frac{\partial^2 P}{\partial \alpha^2} + \left(\frac{1}{h}\frac{\partial h}{\partial P} + \frac{1}{K}\frac{\partial K}{\partial P}\right)\left(\frac{\partial P}{\partial \alpha}\right)^2 + \left(\frac{(R - r_{inj})}{r_{inj} + \alpha\ (R - r_{inj})}\right)\frac{\partial P}{\partial \alpha}\right] \tag{2.18}$$

In addition,

$$\begin{aligned}\frac{\partial h}{\partial t} &= \frac{\partial h}{\partial P}\frac{\partial P}{\partial \alpha}\frac{\partial \alpha}{\partial R}\frac{\partial R}{\partial t} \\ &= \frac{\partial h}{\partial P}\frac{\partial P}{\partial \alpha}\frac{\partial \alpha}{\partial R}\left(-\frac{K}{\mu\phi}\frac{\partial P}{\partial \alpha}\frac{\partial \alpha}{\partial R}\right) \\ &= -\frac{K\alpha^2}{\mu\phi\ (R - r_{inj})^2}\frac{\partial h}{\partial P}\left(\frac{\partial P}{\partial \alpha}\right)^2\end{aligned} \tag{2.19}$$

Hence, from Equations (2.18 & 2.19), the formulation for resin pressure in a radial flow VI process can be written as:

$$\frac{\partial^2 P}{\partial \alpha^2} + \left[\frac{1}{K}\frac{\partial K}{\partial P} + \left(\frac{\phi + \alpha^2}{h\phi}\right)\frac{\partial h}{\partial P}\right]\left(\frac{\partial P}{\partial \alpha}\right)^2 + \left[\frac{(R - r_{inj})}{r_{inj} + \alpha\ (R - r_{inj})}\right]\frac{\partial P}{\partial \alpha} = 0 \tag{2.20}$$

2.2.3 Iterative Solution Procedure

The pressure formulations in Equations (2.10 & 2.20) are non-linear boundary value problems. One can solve them in their current form by using the finite difference method. The solution of the resulting non-linear finite-difference equations can be found using Newton's method. Alternatively, one can convert these equations into two initial value problems using the shooting method. Then, the resulting equations can be solved using a first-order Euler method (Appendix 2.B).

As the exact solutions of Equations (2.10 & 2.20) are not known, the iterative solution will have to be checked for convergence using different discretisation levels. In addition, for such non-linear problems, round off and truncation errors may become significant. Hence, it is desirable to compare results from two different order numerical methods. Many higher order methods such as a fourth-order Runge-Kutta (Appendix 2.C) method can be employed for this purpose.

In any case, all of these methods are iterative and require one to guess an initial value for a solution, which also affects their stability. For the finite difference method, one prerequisite for the solution to converge to the actual solution is that the Jacobian matrix for the system of equations should be non-singular. Calculating the Jacobian for nonlinear system of equations can be challenging, especially if one wants to use higher order methods. Hence, in general, the shooting method is preferred over the finite difference method for solving nonlinear equations (Burden and Faires, 2000; Abdelwahab, 2006).

In the shooting method, the boundary value problem is converted into two initial value problems by replacing the second order equations with two first order equations. Setting $I = \frac{dP}{d\alpha}$, Equation (2.10) can be replaced with:

$$\frac{dI}{d\alpha} + \left[\frac{1}{K}\frac{dK}{dP} + \left(\frac{\phi + \alpha^2}{h\phi}\right)\frac{dh}{dP}\right]\left(I^2\right) = 0 \tag{2.21}$$

$$\frac{dP}{d\alpha} = I \tag{2.22}$$

Then, in the first order Euler's shooting method, the domain is discretised using a fixed number of nodes (m) and Equations (2.21 & 2.22) are replaced with:

$$\frac{I_i - I_{i-1}}{\alpha_i - \alpha_{i-1}} + \left[\frac{1}{K}\frac{dK}{dP} + \left(\frac{\phi + \alpha^2}{h\phi}\right)\frac{dh}{dP}\right]_{i-1} \left(I_{i-1}^2\right) = 0; \;\; i = 2, ..., m \tag{2.23}$$

$$P_i = P_{i-1} + I_{i-1}\left(\alpha_i - \alpha_{i-1}\right); \;\; i = 2, ..., m \tag{2.24}$$

At each iterative step, the value of the pressure gradient at the injection gate (i.e. I_1) is guessed. In this particular case, this value was guessed to be half of the injection pressure. In addition, the injection gate pressure condition is imposed (i.e. $P_1 = P_{inj}$). The resulting simultaneous nonlinear equations are solved for all other nodes inside the flow domain to find the pressure solution at the flow front ($i = m$). If the pressure at the flow front is not equal to the compaction pressure in the dry region of the mould, then a new value for the pressure gradient at the injection gate is guessed and the iterative procedure is repeated. Many algorithms exist for guessing this new value. In this particular case, the entire solution was found in MS-Excel using the in-built goal seek function, which uses a linear search algorithm. One can solve Equation (2.20) in a similar way to find the pressure solution in a radial flow VI process (Appendix 2.D).

Also, the accuracy and convergence of solutions was checked by solving Equations (2.10 & 2.20) using a fourth order Runge-Kutta method (Appendices 2.E & 2.F) for two discretisation levels (with 100 and 1000 nodes) and comparing the results from both the methods and discretisation levels.

2.2.4 Reinforcement Compliance and Permeability Behaviour

To find solutions of Equations (2.10 & 2.20), relationships defining the dependence of the thickness and the permeability on the resin pressure are required. As mentioned earlier, Correia (2004) characterised dry compaction and saturated expansion behaviour of four different architecture reinforcements (Table 2.2).

Table 2.2: Details of the reinforcements whose compliance behaviour was characterised by Correia (2004).

Reinforcement	Architecture	Manufacturer	Surface Density ($Kg\,m^{-2}$)
Unifilo U750/450	Continuous Fibre Random Mat	Saint-Gobain Vetrotex	0.450
UDUC	Unbalanced Bidirectional	Flemings	0.715
RT600	Bidirectional Plain Weave	Saint-Gobain Vetrotex	0.600
FGE 117	Stitched Triaxial	Formax	1.167

In these experiments, 100 mm diameter circular reinforcement samples, placed in an oil bath (HDX 30, Trent Oil Ltd., UK), were initially compressed to a pressure of 90 kPa (which is a normal pressure range in VI) at a constant rate of 10 N/s. Then, the samples were decompressed at the same rate. The results were curve-fitted to an empirical model, similar to the one suggested by Robitaille and Gauvin (1998a) (Equation 2.25), to find distinct values of parameters - V_{f0} and B - for dry compaction and saturated expansion behaviour.

$$V_f = V_{f0}\, P_{comp}^{B}\,, \text{ where } P_{comp} = P_{atm} - P \text{ and } V_f = \frac{n\, S_d}{\rho\, h} \tag{2.25}$$

Table 2.3 lists these values for three layers of reinforcement, while Figure 2.4 shows the goodness of fit of Equation 2.25, using these values, to results from one of the actual saturated expansion experiments. In addition, Figure 2.5 shows the dry compaction and wet expansion curve fitting parameters in Table 2.3, where their inter-dependency as well as the general trend in the compliance behaviour of different reinforcements can be identified. Reinforcements with complex architecture such as FGE 117, which exhibit low compliance behaviour, are concentrated on the right, while simple, highly compliant reinforcements such as Unifilo U750 are concentrated on the left.

Table 2.3: Dry compaction and wet expansion compliance properties of various reinforcements, as reported by Correia (2004) and used in the present work (number of layers = 3, number of cycles = 1).

	Dry Compaction		Saturated Expansion	
	V_{fo}	B	V_{fo}	B
U750/450	0.035	0.150	0.060	0.117
UDUC	0.113	0.108	0.263	0.037
RT600	0.175	0.086	0.368	0.027
FGE117	0.201	0.089	0.456	0.018

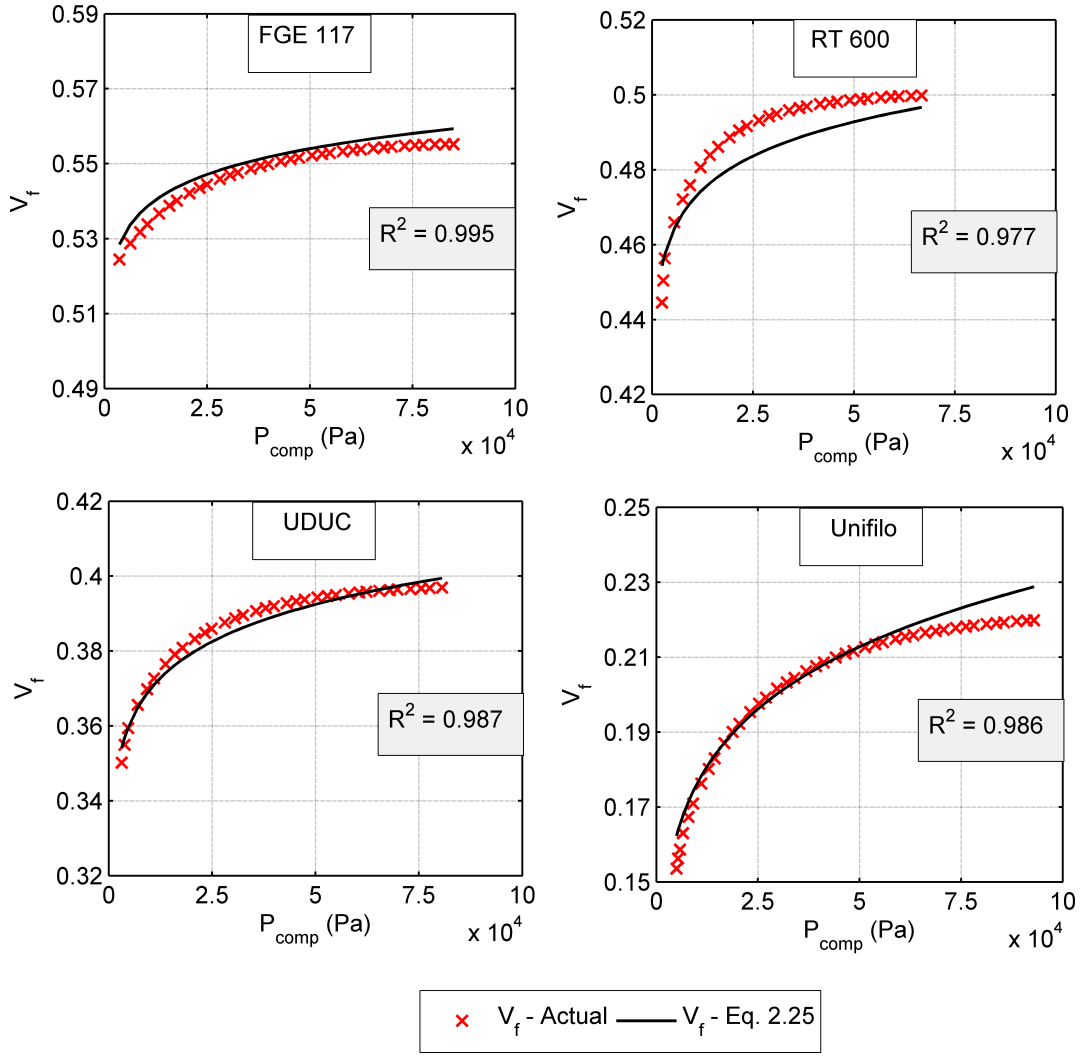

Figure 2.4: Goodness of fit of Equation (2.25) to compliance results from one of the actual saturated expansion experiments. The respective values of the curve fitting parameters are listed in Table 2.3.

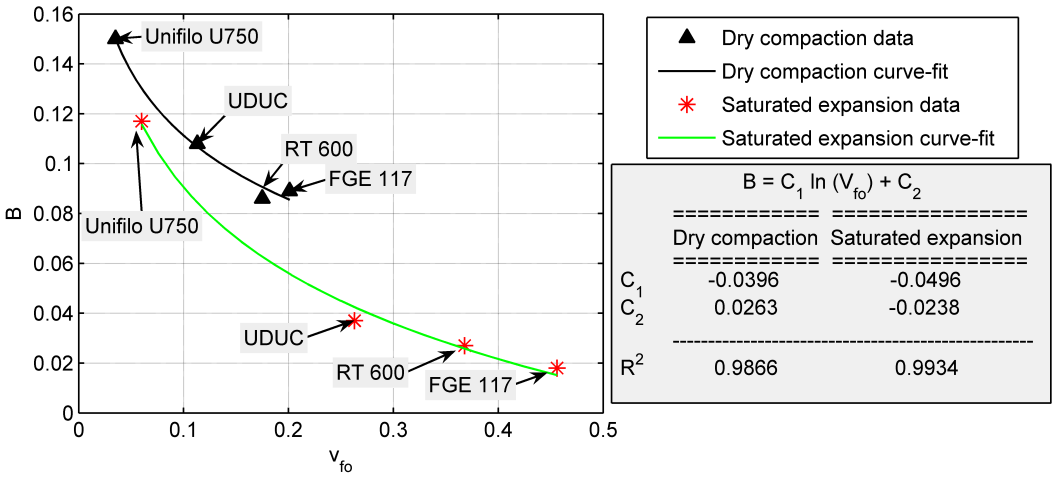

Figure 2.5: The general trend in the values of the curve fitting parameters in Equation (2.25) for different reinforcements (Correia, 2004). Increasing the complexity of the reinforcement architecture shifts the curve downwards and rightwards.

In this analysis, Correia's experimental results in Table 2.3 were used in Equation (2.25) to find the fibre volume fraction (V_f), from which pressure solutions in the rectilinear and radial VI flow processes were calculated using Equations (2.10 & 2.20), respectively. In addition, the well-known Kozeny-Carman equation (Equations 2.26) was used for reinforcement permeability. It is important to note that the pressure solution does not depend on the value of the Kozeny constant (k). However, the permeability (K) does change with (P_{Comp}), which influences the fill-time solution.

$$K = k\,\frac{\phi^3}{(1-\phi)^2} \tag{2.26}$$

From Equations 2.25 and 2.26, one can define the $\frac{dK}{dP}$ and $\frac{dh}{dP}$ terms as follows:

$$\frac{dh}{dP} = \frac{n\,S_d\,B}{\rho\,V_{f0}\,P_{Comp}^{B+1}} \tag{2.27}$$

$$\frac{dK}{dP} = k\,B\frac{\left(-3\,P_{Comp}^{-(B+1)}\,V_{f0} + P_{Comp}^{B-1}\,V_{f0}^{3} + 2\,P_{Comp}^{-2B-1}\right)}{V_{f0}^{2}} \tag{2.28}$$

2.3 Pressure Profile Solution

As mentioned earlier, the pressure formulations in Equations (2.10 & 2.20) are boundary value problems and will need two boundary conditions. For this, the atmospheric, injection and vent pressures were assumed to be 0 kPa (100 kPa absolute), 10 kPa (90 kPa absolute) and 95 kPa (5 kPa absolute) below atmospheric pressure. Thus, the maximum compaction pressure was 95 kPa before the start of the injection. Note that all the pressure results in the present work have been adjusted to show the vacuum pressure to be 0 kPa. In addition, the fibre density and the number of layers were assumed to be 2540 $kg\ m^{-3}$ and 3, respectively.

2.3.1 Rectilinear (1D) Flow

Figure 2.6 shows the iteratively computed analytical pressure solution using Equation (2.10) for Unifilo U750 reinforcement using the Euler and Runge-Kutta methods. The RTM pressure profile is calculated using the closed-form analytical solution. The varying mould thickness leads to a different pressure profile in VI compared to the linear pressure profile in RTM. In addition, the solution does not depend on the order of the numerical method or the discretisation level, which verifies the accuracy of the solution procedure. Hence, for deriving the pressure solution for other reinforcements, the first order Euler method, with a discretisation level of 100 nodes, was used.

Figure 2.6 also shows the pressure profile from LIMS-VI. The profile from LIMS-VI is significantly different compared to the analytical profile. This can be explained by noting that the solution domain in this FE/CV method, which

is the underlying numerical method in LIMS-VI, is defined by nodal fill-factors. At the start of each time step, the pressure profile in the solution domain is calculated using initial set of nodal values for reinforcement properties (i.e. V_f, K, h). Then, from the local pressure values, new values of local reinforcement properties are calculated, from which the pressure profile is recalculated. This iterative process is repeated until the successive change in the pressure profile results in convergence to a predefined tolerance. Then, the fill-factors are updated to advance the flow front and the process is repeated until all the nodes are filled. It is clear that when a node is filled, the thickness of the associated element is assumed to be the initial thickness. Also, once a node is filled, it always forms part of the solution domain and its nodal fill-factor is never allowed to fall below unity in subsequent time-steps. Then, recalculating the thickness and the fibre volume fraction in each element in the filled region, after every time step, while keeping the value of nodal fill-factors constant (equal to 1) leads to violation of law of mass conservation, and hence an erroneous pressure solution. This is because the additional resin volume needed to flow into the empty volume created by recalculation of the thickness and fibre volume fraction is not accounted for.

The changing compliance behaviour, when moving from left to right in Figure 2.5, is reflected in the pressure profile for these reinforcements (Figure 2.7). It is clear that the lower the compliance behaviour (towards the right in Figure 2.5), the greater the similarity in the pressure profile between the VI and RTM processes. In addition, the error level in the LIMS-VI solution depends on the compliance behaviour of reinforcements, which agrees with the previous explanation for the presence of error in the LIMS-VI solution i.e. reinforcements with low compliance behaviour will have lower thickness changes, and hence lower error in the LIMS-VI pressure solution. Also, note that as the analytical formulation is in the non-dimensional form, the pressure profiles in Figures 2.6 and 2.7 do not change with flow progression.

(a) No of Nodes - 100

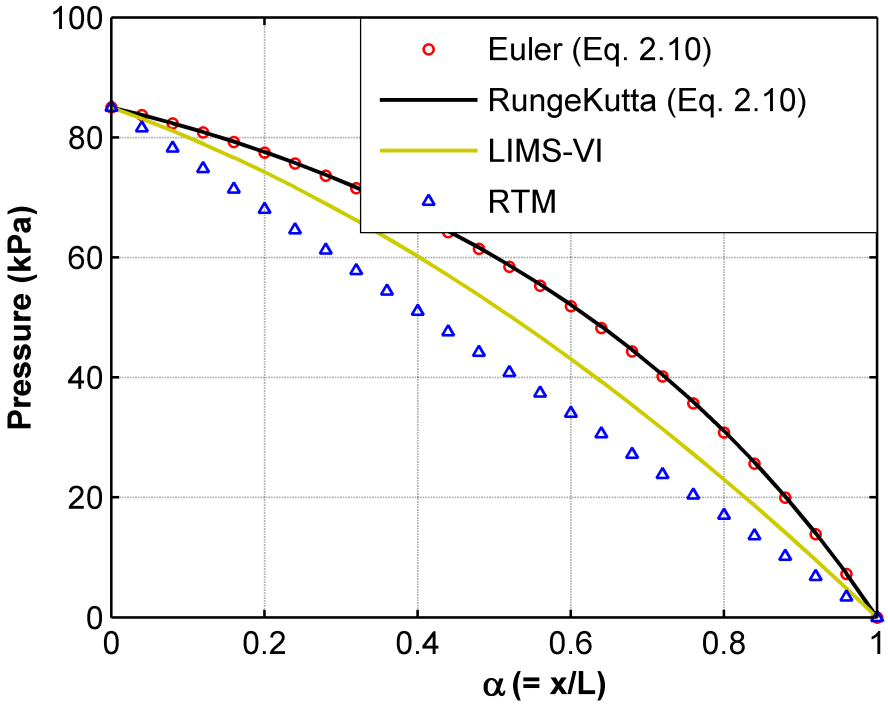

(b) No of Nodes - 1000

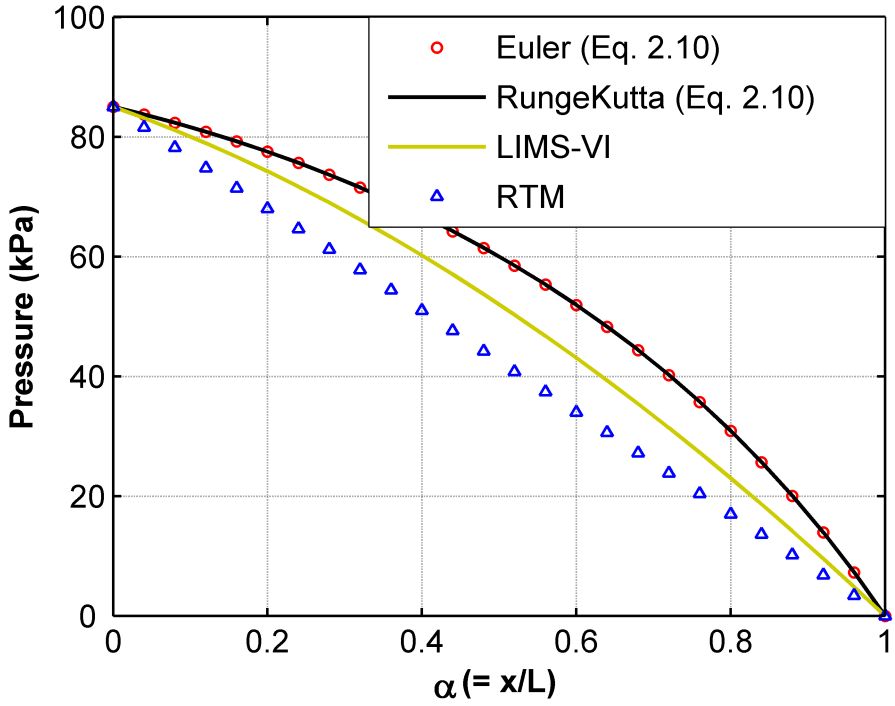

Figure 2.6: Pressure distribution in the rectilinear flow VI process. The mould contains 3 layers of U750 (continuous fibre random mat). The same number of nodes were used for LIMS-VI and the RTM analytical model.

(a) UDUC (Unbalanced Bidirectional)

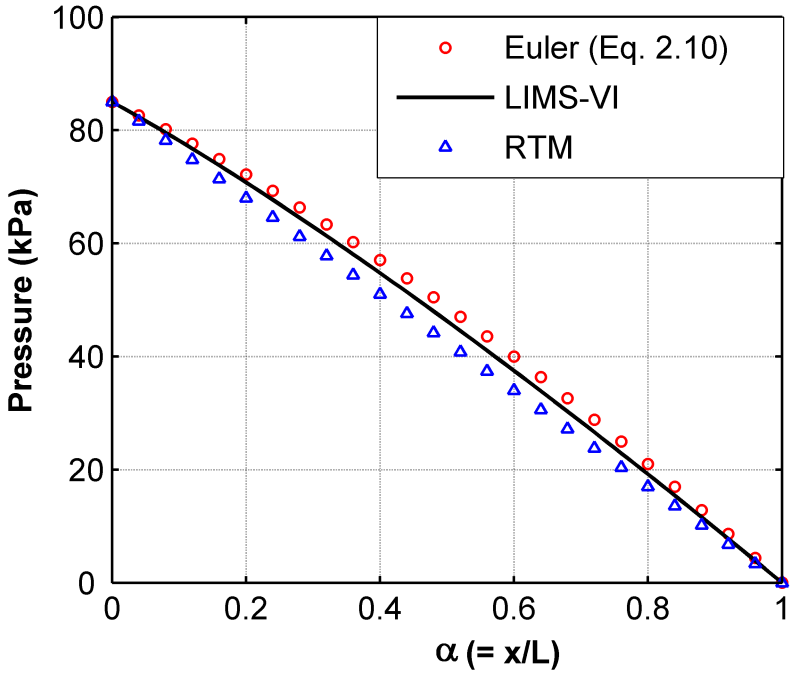

(b) RT 600 (Bidirectional Plain Weave)

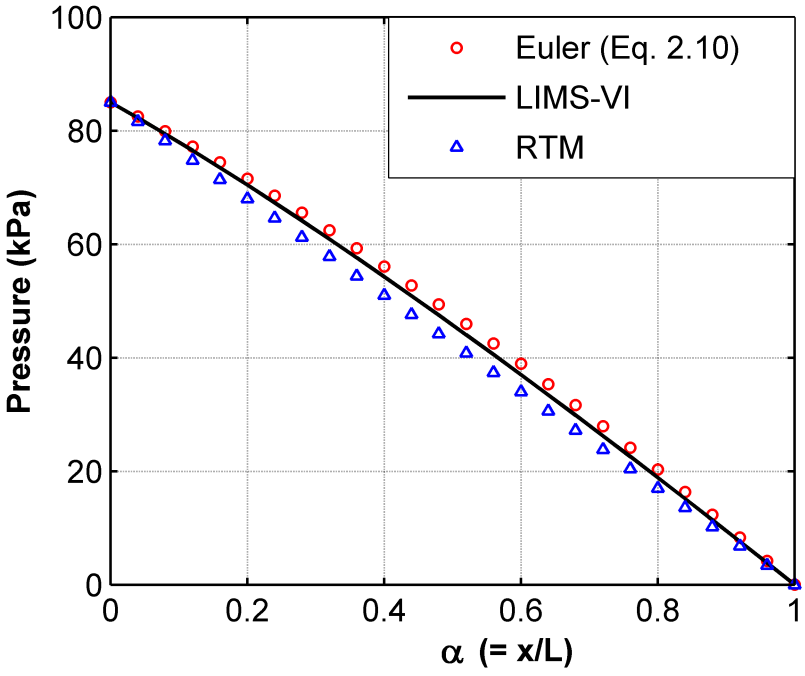

(c) FGE 117 (Stitched Triaxial)

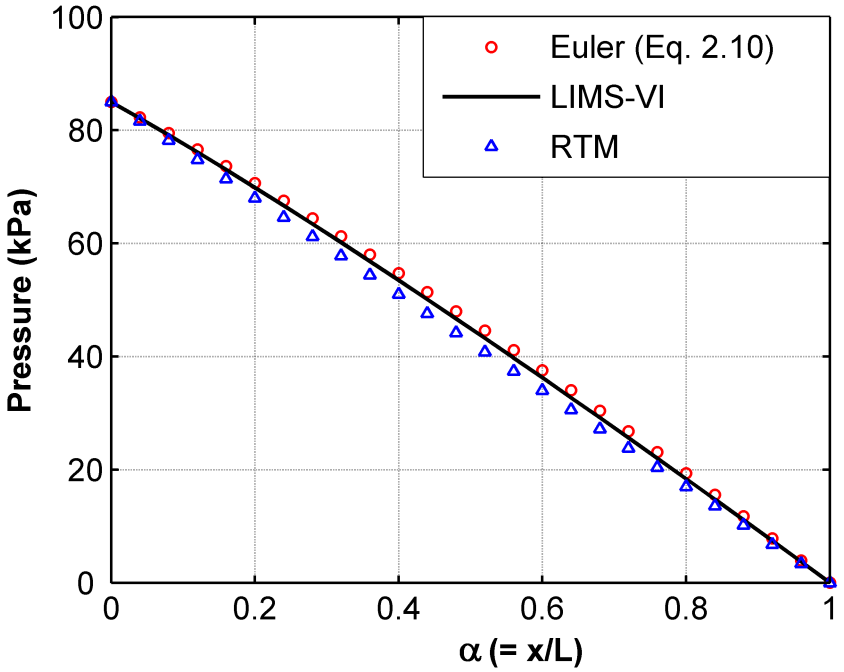

Figure 2.7: Pressure distribution in the rectilinear flow VI process. All results are from numerical models with 100 nodes. The same number of nodes were used for LIMS-VI and the RTM analytical model.

2.3.2 Radial (2D) Flow

Figure 2.8 shows the iteratively computed analytical pressure solution (Equation 2.20) for Unifilo U750 reinforcement using the first order Euler method and the fourth order Runge-Kutta method. The RTM pressure profile is calculated using the closed-form analytical solution. For comparison, the pressure solution using LIMS-VI is also plotted. In this case also, the reinforcement relaxation leads to a different pressure profile in the VI process as compared to the RTM process. The solution does not depend on the order of the numerical method or the discretisation level, which verifies the accuracy of the solution procedure. Hence, the solution for other reinforcements was found using the first order Euler method with 100 nodes. Also, as in the rectilinear case, the

solution from LIMS is errorneous.

Figure 2.9 plots the pressure solution for other reinforcements. It is clear that in this case also, the reinforcement compliance behaviour influences the deviation of the VI pressure profile from the RTM pressure profile as well as the error in the LIMS-VI solution. It is important to note that by its nature, the radial flow solution varies with flow progression and the pressure solutions in Figures 2.8 and 2.9 are for the flow front to injection gate radius ratio of 100.

(a) No of Nodes - 100

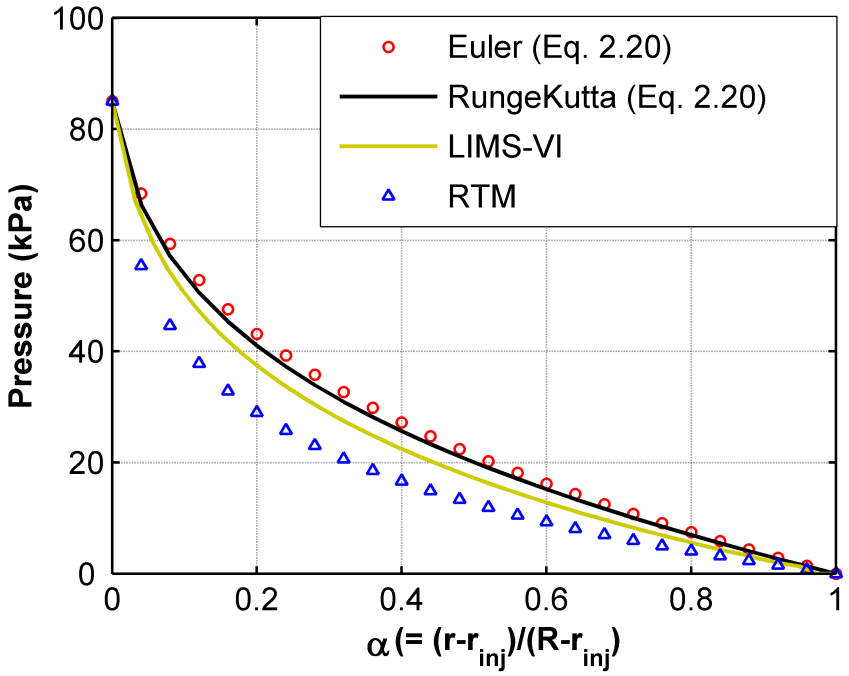

(b) No of Nodes - 1000

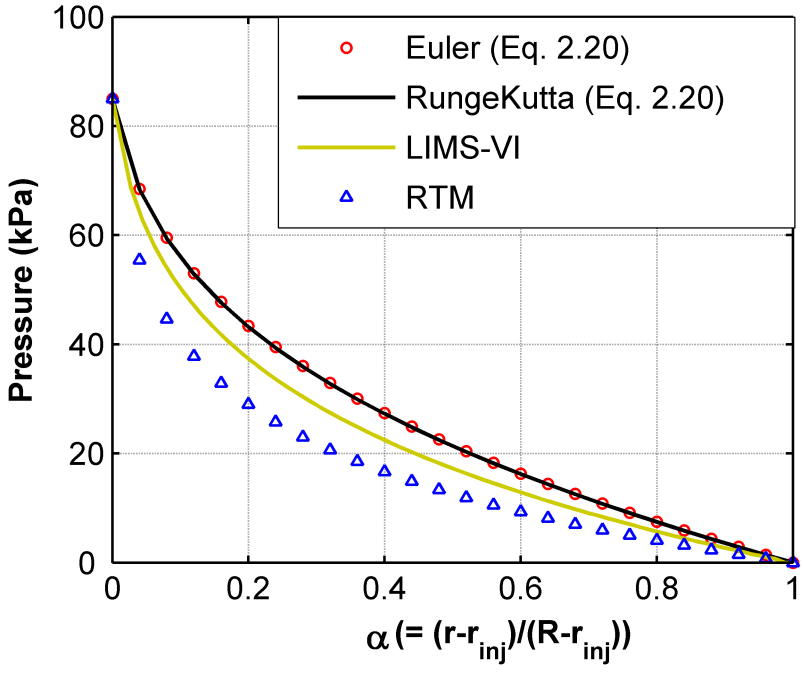

Figure 2.8: Pressure distribution in the radial flow VI process. The mould contains 3 layers of U750 (continuous fibre random mat). The numerical model in LIMS-VI had 1900 nodes. The flow front to injection gate radius ratio is 100.

(a) UDUC (Unbalanced Bidirectional)

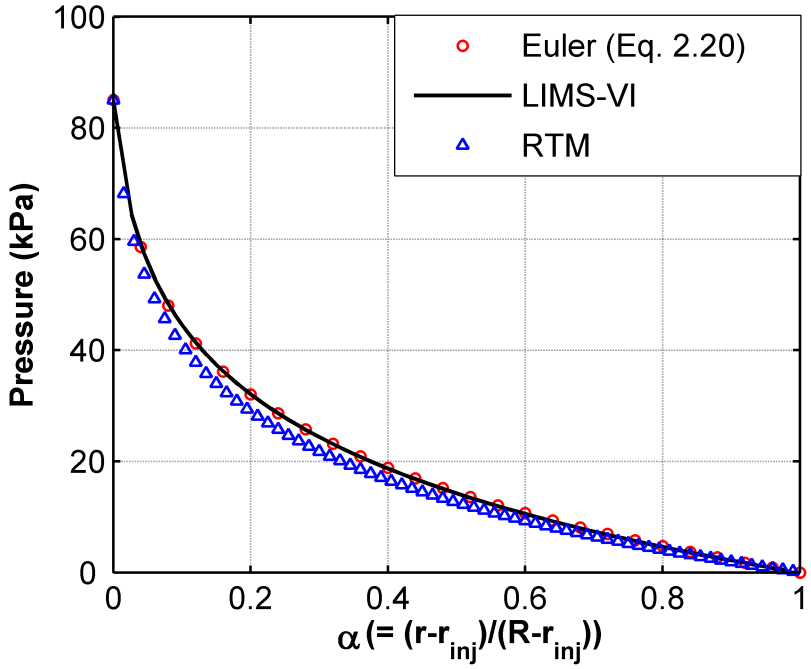

(b) RT 600 (Bidirectional Plain Weave)

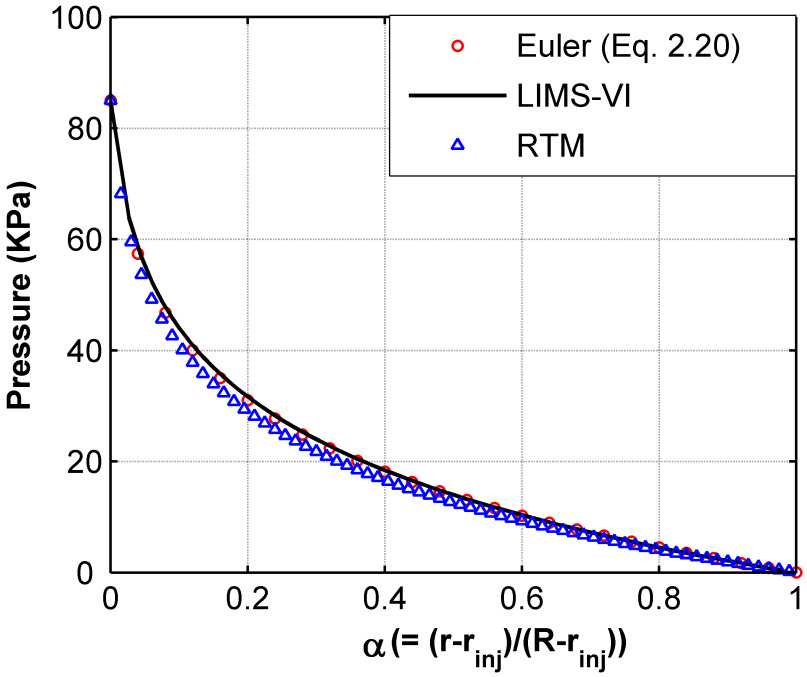

(c) FGE 117 (Stitched Triaxial)

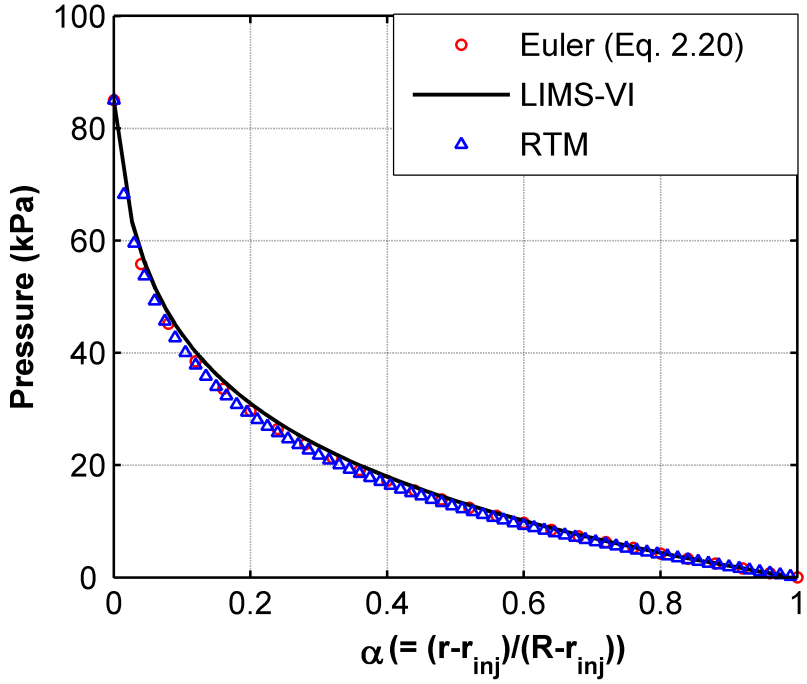

Figure 2.9: Pressure distribution in the radial flow VI process. The numerical model in LIMS-VI had 1900 nodes, while all other models had 100 nodes. The flow front to injection gate radius ratio is 100.

2.4 Fill-time Formulation

2.4.1 Rectilinear (1D) Flow

In the rectilinear flow RTM process, the normalised pressure gradient at the flow front can be written as:

$$\left[\frac{dP}{d\alpha}\right]_{\alpha=1,\,RTM} = -\Delta P \quad \text{where, } \alpha = \frac{x}{L} \tag{2.29}$$

Integrating Equation 2.29, the fill-time for RTM can be written as:

$$t_{RTM} = \frac{\mu\phi L^2}{2K\Delta P} \tag{2.30}$$

It is not possible to express the solution of Equation (2.10) in a closed form. However, for most of the reinforcements, the normalised fluid pressure profile is almost identical in the RTM and VI processes (Figures 2.6 & 2.7) and the VI pressure gradient at the flow front can be assumed to have the same form as the RTM pressure gradient in Equation (2.29) i.e.

$$\left[\frac{dP}{d\alpha}\right]_{\alpha=1,\,VI} = -D_1\,\Delta P \tag{2.31}$$

Then, following the iterative solution procedure outlined in Section 2.2.3, one can calculate the pressure gradient at the flow-front in the rectilinear VI process. From this, using Equation 2.31, one can calculate the value of the constant of proportionality(D_1). Note that, as the presure profiles are normalised and remain constant, only one value of this constant of proportionality (D_1) is required for each reinforcement. In addition, its value will depend on (i) the reinforcement compliance behaviour, and (ii) the applied pressure differential (ΔP).

Then, using Darcy's law, the fluid velocity at the flow front can be written as:

$$\left[\frac{dL}{dt}\right]_{VI} = -\frac{1}{\mu L}\left[\frac{K}{\phi}\,\frac{dP}{d\alpha}\right]_{\alpha=1} \tag{2.32}$$

Substituting Equation (2.31) in Equation (2.32) and integrating, the fill-time in the rectilinear flow VI process can be written as:

$$t_{VI} = \left[\frac{\mu\,L^2}{2\,D_1\,\Delta P}\right]\left[\frac{\phi}{K}\right]_{\alpha=1} \tag{2.33}$$

2.4.2 Radial (2D) Flow

In the radial flow RTM process, the pressure gradient and the fluid velocity at the flow front can be written as:

$$\left[\frac{dP}{dR}\right]_{RTM} = -\frac{\Delta P}{R\,\ln\left(\frac{R}{r_{inj}}\right)} \tag{2.34}$$

$$\left[\frac{dR}{dt}\right]_{RTM} = -\frac{K}{\mu\phi}\frac{dP}{dR} = \frac{K}{\mu\phi}\frac{\Delta P}{R\ln\left(\frac{R}{r_{inj}}\right)} \tag{2.35}$$

Note that the pressure gradient in Equation (2.34), being a function of the flow front radius and the injection gate radius, changes with flow progression, and hence, cannot be normalised as in the rectilinear flow case. In addition, as ΔP is constant, the pressure gradient will vary according to the denominator on the right-side of Equation (2.34). Integrating Equation (2.35), the fill-time can be found as:

$$t_{RTM} = \frac{\mu\phi}{2K\Delta P}\left[R^2\ln\left(\frac{R}{r_{inj}}\right) - \frac{1}{2}\left(R^2 - r_{inj}^2\right)\right] \tag{2.36}$$

In the radial flow VI process also, as shown in Figures 2.8 & 2.9, the pressure profile Equation (2.20) is nonlinear and hence, cannot be expressed in a closed form. However, the assumption that the VI pressure gradient, at the flow front, has the same form as the RTM pressure gradient in Equation (2.34) is still valid. This is because, as in the rectilinear flow case, the RTM pressure profile is almost identical to the VI pressure profile (Figures 2.8 & 2.9) for most of the reinforcements. Then,

$$\left[\frac{dP}{dR}\right]_{VI} = -\frac{D_2\,\Delta P}{R\ln\left(\frac{R}{r_{inj}}\right)} \tag{2.37}$$

Then, one can find the pressure solution for different flow front positions by using the numerical procedure outlined in Section 2.2.3. From this, the value of the constant of proportionality (D_2) can be found by linear regression of the pressure gradient at the flow front as a function of ($\Delta P/R\ln\left(\frac{R}{r_{inj}}\right)$). Figure 2.10 shows such a plot, for the four reinforcements investigated in this analysis. It is clear that the relationship is linear, which validates the assumption of VI pressure gradient having a similar form as the RTM pressure gradient. Note that the value of the constant of proportionality (D_2) depends on (i) the reinforcement compliance behaviour, and (ii) the applied pressure differential (ΔP).

(a) Unifilo U750 (Continuous Fibre Random Mat)

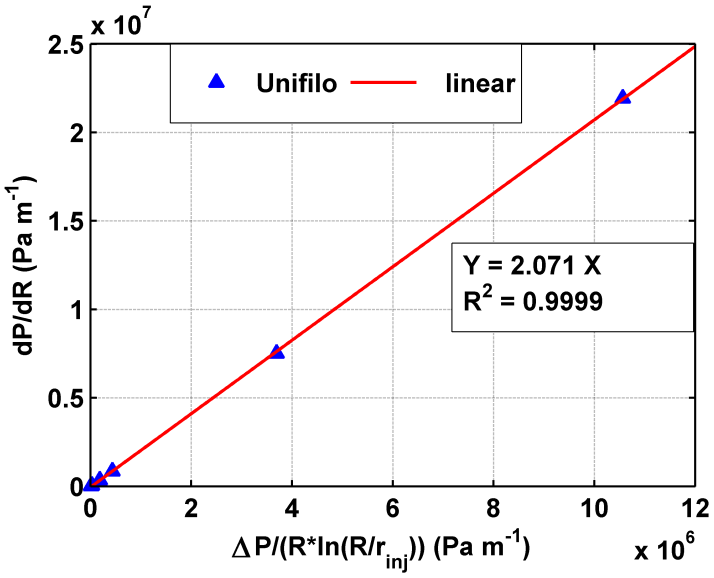

(b) UDUC (Unbalanced Bidirectional)

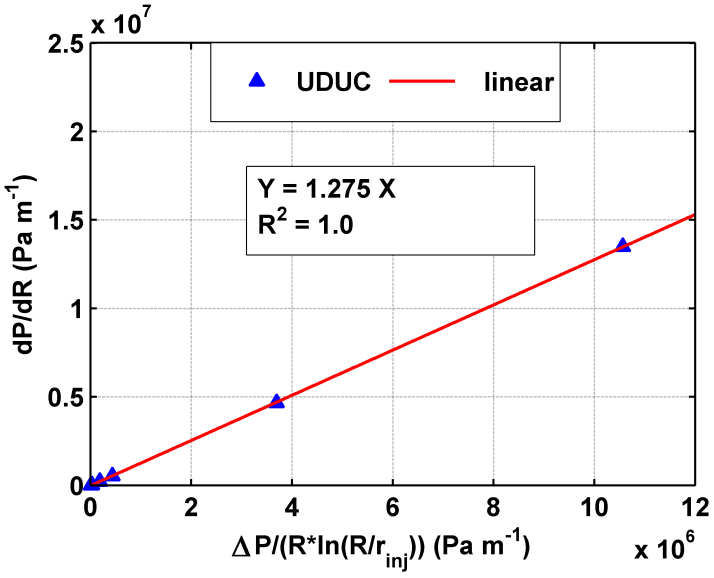

(c) RT 600 (Bidirectional Plain Weave)

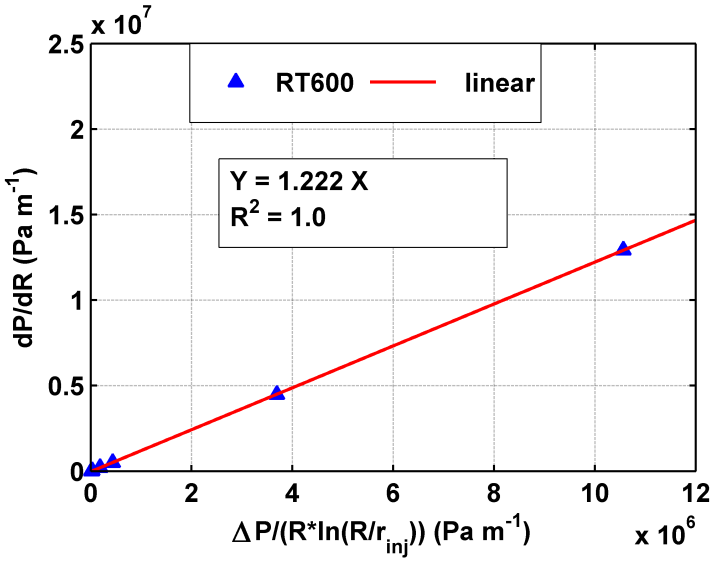

(d) FGE 117 (Stitched Triaxial)

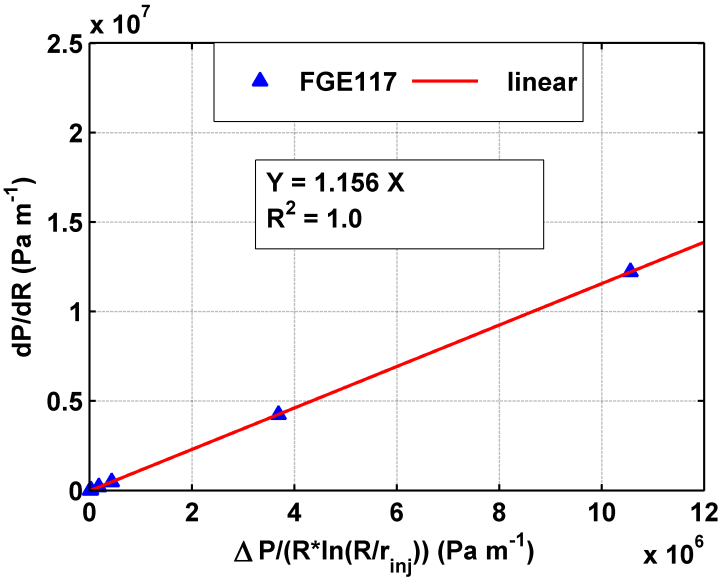

Figure 2.10: Regression analysis of the numerically calculated pressure gradient at the flow front in the radial flow VI process. The linear fit allows one to find the constant of proportionality (D_2), which can be used to find VI fill-time and compare the equivalent RTM and VI processes.

Then, using Equation (2.37), the flow velocity can be written as:

$$\left[\frac{dR}{dt}\right]_{VI} = -\frac{1}{\mu}\left[\frac{K}{\phi}\frac{dP}{dR}\right]_{r=R} = \frac{1}{\mu}\left[\frac{K}{\phi}\frac{D_2\,\Delta P}{R\,\ln\left(\frac{R}{r_{inj}}\right)}\right]_{r=R} \tag{2.38}$$

Integrating Equation (2.38),

$$t_{VI} = \frac{\mu}{2\,D_2\,\Delta P}\left[R^2\,\ln\left(\frac{R}{r_{inj}}\right) - \frac{1}{2}\left(R^2 - r_{inj}^2\right)\right]\left[\frac{\phi}{K}\right]_{r=R} \tag{2.39}$$

2.5 RTM vs. VI Fill-time

2.5.1 Rectilinear (1D) Flow

Correia(2004) exhibited equivalence of the RTM and VI processes using the fill-time ratio (C_t^1) written as:

$$C_t^1 = \frac{t_{RTM}}{t_{VI}} \tag{2.40}$$

Then, using Equations (2.30 & 2.33),

$$C_t^1 = \left[\frac{\mu\phi L^2}{2K\Delta P}\right]_{RTM}\left[\frac{2\,D_1\,\Delta P\left[\frac{K}{\phi}\right]}{\mu L^2}\right]_{VI} \tag{2.41}$$

$$\text{Simplifying, } C_t^1 = D_1\,\frac{\left[\left[\frac{K}{\phi}\right]_{\alpha=1}\right]_{VI}}{\left[\frac{K}{\phi}\right]_{RTM}} \tag{2.42}$$

$$\text{Let, } A = \frac{\left[\left[\frac{K}{\phi}\right]_{\alpha=1}\right]_{VI}}{\left[\frac{K}{\phi}\right]_{RTM}} \tag{2.43}$$

$$\text{Then, } C_t^1 = A\,D_1 \tag{2.44}$$

In the above, it should be noted that:

1. For appropriate comparison of the RTM and VI processes, these processes should be equivalent i.e. the injection and the compaction pressure conditions should be identical in both the processes. Then, the fibre volume fraction and the permeability for the equivalent RTM process can be calculated using Equations (2.25 & 2.26).

2. For valid comparison, it is important to characterise the curve-fitting parameters in Equation (2.25) using appropriate reinforcement compliance experiments. In the RTM process, during mould closure, dry reinforcement is compressed, while during infusion, the reinforcement thickness remains constant. Hence, compliance properties should be derived from dry compaction experiments. For the VI process, as pointed out earlier, these parameters should be charactersied from wet expansion experiments.

3. Table 2.3 lists the values of curve-fitting parameters from wet expansion and dry compaction experiments for the reinforcements investigated in this analysis. The value of C_t^1, in Equation (2.44), was derived using these values.

4. The pressure profile in the rectilinear VI process is normalised and remains constant with flow progression. In addition, the fluid pressure in the VI process is zero at the flow front i.e. the reinforcement is compacted to full compaction pressure. Hence, at the flow front, its porosity remains constant.

5. As both the pressure profile and parameter A remain constant during flow progression, the fill-time ratio will also remain constant.

6. Substituting the Equation (2.26) for reinforcement permeability in Equation (2.43), one can write:

$$A = \left[\frac{(1-\phi)}{\phi}\right]^2_{RTM} \left[\left[\frac{\phi}{(1-\phi)}\right]^2_{\alpha=1}\right]_{VI} \tag{2.45}$$

   i.e. the Kozeny constant in Equation (2.26) is important for calculating individual RTM and VI fill-times. However, when calculating the fill-times ratio of these two processes, it cancels out as shown in Equations (2.43 & 2.45).

7. As described in Sections 2.3.1 & 2.3.2, the pressure solution from LIMS-VI is erroneous and was not used for the fill-times investigation.

2.5.2 Radial (2D) Flow

Using Equations (2.36 & 2.39), the fill-time ratio of radial flow RTM and VI processes can be written as:

$$C_t^2 = \frac{t_{RTM}}{t_{VI}} = \frac{\left[\frac{\mu\phi}{2K\Delta P}\left[R^2 \ln\left(\frac{R}{r_{inj}}\right) - \frac{1}{2}\left(R^2 - r_{inj}^2\right)\right]\right]_{RTM}}{\left[\frac{\mu}{2\,D_2\,\Delta P}\left[R^2 \ln\left(\frac{R}{r_{inj}}\right) - \frac{1}{2}\left(R^2 - r_{inj}^2\right)\right]\left[\frac{\phi}{K}\right]_{r=R}\right]_{VI}} \tag{2.46}$$

From Equations (2.43 & 2.45), $A = \frac{\left[\left[\frac{K}{\phi}\right]_{\alpha=1}\right]_{VI}}{\left[\frac{K}{\phi}\right]_{RTM}} = \left[\frac{(1-\phi)}{\phi}\right]^2_{RTM}\left[\left[\frac{\phi}{(1-\phi)}\right]^2_{r=R}\right]_{VI}$

$$\text{Hence, } C_t^2 = A\,D_2 \tag{2.47}$$

Note that:

1. Irrespective of the flow front position, the fibre volume fraction at the flow front and hence, the value of parameter A will remain constant for a given reinforcement at a given compaction pressure.

2. As ΔP and D_2 are constant, the fill-times ratio will also remain constant.

2.5.3 Results

Table 2.4 lists the process parameters used in this analysis, while Table 2.5 compares the values of the constant of proportionality (D_1, D_2) and the fill-time ratios (C_t^1, C_t^2) for rectilinear and radial flow processes, for four reinforcements used in this investigation. It is clear that, in both the cases, highly porous and compliant reinforcement such as Unifilo has lower VI fill-time as compared to the RTM fill-time. This is because the VI pressure gradient for this reinforcement is significantly greater than the RTM pressure gradient (Figures 2.6 & 2.8, Table 2.5).

Table 2.4: Reinforcement properties and process parameters used for calculating fill-times in the equivalent RTM and VI processes. The fibre volume fraction for the VI process is at the flow front. The fibre volume fraction for the RTM process is calculated using identical compaction pressure as the VI process.

Designation		U750/450	UDUC	RT 600	FGE 117
S_d	$(kg\,m^{-2})$	0.45	0.715	0.6	1.167
V_f	RTM	0.192	0.384	0.464	0.551
	VI	0.226	0.400	0.499	0.559
n		3			
ρ	$(kg\,m^{-3})$	2540			
P_{atm}	(Pa)	100000			
P_{inj}	(Pa)	90000			
P_{vent}	(Pa)	5000			
P_{comp}	(Pa)	95000			

Table 2.5: Analytically calculated constants of proportionality for pressure gradient at the flow front in rectilinear (D_1) and radial (D_2) flow VI processes. The fill-times ratios for rectilinear (C_t^1) and radial (C_t^2) flow processes remain constant, which highlights the similarity between the RTM and VI processes.

Designation	U750/450	UDUC	RT 600	FGE 117
A	0.665	0.903	0.771	0.976
D_1	2.17	1.297	1.241	1.17
D_2	2.071	1.275	1.223	1.157
C_t^1	1.443	1.171	0.957	1.142
C_t^2	1.377	1.151	0.943	1.128

On the other hand, VI processes employing reinforcements with low compliance such as stitched triaxial, will have almost equal fill-times to an equivalent RTM process. This is because these reinforcements exhibit only a minor difference in the fibre volume fraction derived from dry compaction and wet expansion experiments (Table 2.4), which results in the value of parameter A in Equation (2.45) being closer to unity (Table 2.5). In addition, the pressure gradient for these reinforcements is similar in the VI and RTM processes (Figures 2.7 & 2.9, Table 2.5).

Note that lower than unity fill-time ratios for RT 600 is suspected to be an outlier. This suspicion arises from the values of the compliance parameters listed in Table 2.3 and plotted in Figure 2.5. It is clear that the RT 600 does not fit nicely onto the curve-fit. In order to check the validity of this suspicion, the compliance parameters for the three remaining reinforcements were plotted seperately in a modified master curve. Then, assuming the same value for V_{fo}, new values of the parameter B were calculated for RT 600 from the curve-fitting parameters of this plot. These values were found to be different (0.093 and 0.025) from the values reported in Table 2.3 (0.086 and 0.027) for both dry compaction and wet expansion. Calculating new values of pressure gradients, V_f and ϕ for both RTM and VI, the new fill-time ratios were found to be 1.419 and 1.290 for rectilinear and radial flow cases, respectively. This confirms that erroneous values of compliance parameters are responsible for the lower than unity fill-time ratios for RT600. This is also confirmed by the poor curve-fit of Equation 2.25 to the actual results of the compliance characterisation experiments for RT 600 reinforcement (Figure 2.4). Also note that the new values of the fill-time ratios are higher for RT 600 than for UDUC reinforcement in Table 2.5, which does not mean that the fill-time ratios do not follow the master curve. This is because while calculating the compliance parameter values from the modified master curve, one can assume that either, (i) the value of V_{f0} or B remains same, or (ii) both change. Then, one will

get different values of the fill-times ratios, depending upon the assumed values of these parameters. For example, assuming V_{f0} values to be 0.174 (for Dry compaction) and 0.405 (for saturated expansion), one gets corresponding B values of 0.094 & 0.020 from the modified master curve. With these new values, the fill-time ratio in 1D is 1.151, which is between UDUC and FGE 117. It is clear that one needs to find exact values of these parameters to find the exact values of fill-times ratios. This will involve re-characterising the reinforcement compliance behaviour.

Also note that the value of the fill-time ratio is dependent on the assumed RTM equivalence. If one were to assume a different RTM equivalence e.g. by imposing identical average thickness, then the value of fill-times ratio would be different. In addition, the selection of compliance experiments to characterise the curve-fitting parameters will also affect this ratio. In any case, the trend should be similar to the one observed in the present analysis.

2.6 Conclusions

The flexible nature of the mould top half in the VI process leads to dynamically varying mould thickness, fibre volume fraction and permeability. An analytical formulation for the pressure profile in such a process was developed. Two cases, involving rectilinear (1D) and radial (2D) flow, were investigated. The coupled formulations were solved using an iterative numerical procedure. Following a previously reported approach, the infusion process was also modelled using LIMS-VI, a custom implementation in the FE/CV method based flow modelling tool LIMS. In addition, analytical solutions were also developed for fill-times in the rectilinear and radial flow VI processes.

The fluid pressure, in the filled region of the mould, was found to be higher in the VI process as compared to the RTM process. In addition, with increasing reinforcement compliance, the analytical pressure profile in the VI process

diverged from the RTM pressure profile. Results from numerical flow simulations showed a similar behaviour. Due to the technique used by the FE/CV method to track the flow front, the results from the flow simulation tool were found to be erroneous. The level of error depended on the compliance of reinforcements i.e. for reinforcements involving lower thickness changes, the error in the solution was lower.

The RTM and VI fill-time ratio, for both the rectilinear and the radial flow processes, was predicted to remain constant with flow progression. An important implication of the study is that simulation tools developed for the RTM process can be used to model the VI process without any major modifications. However, before this can be done with confidence, these analytical results need to be validated experimentally, which is the focus of the next chapter.

Chapter 3

Experimental Investigation of Pressure Profile and Flow Progression in the Vacuum Infusion (VI) Process

3.1 Introduction

In the previous chapter, analytical formulations for rectilinear and radial flow VI processes were developed. As these were coupled formulations, their solutions were derived using numerical methods. In the absence of a closed form solution, their validity can only be checked using experimental results. The main focus of this chapter is to describe an experimental set-up for this purpose. The validation of the analytical formulation through comparison with experimental results is also presented.

For rectilinear and radial flow RTM processes, one can easily derive analytical solutions for the fluid pressure profile and flow progression. The experimental validation of these formulations is also straightforward (DeParseval et al., 1995; Breard et al., 2003). However, as demonstrated in the previous chapter,

this is not the case for VI i.e. it is not possible to derive closed form analytical solutions for the rectilinear and the radial flow VI processes and hence, numerical solutions are necessary. The validity of these solutions will need to be checked with experimental results.

The majority of VI-related experimental work reported in the literature is focused on either measuring the thickness variation due to the reinforcement compliance behaviour (Williams et al., 1998; Andersson et al., 2003b) or measuring the lead-lag distance in the VI process with a distribution medium on top i.e. in the SCRIMP^{TM} process (Mathur et al., 2001; Ragondet, 2005). In fact, the only experimental effort to measure pressure profiles and fill-times is by Correia (2004). This was to validate his analytical formulation for a rectilinear flow VI process. The author measured fluid pressure at three locations along the flow direction for unsaturated as well as saturated flow. It was noted that instead of rising to its full value immediately after the start of injection, the injection pressure evolves with flow progression. The author attributed this evolution of the injection pressure to the permeability of the reinforcement and the resistance of the injection pipe and argued that one should only use the pressure results from inside the mould once the full injection pressure has been realised. Hence, fluid pressure results from saturated flow were used to validate the analytical formulation. The numerical results of the analytical formulation compared well with the experimental results, proving its validity. These experimental results also gave an important insight into the VI process, and for the first time, demonstrated the pressure profile in a rectilinear flow VI process to be non-linear as suggested by various formulations. Correia (2004) also reported experimental validation efforts for his rectilinear flow fill-time formulation. In his experiments, the author had used a woven material, which had complex architecture and hence, low permeability. The resulting high variability in the experimental results of the normalised fill-time vs. driving pressure led him to state that the approach was not reliable to validate the

analytical model.

In this chapter, new experimental set-ups, for the rectilinear and the radial flow VI processes, are described. These set-ups allow one to measure an unsaturated flow pressure profile and its evoluation with flow progression. In Section 3.3, the experimental results are presented and the validity of analytical formulations reported in the previous chapter is investigated.

3.2 Experimental Set-up

The aim of this new experimental set-up was to facilitate measurement of the fluid pressure distribution and its evolution in an unsaturated flow VI processes.

3.2.1 Rectilinear (1D) Flow Set-up

The pressure profile in a rectilinear flow VI process can be measured using Correia's (2004) experimental set-up. However, in this set-up, only two transducers are used inside the mould i.e. the expected non-linear pressure profile will have to be generated from only two pressure readings. The accuracy of the generated pressure profile can be increased by using more transducers along the mould length. In addition, more transducers are also needed for measuring the pressure profile evolution with flow progression. In addition, the transducers in the original set-up are placed along the centre-line of the mould. A minimum distance between these transducers needs to be maintained and hence, the maximum number that one can accomodate will be affected by the size of transducers. In summary, in order to increase the accuracy of experimental results and to measure the pressure profile evolution with flow progression, one will need to accomodate more transducers by changing the mould design.

In the new set-up for the rectilinear flow VI process, the top half was made

from an aluminium frame, while the bottom half was made from a 25 mm thick clear perspex sheet (Figure 3.1). Using a sealant tape, a flexible plastic bag was attached to the top side of this frame, while a draught excluder was attached to the mould side of the frame. The use of a draught excluder allows one to make a flexible mould sealing arrangement for easy, fast and repeatable experiments.

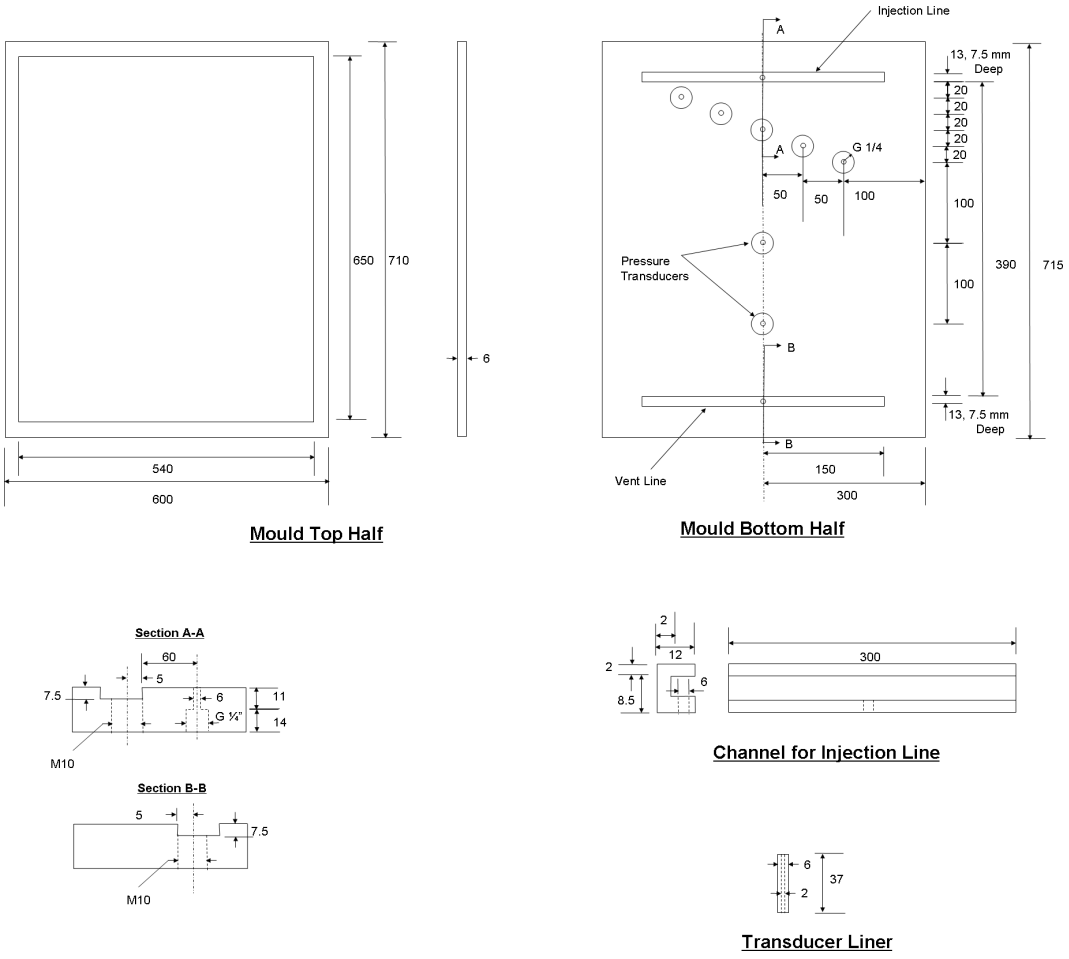

Figure 3.1: Experimental set-up for the rectilinear flow VI process. More pressure transducers are accomodated in this set-up by placing them across the width of the mould.

The transducers (Part: 348-8093, RS Components Ltd., UK[1]), with a diameter of 25 mm, need to be spaced apart by at least 50 mm to allow easy installation

[1]http://rswww.com

and removal. Starting from the injection line, a total of six transducers were placed in the first half of the mould. In addition, a transducer was also placed at the injection line. To create exact injection conditions for rectilinear flow, a groove was cut in the mould. A C-shaped channel (Figure 3.1), with a centre hole for fluid injection, was placed inside this groove to serve as an injection line. The channel height was set such that the open section of the channel remained in line with the reinforcement. Then, the fluid injected from the centre hole first filled the channel before starting to infuse the reinforcement. This ensured that the fluid was injected through the entire thickness of the reinforcement. In addition, to ensure faster sensing of fluid arrival at any pressure transducer, a liner was placed inside each transducer (Figure 3.1).

After placing the reinforcement on the mould bottom half, it was covered with the mould top half. Starting the vacuum pump evacuated the mould, driving infusing fluid through the injection line.

3.2.2 Radial (2D) Flow Set-up

In the radial flow VI process also, one will need to design the set-up such that more transducers can be accomodated, especially near the injection gate. Figure 3.2 shows the experimental set-up. In this case also, the design of the mould top and bottom halves was identical to the rectilinear case.

By aligning transducers along different radial axes, a total of seven transducers, including one at the injection gate, were accomodated in a radius of 100 mm. In addition, to prevent the vacuum bag from blocking the injection gate by sagging into it, a small, rigid piece of plastic (2 mm thick) was placed between the reinforcement and the plastic bag, directly above the injection gate. A centre hole, of 5 mm radius, was cut into the reinforcement to create uniform plug-flow injection conditions. Then, the fluid injected from the injection gate, first filled this circular hole, before starting to infiltrate the reinforce-

ment. Also, faster sensing of the fluid arrival at any pressure transducer was facilitated by a liner placed inside the transducer (Figure 3.1).

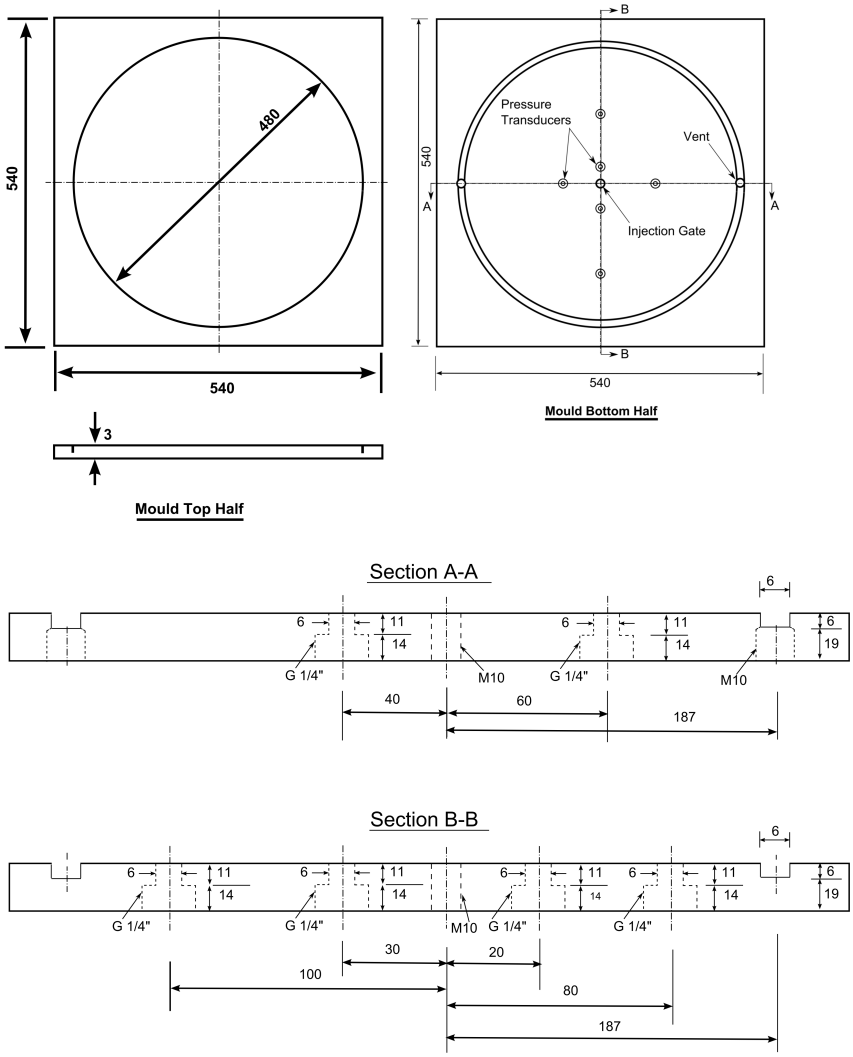

Figure 3.2: Experimental set-up for the radial flow VI process.

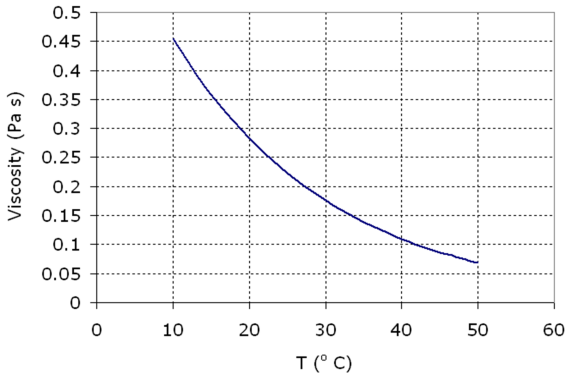

Figure 3.3: Viscosity of the infusing fluid (HDX-30 hydraulic oil) as a function of temperature.

In total, four infusion experiments were performed for both the rectilinear and the radial flow cases. The infusing fluid (hydraulic oil, HDX 30, Trent Oil Ltd., UK) was injected from a bucket, using a 0.5 metre long plastic injection pipe. All infusion experiments were performed in a climate controlled room with a set temperature of 18 ^{0}C. Nonetheless, in all experiments, the temperature of the infusing medium (hydraulic oil) was also measured before the start of the injection and did not show any major variations. Figure 3.3 shows the oil viscosity, measured seperately as a function of temperature, using a Brookfield rheometer (model DV-II). From this, the viscosity of oil was assumed constant at 0.3 Pa s and this was used for comparing the fill-time results.

In both the rectilinear and the radial flow cases, all the transducers were calibrated initially for the full pressure range. Also, a computer connected through a data acquisition box logged the transducer readings at a sampling frequency of 10 Hz.

In addition, the compliance properties measured by Correia (2004) and relisted in Table 2.3 were for Unifilo U750/450 reinforcement. However, this material was not available at the time of experiments. Hence, Unifilo U750/375, which is a similar material but with a lower areal surface density (0.375 Kgm^{-2}), was used in these experiments. The difference in the areal density was compensated

for by using four layers of U750/375 in place of three layers of U750/450. In all experiments, the atmospheric pressure was assumed to be 0 kPa (i.e. 100 kPa-absolute), while the pressure at the injection and the vacuum port was maintained at 5 kPa (i.e. 95 kPa absolute) and 65 kPa (i.e. 35 kPa-absolute) below atmospheric pressure, respectively. Thus, the maximum driving pressure was 60 kPa, while the maximum and minimum compaction pressures on the reinforcement were 65 kPa and 5 kPa, respectively. Note that due to the limited working range of the available pressure transducers, full vacuum pressure could not be used. All the experiments were recorded with a digital camera at a rate of 30 frames per second, from which the fill-time was calculated.

3.3 Results and Discussion

3.3.1 Pressure Profile Results

Figure 3.4 shows typical pressure measurements in the rectilinear and the radial flow VI processes. An important point to note is that, in the rectilinear flow process, realisation of the full injection pressure is not immediate at the start of injection but needs some time. This is because the fluid is being pulled by the applied vacuum rather than being pushed under positive pressure as in the RTM process. Hence, the pressure achieved at the injection gate depends on the resistance faced by the entering fluid. Reinforcement permeability and the type of flow are two main factors affecting this resistance. Correia (2004) also reported similar results and noted that the slow rise in the injection pressure is due to it being a function of the resistance in the piping and the reinforcement permeability. The radial flow experiments conducted in the present work provide further supporting evidence for this conclusion, where high flow resistance leads to an immediate realisation of the full injection pressure.

(a) Rectilinear Flow

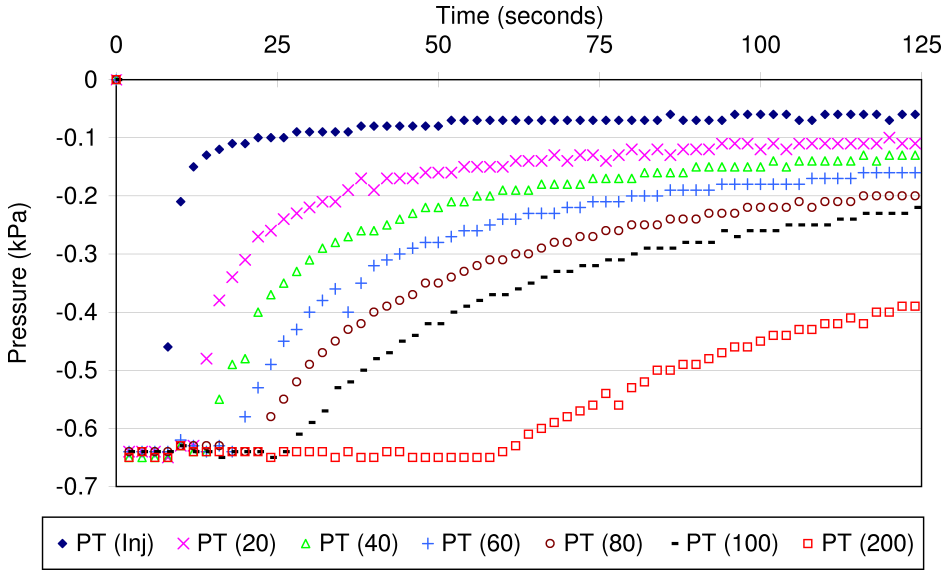

(b) Radial Flow

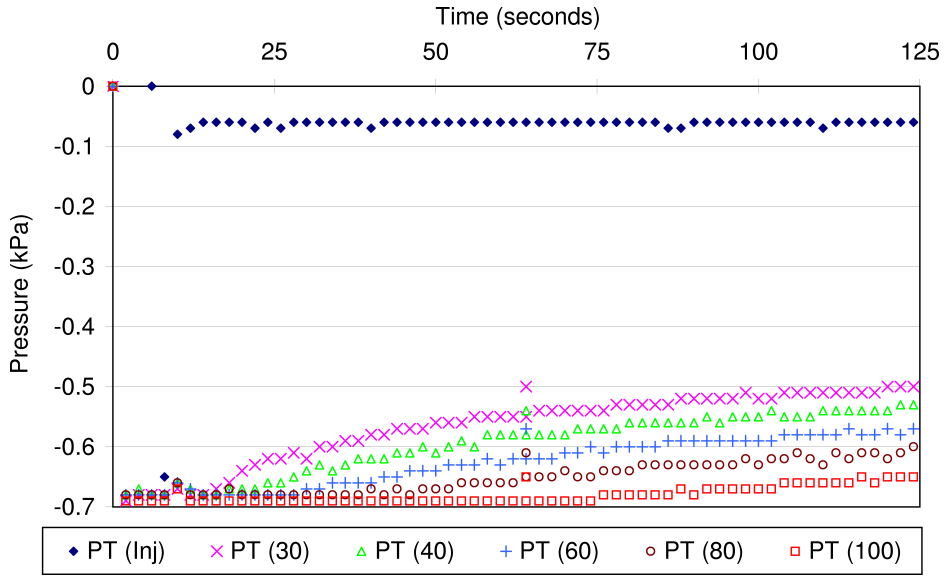

Figure 3.4: Pressure measurements in the rectilinear and the radial flow VI processes (PT = Pressure Transducer).

Figures 3.5 and 3.6 show an average presure profile and its evolution with flow progression in the rectilinear and the radial flow VI processes, along with the scatter in results from four identical experiments. The RTM pressure profiles in these figures were calculated from Equations 3.1 and 3.2, while the analytical

VI pressure profiles were calculated using Equations 2.10 and 2.20.

$$P = P_{inj}\left(1 - \frac{x}{L}\right) \tag{3.1}$$

$$P = P_{inj}\left(\frac{ln\left(\frac{r}{R}\right)}{ln\left(\frac{r_{inj}}{R}\right)}\right) \tag{3.2}$$

In both the flow processes, the initial pressure profile in the filled region is below the RTM analytical pressure profile (Figures 3.5-a & 3.6-a). Furthermore, with flow progression, the pressure profile in the rectilinear flow process levels with the RTM pressure profile (Figures 3.5-b,c) before rising above it to give a non-linear pressure profile (Figure 3.5-d). In radial flow experiments, although the pressure profile has not risen to match with analytical predictions, it does show a similar behaviour. This dynamic behaviour in the pressure profile is contrary to one's expectation. First, the rectilinear and radial flow pressure profiles should be above the RTM pressure profiles. Second, the pressure profile in the rectilinear flow VI process is non-dimensional, and hence, should remain constant with flow progession. On the other hand, in the radial flow RTM process, the pressure profile varies with flow progression and cannot be normalised. However, it should vary in a similar fashion in both RTM and VI.

(a) Infused Length = 60 mm

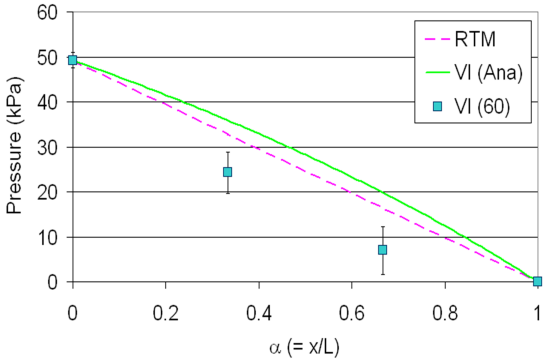

(b) Infused Length = 100 mm

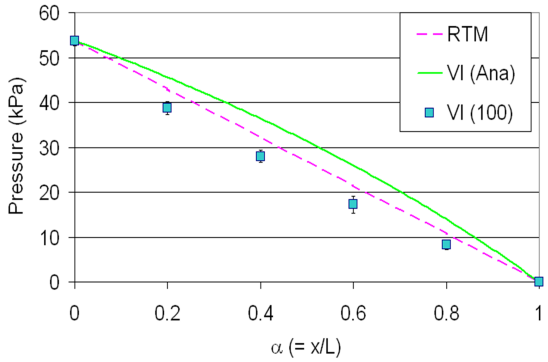

(c) Infused Length = 200 mm

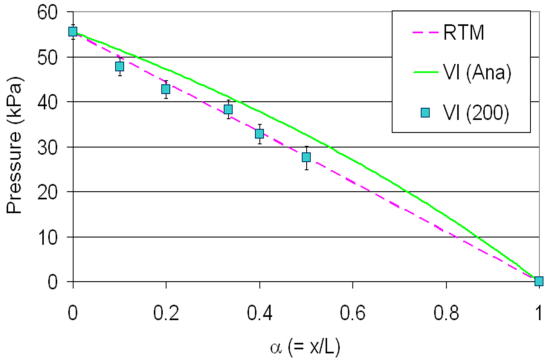

(d) Infused Length = 300 mm

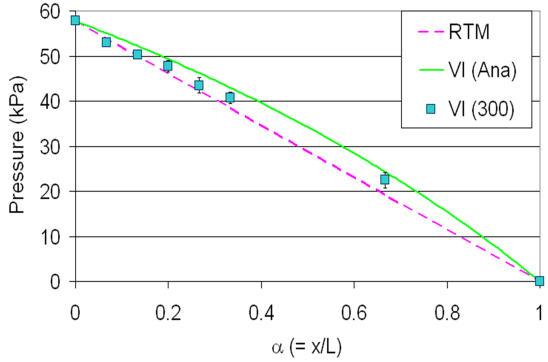

Figure 3.5: Pressure profile evolution with flow progression in one of the rectilinear flow VI experiments.

(a) Infused Radius = 80 mm

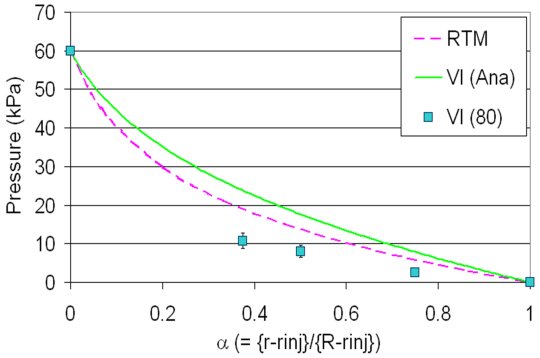

(b) Infused Radius = 100 mm

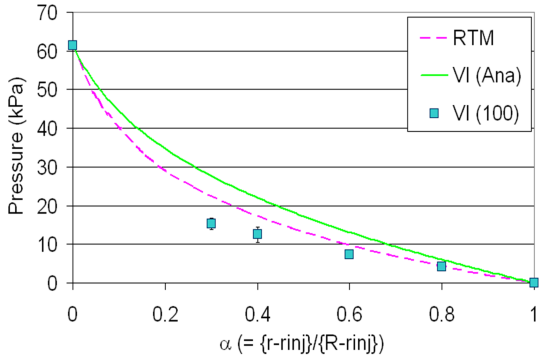

(c) Infused Radius = 160 mm

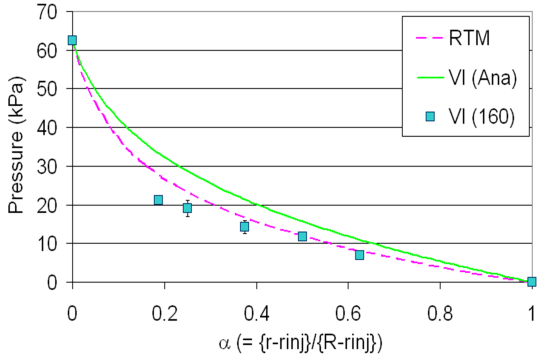

Figure 3.6: Pressure profile evolution with flow progression in one of the radial flow VI experiments.

Correia (2004) suggested that because of the varying injection pressure, one should only measure the pressure distribution in the mould, once the injection pressure has achieved its full value. However, the analytical solution suggests that irrespective of the injection pressure, the pressure profile should be above the RTM pressure profile. This should at least be the case for the radial flow experiments, where the full injection pressure is realised immediately at the start of the injection. Hence, it can be concluded that the observed pressure profile variation is a consequence of the process physics.

As the analytical formulations were derived using fundamental laws (i.e. conservation of mass law and Darcy's law) without any limiting assumptions and the experimental results from both the flow experiments show a rising behaviour that leads to converging pressure profiles towards the analytical solutions, one can justly assume the validity of both of them. Then, as the analytical pressure formulations did not show any transient terms, the variation in the pressure profile can only be explained through the reinforcement compliance behaviour. Considering the actual events in the compliance characterisation experiments, first a pre-wetted reinforcement is compacted to the required compaction level between two solid tool surfaces. During this phase, extra fluid in the intra-tow and inter-tow spaces is forced out. Then, during the expansion or unloading phase, the tools are moved apart mechanically to remove the compaction pressure. However, no fluid is available at this stage to fill the empty spaces created due to the reinforcement expansion. Hence, it can concluded that during the expansion phase, a significant proportion of the load is supported by the reinforcement (Figure 3.7-a).

In the actual VI process, the flexible bag is supported at the fibre/tow contact points, while it sags (i.e. is pulled or deformed) into in the inter-tow spaces. The reinforcement compaction is also due to this sagging and the related tension in the plastic bag (Figure 3.7-b). After fibre wetting and compaction due to the arrival of fluid, the rising fluid pressure acts against the atmospheric

compaction pressure. In addition, it also reduces the bag sagging, leading to a further reduction in the reinforcement compaction. It is clear that at least some, if not all, of the compaction pressure is supported by the infiltrating fluid. In addition, the stresses in the plastic bag may be important. This difference in events may lead to a different compliance behaviour, possibly resulting in a different empirical model that will lead to a rising pressure profile in both the flow cases. However, it is clear that to verify this hypothesis, a new set of compliance characterisation experiments needs to be done, which is discussed in the future work section of the last chapter.

(a) Events in the Reinforcement Compliance Experiment

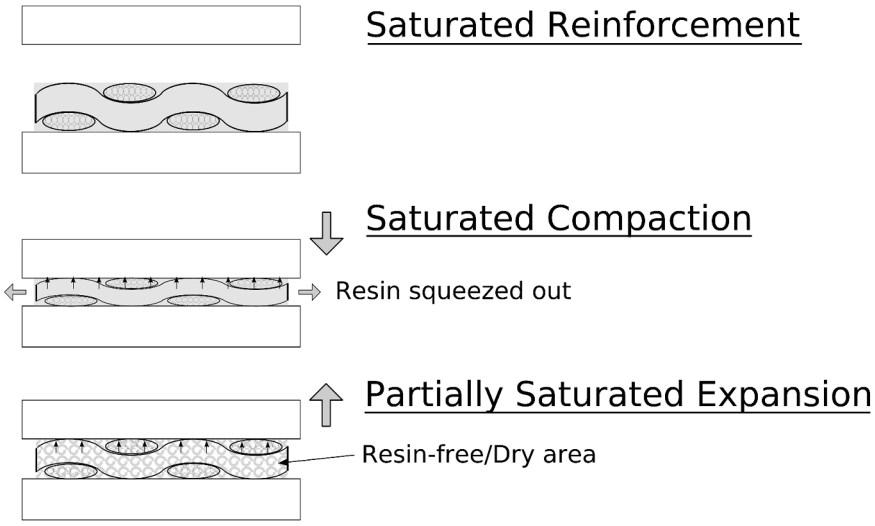

(b) Events in the Actual VI Process

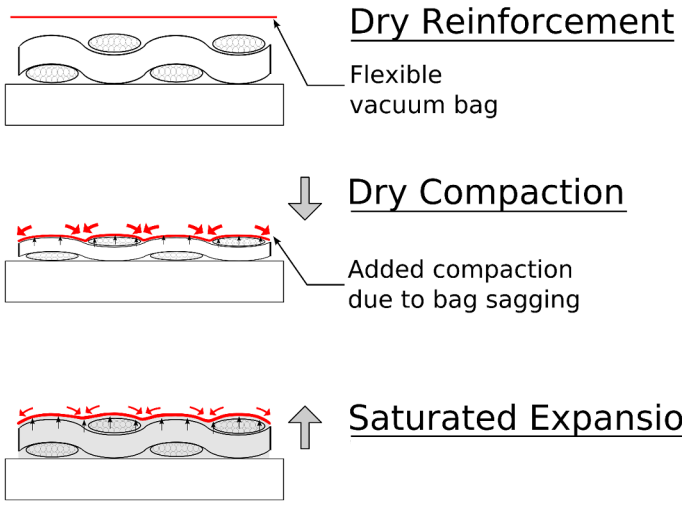

Figure 3.7: Comparison of events in the reinforcement compliance experiment and the actual VI process.

3.3.2 Fill-time Results

Figure 3.8-a shows an average flow-front progression with time in the rectilinear flow VI process, along with the scatter in results from four identical experiments. The RTM fill-time was calculated using Equations 2.30 and 2.36 using the values of various parameters listed in Table 3.1. The value of porosity was calculated using dry compaction parameters listed in Table 2.3 with the compaction pressure of 65 kPa, while the value of permeability was taken from Rudd et al. (1997). It is clear that the fill-time does not increase directly in proportion to the square of the infused length. As a direct consequence of the pressure profile evolution, one can see that when the pressure profile is lower in VI than in RTM, correspondingly the fill-time is higher in VI than in RTM. As the pressure profile rises towards the RTM profile, the fill-time becomes equal to the RTM fill-time. A further rise in the VI pressure profile reduces the fill-time to below the RTM case as expected.

Table 3.1: Parameter values used to calculate the analytical fill-time for RTM process. The value of porosity was calculated using dry compaction parameters listed in Table 2.3 with the compaction pressure of 65 kPa, while the value of permeability was taken from Rudd et al. (1997).

$\mu\,(Pa\,s)$	ϕ	$K\,(m^2)$	$\Delta P\,(Pa)$
0.3	0.815	10^{-09}	60000

(a) Rectilinear Flow

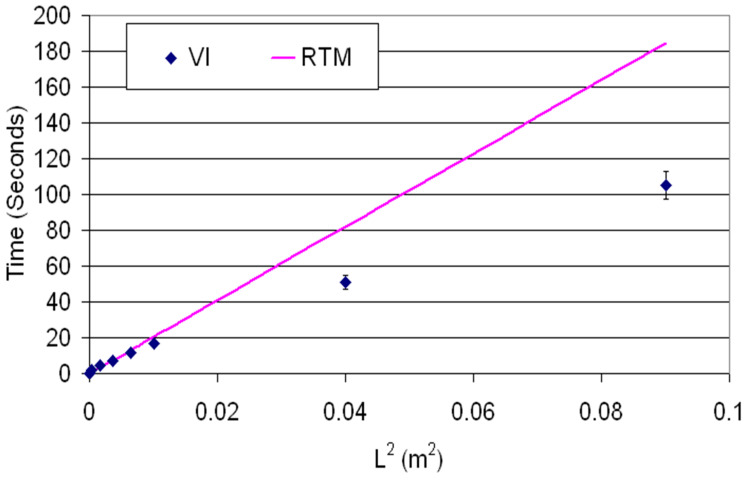

(b) Radial Flow

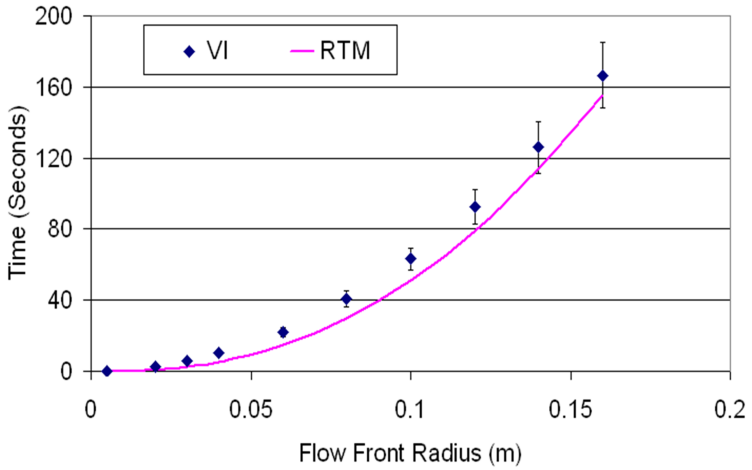

Figure 3.8: Flow progression with time in (a) a rectilinear flow, and (b) a Radial Flow VI mould.

Figure 3.8-b shows an average flow-front progression with time as well as the scatter in the results from radial flow VI experiments. In this case also, the lower than RTM pressure profile leads to longer fill-time in the VI process. It can be reasonably expected that once the VI pressure profile rises above the RTM profile, it will lead to a reduced fill-time in VI than RTM.

From Figure 3.8, one might suspect that the VI fill-times follow the RTM fill-times trend more closely in 2D than in the 1D flow case. However, this sus-

picion is not valid and can be explained by observing that the pressure profile in the radial flow case has not even levelled with the RTM profile (Figure 3.6). Fill-time results in 1D case for similar conditions, i.e. near the origin in Figure 3.8-a when the VI pressure profile is below the RTM profile, also show good agreement with the RTM fill-times trend. Also note that the match between the RTM and VI fill-times depend on the assumed value of the reinforcement permeability in Table 3.1.

In addition, one can also plot the ratio of the RTM fill-time and the experimental VI fill-time as a function of flow progression. Figure 3.9 plots this fill-time ratio for both the rectilinear (1D) and radial (2D) flow processes, where its variation can be clearly seen. This is in contrast to the observation in Chapter 2 (Table 2.5) that, in both types of flow processes, the RTM and VI fill-time ratio remains constant. Also, it is clear that as the pressure profile in 1D converges towards the analytical prediction, the fill-time ratio also converges, although to a different value from the prediction in Table 2.5. Again, this depends on the assumed value of the reinforcement permeability in Table 3.1.

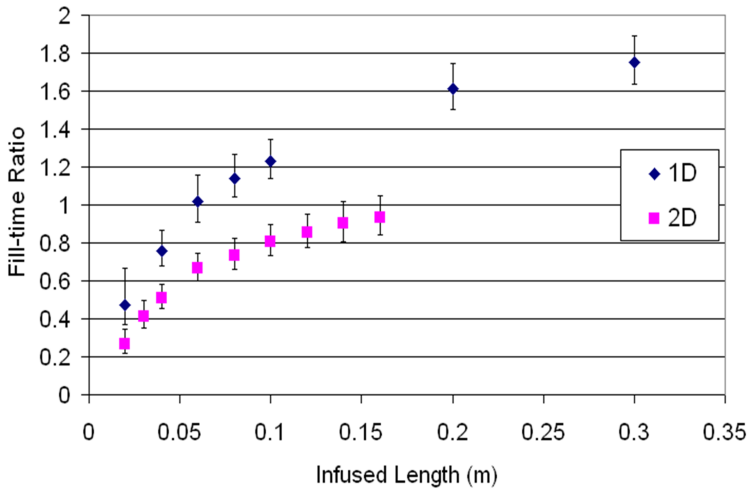

Figure 3.9: RTM vs. VI fill-time ratios calculated as a function of flow progression in the rectilinear and the radial flow processes.

For a rectilinear flow VI process, Correia (2004) reported a similar trend and

attributed it to the variation in the injection pressure. However, as can be seen from radial flow experiments, the variation in the pressure profile rather than variation in the injection pressure is responsible for this behaviour.

3.4 Conclusions

The lack of published experimental validation of pressure and fill-time formulations in the rectilinear and the radial flow VI processes is highlighted. In particular, no detailed studies for an unsaturated flow progression have been published. Two new mould set-ups were developed for measuring pressure profiles, their evolution with flow progression and fill-times in an unsaturated flow rectilinear and radial flow VI processes. The expected pressure profiles were of a non-linear nature. Hence, to increase the accuracy of the measured pressure profiles, the arrangement of pressure transducers was modified such that at least five could be incorporated in the first 100 mm of the infused length. This also facilitated, for the first time, measurement of the pressure profile evolution with flow progression.

The results from the rectilinear flow VI process showed that in an unsaturated flow process, the full injection pressure is not realised immediately. Also, the pressure profile is initially lower than the RTM pressure profile. With flow progression, it rises to level with and ultimately exceed the RTM pressure profile. A similar trend is also observed in the radial flow VI process, although here full injection pressure is realised at the start of the injection. This is in contrast to analytical formulations, which suggest that the fluid pressure profile should remain constant or move in a similar direction as the corresponding RTM profile. Hence, it is concluded that this variation in the pressure profile is an integral part of the process physics. It was hypothesised that the time-dependent pressure profile evolution is due to the difference in events in the reinforcement compliance characterisation and actual VI experiments and thus, the current

empirical model for the reinforcement compliance may not be appropriate for VI. However, this hypothesis cannot be verified at present due to the lack of accurate saturated expansion data and this should be investigated in future.

In addition, fill-time results from the rectilinear flow VI process showed that fill-time is not proportional to the square of the infused length. A similar observation in the radial flow VI process showed that fill-time in VI is higher than for the RTM process. This variation, in direct relation to the pressure profile evolution, invalidated the previous understanding of Correia (2004) that this was entirely due to the evolution of the injection pressure.

It is clear that the fundamental investigation of the VI process can be very involved. Also, the knowledge gained does not ensure one of complete success as the process can be influenced by factors such as reinforcement and process heterogeneity. In such cases, other alternatives that help in improving the process reliability and repeatability need to be explored. One such approach, using active flow control, is developed in the next chapter.

Chapter 4

Active Control of the Vacuum Infusion Process

4.1 Introduction

As discussed in previous chapters, in the majority of flow scenarios in liquid composite moulding processes, moving boundaries of the flow domain make analytical treatment almost impossible and numerical treatment is necessary. For this, permeability and fibre volume fraction are two very important reinforcement properties. However, the dynamic nature of the process makes evaluation of these properties in VI extremely difficult. In addition, there is an inherenet heterogenity involved in the VI process, mainly due to operator dependency, reinforcement heterogeneity, non-uniform bag folding etc. This leads to low process repeatability and reliability, despite being aided by process simulation tools.

Possible methods of improving the process reliability include resin bleeding and off-line controls. In the resin bleeding approach, resin injection is continued after the flow has reached the vent. This increases the chances of infusing any remaining dry patches in the mould. However, most of the resin thus injected flows out of the vent creating significant waste, which could be avoided with

improved design and control strategies. In addition, resin gelation can start before complete infusion, leading to higher rejection rates or increased salvage costs.

In off-line or passive control systems, a database of possible flow scenarios is generated from numerical flow simulations. Input parameters in the numerical models are defined from a set of pre-defined possible perturbations in either material properties or boundary conditions. Simulation results are then analyzed to arrive at an optimum mould design with suitably placed injection gates and vents to achieve the maximum probability of success for the infusion process. Chan and Morgan (1992), Mychajluk and Mahoochehri (1994), Boccard et al. (1995), Lin et al. (2000), Gokce et al. (2002; 2004), have previously reported efforts in this direction.

However, passive control systems offer limited improvements in infusion efficiency, quality as well as process reliability due to limitations in modelling and replication of various aspects of the process such as edge effects, wrinkling of the vacuum bag, and local reinforcement heterogeneities. In addition, exact evaluation and assignment of various material properties may be difficult in many cases. This has led researchers to develop advanced on-line or active control systems.

4.2 Background

4.2.1 Active Control

In on-line or active control systems, a set of sensors are used to collect information about the infusion state. These systems can be divided into two categories, depending on whether the simulations to be used in arriving at a suitable corrective action are performed prior to the start of infusion or in real-time i.e. during the infusion. One of the main challenges of real-time

simulations is that the simulation must be fast and run times singnificantly lower than the mould fill time. Hence, in many on-line control systems, proxy simulators such as neural networks are used to predict flow progression. It is important to note that on-line control systems, with original or proxy simulators, also suffer from similar modelling related limitations as off-line control systems. However, active and continuous input from the process facilitates continuous feedback and improved process modelling. Irrespective of the simulation approach, an appropriate corrective action is implemented through computer-controlled injection gates and vents.

Early studies of on-line control aimed at managing pressure and flow rate conditions (Mogavero et al., 1997). To control flow progression in RTM, Lee et al. (1998) used a system to regulate either the resin viscosity through modulation of the mould temperature or the flow rate at various injection gates. Flow progression was sensed using a DC resistance sensor grid. The system was validated for rectilinear flow patterns with artificially created local heterogeneities in the reinforcement permeability and fibre volume fraction. The authors reported significant qualitative improvements in the flow progression in controlled experiments. However, no parameters were used to quantify these improvements. Although an innovative approach, control of flow progression through alteration of resin viscosity is challenging as it requires detailed and accurate characterisation of resin cure behaviour.

Bickerton et al. (2001) reported an RTM flow monitoring and control system. Flow simulations were performed in advance for a number of predefined scenarios. Then, from the information provided by flow sensors, a specific disturbance pattern was identified and appropriate corrective action was taken. To validate the control system, a complex shaped part, with artificially generated edge effects or race-tracking disturbances, was designed. This part was filled from multiple injection gates under constant flow-rate injection conditions. The control system met the primary objective of avoiding major voids.

However, the comparison between uncontrolled and controlled experiments is not valid as one additional vent was used in the actively controlled experiments.

Nielsen and Pitchumani (2001) used a neural network to control a constant flow rate RTM process. The neural network was initially designed and trained from numerical simulations for a set of pre-defined process parameter values. In the experimental implementation, digital cameras were used to capture images of flow progression at fixed intervals, which were then analyzed and fed to the neural network. Based on these inputs, the neural network calculated flow advancement results. The parameter optimisation was performed using a simulated annealing (SA) approach- a stochastic optimisation method fast enough to match mould filling times as well as being able to perform a global search for an optimum solution. For control of a constant injection pressure RTM process, Nielsen and Pitchumani (2002a) used the same system with a fuzzy-logic based on-line permeability estimator. Reinforcement permeability was estimated from the measurements of the actual flow front position and injection pressure. The main limitation of both of the above-mentioned control systems is that they employ a proxy simulator, in this case neural network, to predict the flow advancement. It is widely acknowledged that the accuracy of results from such a network is influenced by the training parameters. For a constant flow rate RTM process, Nielsen and Pitchumani (2002b) also reported an active control approach employing real-time flow simulations. In all of their work, the control systems were validated through infusion experiments of a rectangular mould, with inhomogeneous reinforcement lay-ups. The efficacy of the system was demonstrated qualitatively and no quantitative comparisons were reported.

Lawrence et al. (2002) used a genetic algorithm based optimisation approach in an active control system for RTM. In the design stage, various flow disturbances were identified and simulations were carried out to investigate the resulting flow patterns. From this information, optimum sensor locations were

identified. The system was demonstrated in a mould with various geometric features such as rib structures and tapered regions. These features allowed preferential flow and thus created flow disturbances. During infusion, the information collected by point sensors was fed to the optimisation algorithm. Parts made using the actively controlled injection system showed complete infusion. Note that, similar to many other control systems reported here, the mould was infused under constant flow rate injection conditions. Employing these systems for flow control in constant flow rate or constant pressure injection VI is problematic. First, the limited driving pressure range in VI and the resulting low flow rates puts severe restrictions on the design of the flow control system. Also, as reported by Berker et al. (Berker et al., 1998), the effectiveness of flow control system remains constant, with flow progression, for the constant flow rate injection conditions, but decreases for the constant pressure injection conditions i.e. the effectiveness of all of the above-mentioned systems will be different, possibly lower, for constant pressure injection conditions.

It is clear that proper design and implementation of an on-line control system can give higher probability of success for the infusion process. However, such systems are difficult to design and implement, and their success depends on the underlying sensor system i.e. for an efficient and effective control system, a fast, accurate, reliable, low-cost and minimally intrusive sensor with an ability to interface with control hardware is desirable.

4.2.2 Flow Sensing Technology

In the past, pressure transducers (Lai et al., 1997; Lynch et al., 1999; Bickerton et al., 2000; Amico and Lekakau, 2001), SMARTWeave conductive sensors (Walsh, 1993; Vaidya et al., 2000; Mathur et al., 2001; Green et al., 2003), dielectric (Skordos et al., 2000), TDR (Dominauskas et al., 2003), photo (Kang et al., 2000), fibre optic (Ahn et al., 1995; Bernstein and Wagner, 1997; Kueh et al., 2000, 2002) sensors and digital cameras (Mathur et al., 2001; Grimsley

et al., 2001; Nielsen and Pitchumani, 2001, 2002a,b; Nedanov and Advani, 2002; Sayre and Loos, 2003) have been employed in LCM processing, mainly for flow monitoring and reinforcement permeability characterisation purposes. Table 4.1 lists the specific advantages and disadvantages of these sensor systems. Most have features that make them unsuitable for use in a generic VI mould e.g. most of these sensors are of point contact type; they provide flow information at a particular point in the mould. Hence, a generic VI mould with a large surface area will require a large number of sensors to continually and effectively monitor flow progression. This can increase the intrusiveness of the sensing system, to a point where the infusion process is disturbed to an unacceptable level. Mounting of these sensors may also require the mould to be machined, which will reduce the flexibility in selecting and/or modifying sensor locations and will also increase the overall cost. In addition, it is possible that additional inacuracies e.g. in the reconstruction of the flow front from point sensor data (Lawrence et al., 2005), are introduced. It is desirable to avoid as many of these artefacts as possible.

Table 4.1: Advantages and disadvantages of various sensors used by previous researchers for flow monitoring in LCM processing.

Sensor	Advantages	Disadvantages
Pressure	high signal-to-noise ratio (SNR), ease of real-time interfacing, low user intervention	localised sensing, increased intrusiveness, requires the mould to be machined
SMARTWeave	(N+M) channels for (NxM) sensors, possible cure monitoring	low reliability due to possible shifting of sensor during reinforcement lay-up, low SNR due to electromagnetic interference, cumbersome configuration (no connections should touch each other)
Dielectric	small size	localised sensing, increased intrusiveness
TDR (Time-Domain Reflectometry)	good accuracy, high repeatability, possible monitoring of multiple flow fronts	possible shifting of sensor during reinforcement lay-up or infusion

(contd..)

Table 4.1 (contd..)

Sensor	Advantages	Disadvantages
Photo	small size, high SNR, ease of mounting, ease of interfacing with other hardware	localised sensing, increased intrusiveness
Fibre optic	miniature size, low intrusiveness, compatible with glass fibre, minimum impact on structural properties	high minimum bending radius, high cost of hardware, high labour cost
Digital Camera	non-intrusive, ease of implementation, ease of real-time interfacing, possible flow sensing over large area	requires at least one half of the mould to be transparent, difficulty in monitoring flow beneath the top surface of mould

4.2.3 Outline

The active control systems reported in the literature suffer from various limitations. As discussed previously, many of the systems involve resin injection under constant flow rate conditions. In addition, many of them employ proxy simulators and were designed for the RTM process. In the absence of any quantitative data, it may be difficult to evaluate their performance and applicability for the VI process. The work reported here is focused in this direction.

The objective of this work is to develop and demonstrate a fully automated control system for closed moulding processes, where the flow progression is visible from one (top) surface. Its initial concept was first reported by Correia (2004). This control system should monitor flow progression, identify any deviations from the expected or ideal flow patterns, and take appropriate corrective actions. A deviation is any flow disturbance due to unforeseen or unpredictable reasons, such as operator-dependency, reinforcement heterogeneities, race-tracking due to the vacuum bag folding etc. It is an enhancement, rather than an alternative, to other optimisation approaches such as off-line control and is meant to enable one to control the infusion process to achieve the required part quality and reduce part rejection rates.

This new system employs a novel approach for continuous flow monitoring. A digital camera, which allows one to meet key requirements of minimum intrusiveness, low probability for introducing any artefacts, ease of interfacing and low-cost, is used in this approach. Unlike previous efforts, the collected information is processed and used in real-time for active process control. The accuracy of a proxy simulator depends on its design parameters, whereas the present system uses an original flow simulator, based on a proper mathematical formulation.

The remainder of the chapter is organized in five sections. In the next section, the development of the proposed control scheme is described. It is important

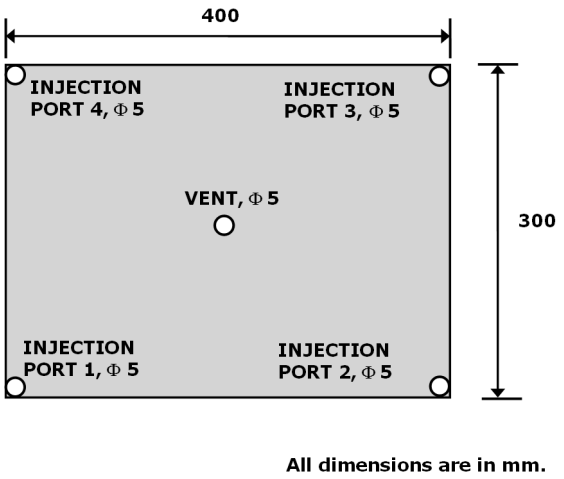

Figure 4.1: Schematic of the demonstration mould set-up.

to note that some of the steps in this scheme are peculiar to the case-study (Figure 4.1) presented here and will need to be redesigned for other cases, while others are more general. In this case-study, the mould had four injection ports located in the four corners, while the vent was located in the centre (Figure 4.1) i.e. the mould had a geometric symmetry about centrelines in the length and width directions, resulting in four equal quarters. In Section 4.4, the system is first validated through virtual (simulation based) mould filling experiments. Results from actual uncontrolled and controlled infusion experiments are presented next, where variability in the flow patterns as well as the efficiency of the proposed system is highlighted. In Section 4.5, possible extensions of the control system for variants of the VI process such as SCRIMP, are discussed. Finally, some conclusions are drawn regarding the advantages and the limitations of the system.

4.3 On-line Flow Control with Image Analysis: Approach

The on-line control system developed in this work utilizes an image acquisition and analysis system to monitor flow progression inside a closed mould with at least one transparent side. This information is used to define initial conditions for mould filling simulations. With a pre-defined set of port configurations (injection schemes or boundary conditions) and the initial conditions, mould filling simulations are performed to predict flow advancement over the next time period. Then, the optimisation algorithm uses a pre-defined cost function to select an optimum injection scheme i.e. from the simulation results, a value of a cost function for each port configuration is calculated and the configuration with the lowest value is relayed to computer controlled injection valves to correct the flow deviations. The strategy is repeated during the entire infusion phase. Figure 4.2 shows a flow chart for all the steps involved in the system, while Appendix 4.A lists the MATLAB implementation code for the same. Next, the development of each individual step is described.

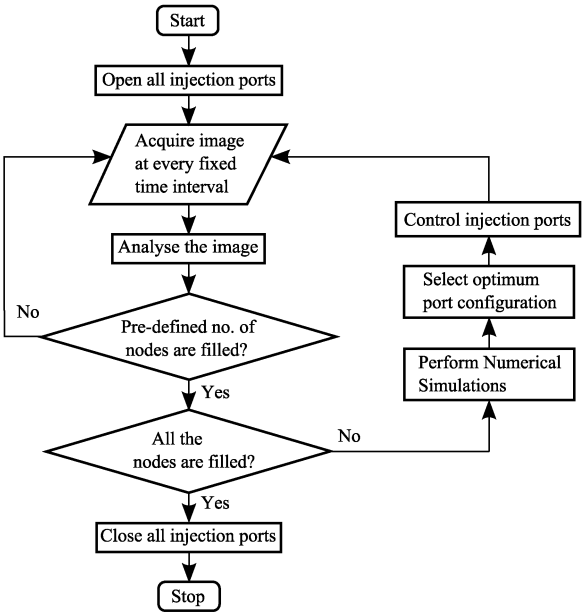

Figure 4.2: Flow-chart of the proposed control system.

4.3.1 Image Acquisition

To reduce the overall cost of the system and for ease of real-time interfacing, it was decided to use a web camera for image acquisition. Almost all cameras available on the market have programmable image acquisition capabilities. For this specific work, a Fire-i^{TM} camera and software (version 2.5) from Unibrain[1] was used to capture images of the infusion phase from the top side of the mould. All images had 640x480 pixels resolution and were captured at fixed time intervals (one second).

[1] www.unibrain.com

4.3.2 Image Analysis

The analysis of the captured images is performed in MATLAB[2] using the native image analysis toolbox. The captured images are processed to select a region of interest. In addition, as the camera and the mould planes may not be parallel to each other, the images are processed to remove perspective (Russ, 2002). Then, they are passed through an averaging and a high-pass filter to convert them into binary images (Appendix 4.A). As the relative position of the camera with respect to the mould can vary between experiments, the entire image acquisition and analysis system is calibrated before the start of the infusion process. This is done by setting up the mould for an experiment and calling the image acquisition and analysis program to select the region of interest. Once a satisfactory region is selected, all the relevant data is saved in a data file, which is then used during the actual infusion phase.

4.3.3 Numerical Simulations

As discussed in the second chapter, for 1D and 2D flow, in theory the ratio of pressure gradients at the flow front remains constant in RTM and VI, which leads to constant fill-times ratios. In chapter 3, the experimental results showed that the pressure profiles vary dynamically in 1D and 2D flow VI. Hence, the RTM vs. VI fill-time ratios also vary with flow progression. However, irrespective of the injection pressure, pressure profile or fill-times, the flow patterns remain straight and circular in 1D and 2D RTM and VI processes. This is because the flow patterns depend on the temporal distribution of the permeability field. If one assumes a similar spatial variability in the permeability field in RTM and VI then, the flow patterns in RTM and VI are identical in space and differ only in time, i.e. the thickness induced permeability and porosity changes can be neglected for flow pattern predictions.

[2] www.mathworks.co.uk

Then, the results from simulation tools modelling the infusion inside a rigid mould can be used to predict flow patterns for a flexible mould. Hence, the flow advancement simulations in this work were carried out using LIMS.

Before starting the infusion, a set of sixteen simulation models of the mould, corresponding to the 16 individual permutations of the possible port configurations for the four injection ports, is generated. Each port can be either open or closed. Then, appropriate material properties (i.e. porosity and permeability) are supplied to these models. In addition, the entire mould filling phase is divided into a number of equal control-steps such that in each step, a pre-defined number of nodes are required to be filled (a filled node lies in the infused region). It is important to distinguish between a time-step and a control-step; a time-step is inherent to the FE/CV method for advancing the flow (Sec 1.4.2) , while a control-step is a collection of time-steps and is only relevant for the control system.

In the first control-step, all the injection ports are opened. For subsequent control-steps, the current flow front status in the experiment is used to describe the initial conditions (or nodal fill-factors) for all numerical models. This is done by setting the fill-factor of each node in the filled region equal to one, whilst those outside are assigned a fill-factor of zero (Figure 4.3). Numerical simulations are performed to advance the flow in all models individually until the end of the current control-step. Note that performing flow simulations to the end of infusion will increase the simulation time, which could affect the performance of the control system. At the end of the last control-step, all the injection ports are closed.

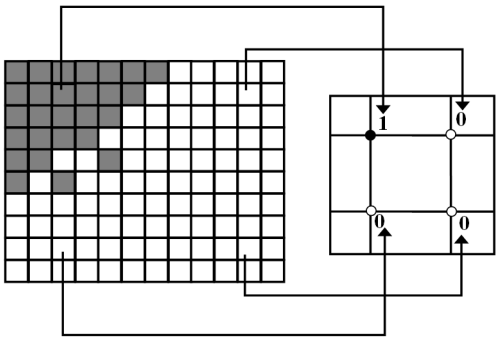

Figure 4.3: Definition of nodal fill-factors in the simulation model from the captured and analysed binary image.

4.3.4 Control Algorithm Design

To select an appropriate corrective action from the available choices, the design of a port configuration selection strategy is necessary. This involves defining a cost function as well as its preferred optimum value (maximum or minimum). Various cost functions such as fill-time, ratio of resin wasted via bleeding to the porous volume of the mould, distance between the centroid of an unfilled region and the vent (henceforth, denoted as the centroid scheme) etc. were considered. The centroid scheme, with minimum as the optimum value, was chosen as it indirectly reflects other cost functions i.e. if the distance between the centroid of an unfilled region and the vent is minimum at any time, the filling pattern will resemble an ideal filling pattern and the mould will be filled in the shortest possible time, with minimum amount of bleeding required through the vent.

Figure 4.4 shows a schematic of the centroid scheme. Using the simulation results, the centroid of an unfilled region, and hence the value of the cost function (the distance between the centroid and the vent), is calculated for all port configurations. The configuration with the lowest value of the cost function is selected as an optimum injection strategy for the next step.

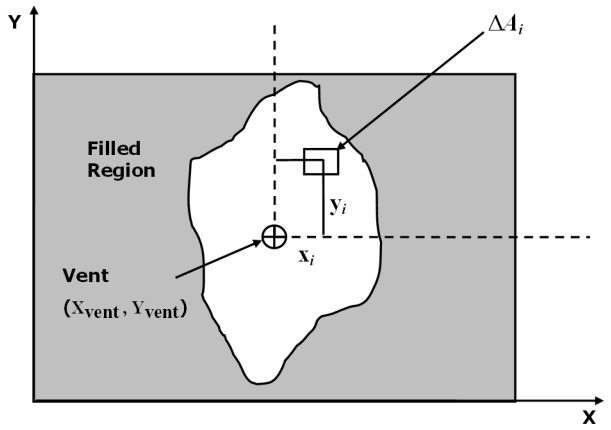

$$\overline{X} = \frac{\Sigma x_i \Delta A_i}{\Sigma \Delta A_i};\ \overline{Y} = \frac{\Sigma y_i \Delta A_i}{\Sigma \Delta A_i};\ D = \sqrt{\left(\overline{X} - X_{vent}\right)^2 + \left(\overline{Y} - Y_{vent}\right)^2}$$

Figure 4.4: Calculation of distance between the centroid of an unfilled region and the vent. The port configuration with the minimum value of this distance is selected for the next infusion phase.

For example, assume that the same mould as shown in Figure 4.1 has to be filled in five control-steps and that the meshed model has 1000 nodes. Figure 4.5-a shows the infusion status in the meshed model at the end of the second control-step, when 400 nodes are filled. For simplicity, also assume that there are only two possible port configurations. In the first configuration, the first three injection ports are open, while in the second configuration, only the first injection port is open. Following the strategy outlined above, flow simulations are carried out for both port configurations to advance the flow until the end of the third control-step, when 600 nodes are filled. Figure 4.5-b & c show the simulation results of the flow advancement. It is clear that for the first configuration (Figure 4.5-b), the centroid of the unfilled region is closer to the vent than for the second configuration (Figure 4.5-c). Hence, the first port configuration is chosen as the optimum injection strategy for the next control-step.

(a)

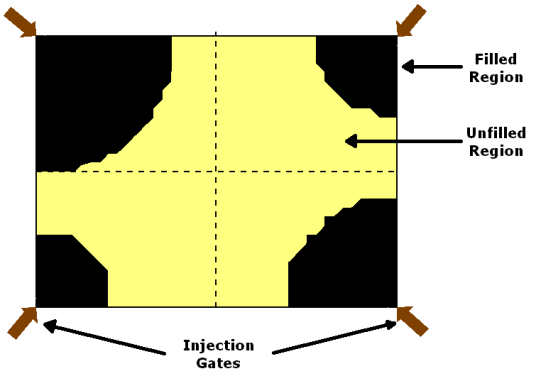

(b)

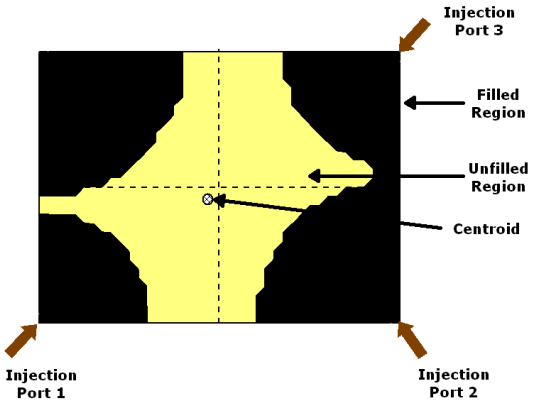

(c)

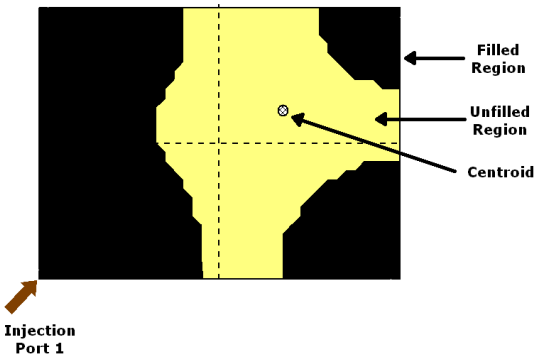

Figure 4.5: (a) Flow front positions inside the mould at the end of the second control phase. The mould has to be filled in five control-steps. (b, c) Simulation results of flow advancement for the third control-step. In (b), resin is injected from ports # 1, 2, 3 while in (c), it is injected from port # 1. The centroid of the unfilled region is closer to vent for the first port configuration (b) than for the second port configuration (c).

4.3.5 Control Implementation

The optimum port configuration as selected by the control algorithm is relayed to solenoid valves, which actually control the resin injection and hence the infusion process. In this work, each injection port was connected to a solenoid valve (Type 6213, Burkert Contromatic[3]) having a response time of 700 milliseconds. These valves were controlled by a computer through a digital input/output board (DAQCard DIO- 24) and control modules (SSR series) from National Instruments[4].

4.4 Validation

The validity of the proposed algorithm was investigated using a rectangular mould (Figure 4.1) infused using a VI process. Three different infusion cases, stemming from three different lay-ups (Table 4.2), were investigated. The first lay-up consisted of six layers of continuous fibre random mat (CFRM, Unifilo U750 / 450), while two layers of plain weave (RT 600) were used in the second lay-up. In the third lay-up, three rectangular layers of bi-axial reinforcement (-/+ 45, FGE 106, Formax UK), of quarter the mould size, were placed between two layers of CFRM (Unifilo U750/450) (Figure 4.6).

The reinforcement layers were infused with hydraulic oil (HDX 30, Trent Oil Ltd., UK) (Figure 3.3) with a viscosity of 0.3 Pa s (at 18 ^{0}C temp), while the vacuum pressure inside the mould was 90 KPa. In uncontrolled experiments, all the injection ports were simultaneously opened at the beginning of the infusion and closed at the end of infusion. For controlled experiments, the injection ports were computer controlled and the infusion was completed in eleven control-steps.

[3]www.bci.burkert.com
[4]www.ni.com

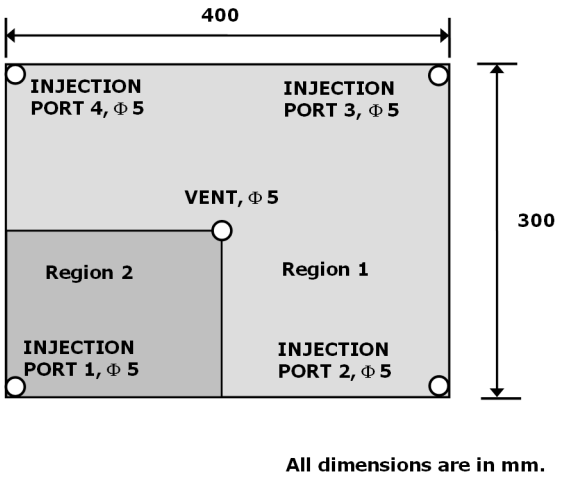

Figure 4.6: Schematic of the demonstration mould set-up for the third lay-up. Region 1 is packed with two layers of CFRM, while region 2 is packed with three layers of bi-axial reinforcement placed between two layers of CFRM.

To compare flow progression in various experiments, all experiments were recorded with a camera. In addition, in any single experiment, flow progression was also compared between different quarters (or injection ports). In all, the experimental programme included four uncontrolled and controlled experiments (for plain weave, only three controlled experiments were performed) for all three lay-ups. For quantitative comparison, three parameters were identified and monitored for each experiment. They were: (1) the distance between the vent and the centroid of an unfilled region, when resin reached the vent, (2) the unfilled area (as fraction of the mould area), when resin reached the vent, and (3) the amount of resin bled through the vent, as a fraction of the mould porous volume (calculated from the amount of resin injected inside the mould and the amount of resin bled through the vent), for complete infusion of the mould.

Table 4.2: Reinforcement lay-ups and their material properties for the cases investigated. The permeability value for region 2 of the third lay-up is calculated from the individual reinforcement permeabilities following a volume-averaged approach. Reinforcement fibre volume fraction (calculated using compaction data at 90 kPa pressure) and permeability values were also obtained from Rudd et al. (1997).

Lay-up	Material	Manufacturer	Surface Density	No of Layers	Permeability (m^2)	Fibre Volume Fraction	Thickness (m)
I	CFRM, Unifilo U750	Saint-Gobain Vetrotex	450 GSM	6	1.0 x 10^{-08}	0.18	0.0045
II	Plain Weave, RT600	Saint-Gobain Vetrotex	600 GSM	2	1.0 x 10^{-10}	0.5	0.001
III	CFRM, Unifilo U750 +	Saint-Gobain Vetrotex	450 GSM	2	1.0 x 10^{-08}	0.18	0.0015
	(-/+) 45, FGE 106	Formax	950 GSM	3	2.74 x 10^{-09}	0.412	0.004

In addition, for preparing simulation models, one needs to select values for various simulation parameters such as mesh size, reinforcement permeability values etc. Differing mesh requirements and parameters for different moulds make it difficult to suggest or use any general guidelines for selecting appropriate values of these simulation parameters. Then, one has to select optimum values, while meeting other constraints such as infusion time, level of control required etc.

The assignment of reinforcement permeability requires caution. The first two lay-ups contain only one reinforcement. Even though fibrous reinforcements are in general heterogeneous, it is difficult to measure and replicate the actual permeability distribution. Therefore, it is necessary to assume isotropic homogeneous permeability for both of these reinforcements. Accordingly, the elements in the corresponding simulation models were assigned isotropic homogeneous permeability values (Table 4.2) (Rudd et al., 1996). On the other hand, the third lay-up contains different reinforcement regions. Again, it is not possible to establish the eaxct permeability distributions within each region. However, it is possible to establish the difference in the expected mean value of the permeability in these regions; failure to do this may result in inaccurate flow forecasts and hence, poor flow control. Therefore, different permeability values were used for different regions in the numerical model of this lay-up (Figure 4.6, Table 4.2). The permeability for region 2 was calculated from the individual reinforcement permeabilities following a volume-averaged approach.

In the present analysis, the mesh density for the numerical model of the mould was selected based on (i) the simulation time, (ii) the accuracy of the flow pattern predictions, and (iii) the accuracy of the pixel-to-node correlation. The simulation time for a numerical model with 336 nodes was 0.13 seconds. This increased to 0.59 and 67.35 seconds for models with 1271 and 7676 nodes, respectively. In addition, Figure 4.7 shows flow pattern predictions for three different mesh refinement levels, while Figure 4.8 shows pixel-to-node correla-

tion of a sample image for same meshed models. The meshed model with 1271 nodes and 1200 elements has reasonable simulation time and gives acceptable accuracy levels. Hence, it was used in the present analysis.

(a) Number of Nodes = 336

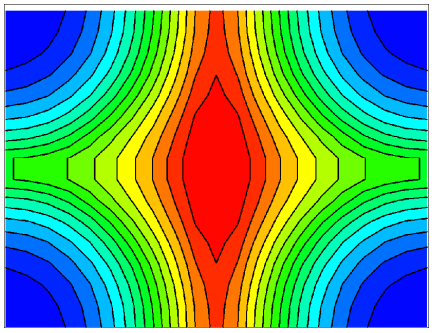

(b) Number of Nodes = 1271

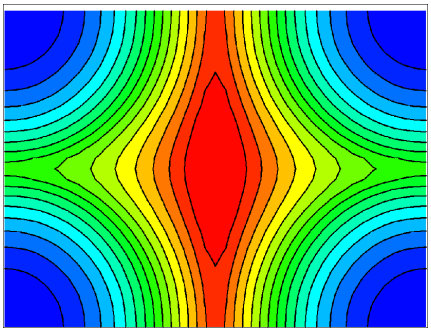

(c) Number of Nodes = 7676

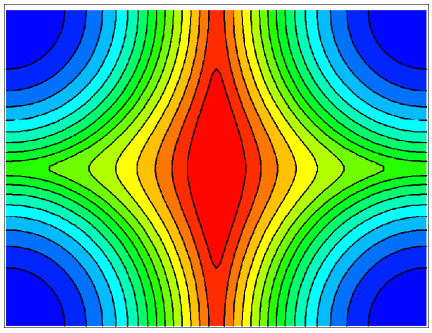

Figure 4.7: Influence of the mesh refinement level on the accuracy of flow pattern predictions. The meshed model had isotropic, homogeneous permeability distribution.

(a) Original Image

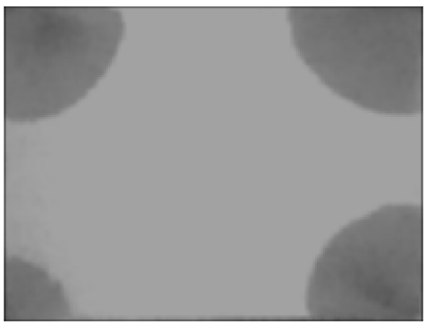

(b) Number of Nodes = 336

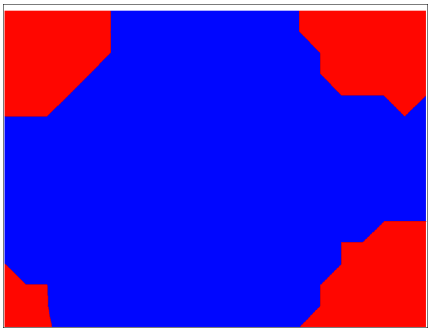

(c) Number of Nodes = 1271

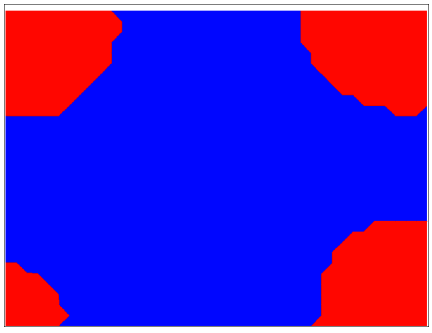

(d) Number of Nodes = 7676

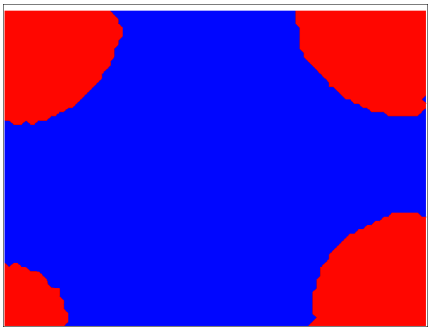

Figure 4.8: Influence of the mesh refinement level on the accuracy of pixel-to-node correlation. As the mesh with 1271 nodes gives acceptable accuracy with reasonable processing time, it was used in active control of the VI process.

Care is also needed in selecting the number of control-steps to be used for complete infusion of the mould. Fibrous reinforcements are known to be heterogeneous, which makes it necessary to monitor the flow as closely as possible. In contrast, in each control-step, enough time is required to perform flow simulations, select and implement an appropriate corrective action and realise its effect on the flow progression. The total processing time for flow simulation consists of an actual simulation time as well as the time to read the mesh file, impose initial conditions and save results at the end of a simulation. Table 4.3 lists the total processing time for the chosen mesh-size (1271 nodes,

1200 elements) for various numbers of control-steps. It is clear that beyond a limit, increase in the number of control-steps does not lead to a significant decrease in the total processing time. On the other hand, increasing the number of control-steps reduces the time-span for each control-step and hence, the window of opportunity for the corrective action to be reflected in process improvements.

Table 4.3: Influence of the number of control-steps on the processing time for flow simulations for a single control-step. The meshed model had 1271 nodes and 1200 quadrilateral elements.

Number of control-steps	Total processing time for one control-step (seconds)
4	6.00
6	4.09
11	3.22
21	3.01

For example, assume that the mould infusion time is two minutes and in any control-step, the time required for selecting and implementing the corrective action is one second. Then, completing the infusion in four control-steps will result in a thirty second time-span for each control-step. As the total processing time is six seconds (Table 4.3), 23 seconds are available for the effect of the corrective action to be realised before the start of the next control-step. However, if one uses eleven control-steps, then the time-span for each control-step is reduced to approximately eleven seconds, and the effective time available for flow correction is reduced to less than seven seconds. Note that this effect is made more severe as the flow continues to progress while one is performing flow simulations and selecting and implementing the corrective action.

In the present analysis, the infusion time for the mould was expected to be

of the order of minutes. Hence, eleven control-steps, giving ten computer controlled corrective actions, were used. The efficacy of the number of control-steps was investigated using virtual experiments, as described in the next section.

4.4.1 Virtual Experiments

The control scheme was first validated using virtual experiments for the first lay-up. For this, the mould was replaced by a virtual (meshed) model. The elements in this model were assigned random permeability values following a Normal distribution (Ghanem and Dham, 1998; Lundstorm et al., 2000; Pan et al., 2000; Hoes et al., 2004; Lundstorm et al., 2004) with a mean value of 1 x 10^{-08} m^2 and standard deviation of 2.29 x 10^{-09} m^2 . In addition, to investigate the influence of the number of control-steps used in the infusion process on the efficiency of the algorithm, the same mould was infused with a range of total control-steps (three, five and ten). Figure 4.9 shows the simulation results for various models, while Figure 4.10 shows the location of the final filling point for various numbers of control-steps. It is clear that in an uncontrolled infusion, material heterogeneity can lead to significant deviation in the flow progression from the ideal flow pattern in a homogeneous material and the final filling point can be moved a significant distance from the vent. The control system is able to identify such deviations and take corrective action such that the flow converges uniformly towards the vent i.e. the final filling point moves towards the vent.

It is important to note that virtual experiments can only be used for initial conceptual validation and a thorough comparison between virtual and real experiments is not possible. This is because the accuracy of such a comparison will strongly depend on the modelled permeability distribution. As noted earlier, it is extremely difficult to identify and replicate the actual permeability distribution in the mould.

(a) Without Controls

(b) 3 Control Steps

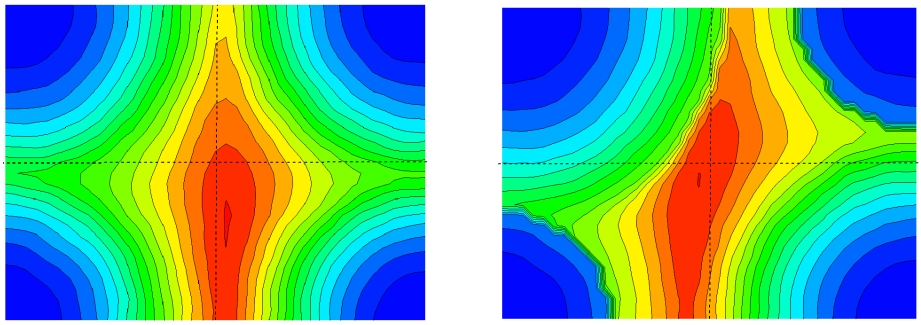

(c) 5 Control Steps

(d) 10 Control Steps

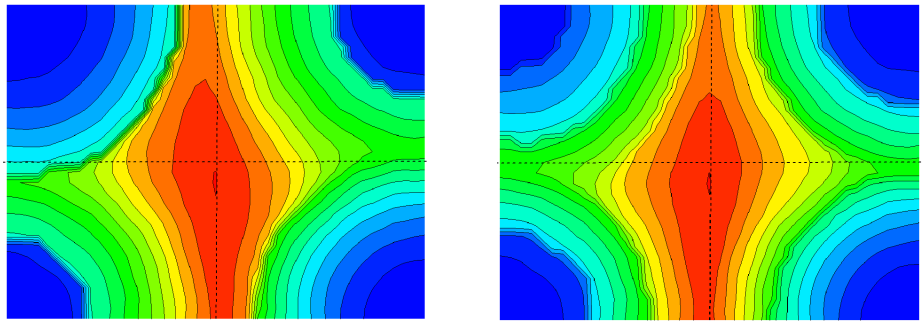

Figure 4.9: Simulation of infusion in heterogeneous porous media. (a) Without controls, the flow pattern is non-uniform. (b, c, d) With controls, the flow converges towards the vent, resulting in lower fill-time and resin wastage through the vent.

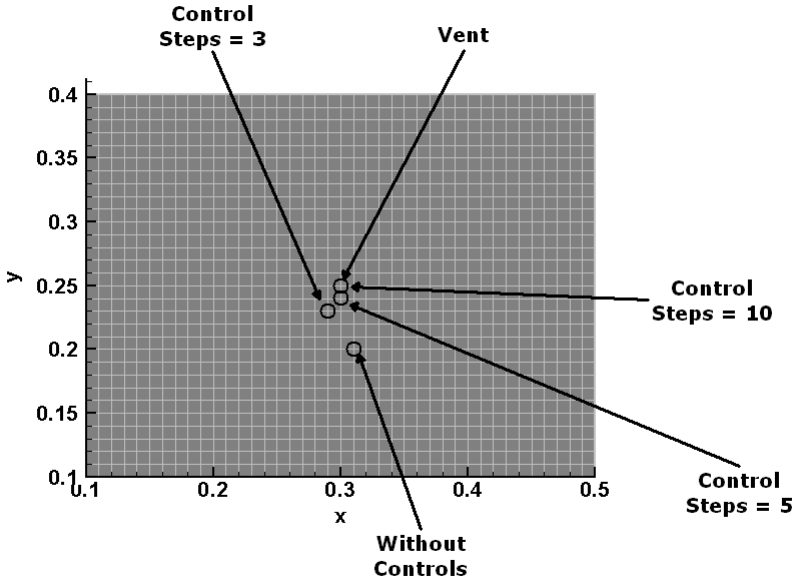

Figure 4.10: Due to material heterogeneity, the final filling point in an uncontrolled infusion is far away from the vent. The control system takes corrective action such that the flow converges uniformly towards the vent.

4.4.2 Infusion Experiments: Lay-up # 1 (CFRM)

The experimental results show that in any single uncontrolled infusion experiment, there is a considerable variation in the flow front progression from different injection ports. In addition, these variations were random in nature between experiments (Figure 4.11). As a result, the size of the unfilled region, when resin reached the vent, was large and the shape was unpredictable. This also moved the location of the final filling point away from the vent in an unpredictable manner (Figure 4.12). Hence, higher resin wastage through vent bleeding was necessary to ensure a complete infusion of the mould (Table 4.4). For the same lay-up, controlled infusion experiments showed slight or no reduction in the size of the unfilled area, when resin reached the vent (Figure 4.13, Table 4.4).

(a) Experiment # 1

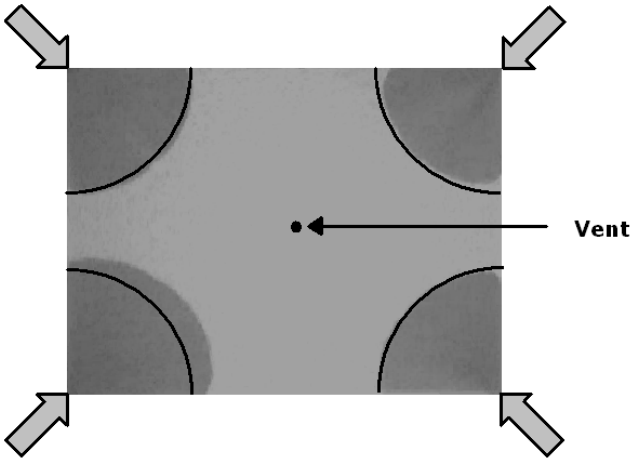

(b) Experiment # 2

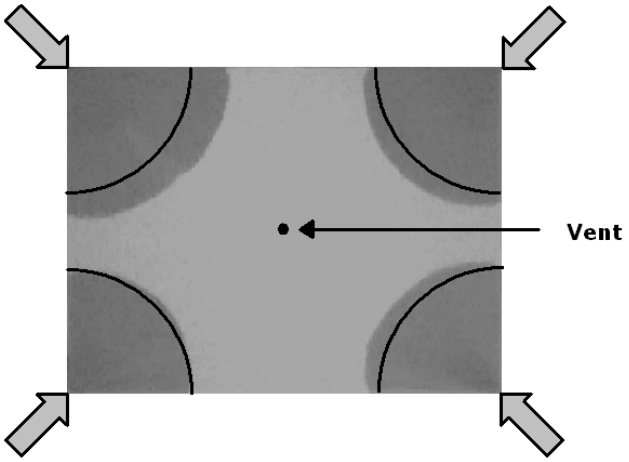

Figure 4.11: Variation in the flow progression due to the reinforcement heterogeneity in uncontrolled infusion experiments. Injection is from four corner injection ports. The circular lines show the expected flow patterns for a homogeneous reinforcement (Reinforcement: CFRM).

(a) Experiment # 1

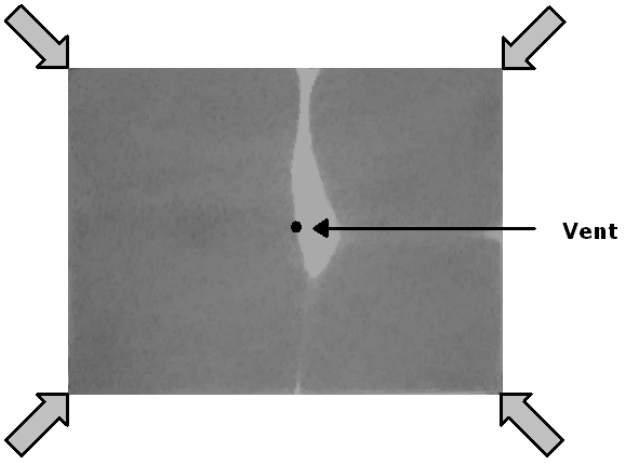

(b) Experiment # 2

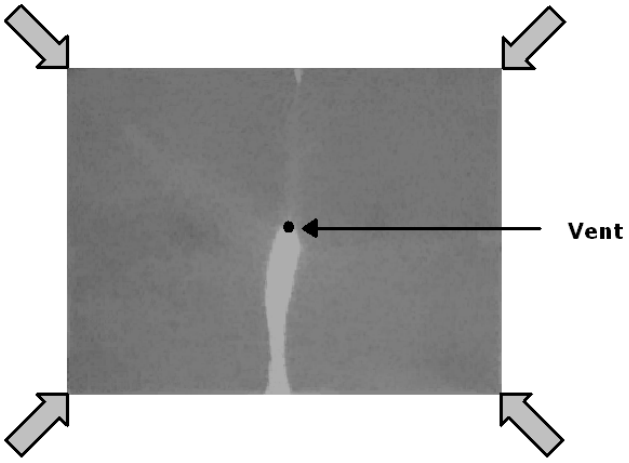

Figure 4.12: Flow front positions and unfilled region, when resin reached the vent, in uncontrolled infusion experiments. The infusion is from all the four corner injection ports. Uneven flow patterns necessitates resin bleeding through the vent for complete infusion of the mould (Reinforcement: CFRM).

(a) Experiment # 1

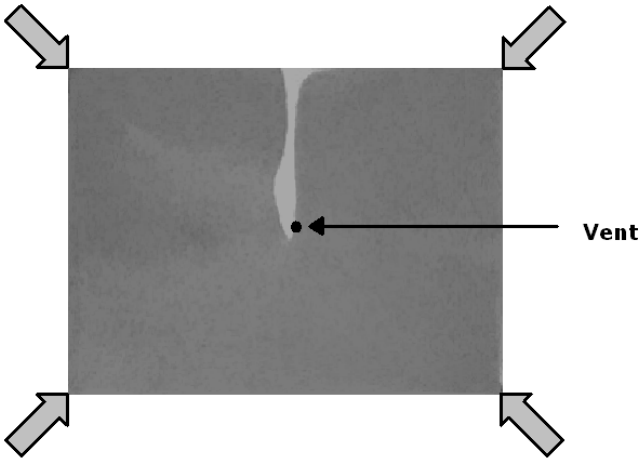

(b) Experiment # 2

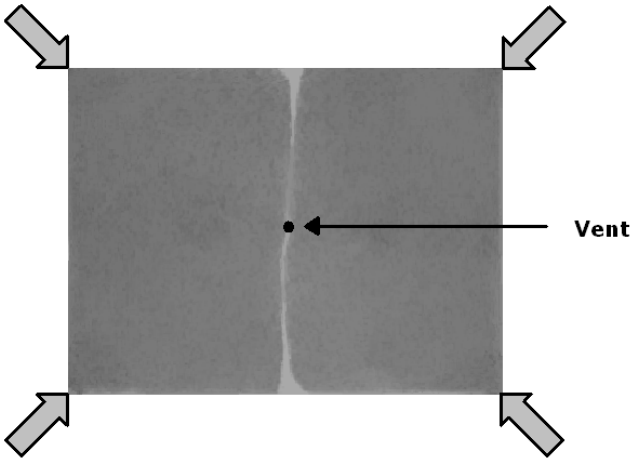

Figure 4.13: Flow front positions and unfilled region, when resin reached the vent, in controlled infusion experiments. All the injection ports are computer controlled and can be in open or closed configuration. High flow velocity, due to high reinforcement permeability, lowers the potential for improvement in the infusion efficiency by the control system (Reinforcement: CFRM).

Table 4.4: Final values of the parameters characterising the efficiency of the control system. Controlled experiments do not show any major improvements in the infusion efficiency as compared to uncontrolled experiments (Reinforcement: CFRM).

CFRM (Unifilo U750/450)							
Uncontrolled Experiments				*Controlled Experiments*			
	Distance (m)	**Area (%)**	**Resin Wastage (%)**		**Distance (m)**	**Area (%)**	**Resin Wastage (%)**
I	0.02243	0.541	5.52	I	0.06472	1.875	9.09
II	0.03151	5.0417	6.48	II	0.05255	2.2917	6.32
III	0.06639	3.625	8.2	III	0.06666	3.5833	7.95
IV	0.02167	3.3333	5.4	IV	0.3735	2.3333	10.35

The low level of improvement in this case is due to the following reasons. For effective implementation of the control system, it is critical that the filling simulations are performed faster than the actual flow front progression. For high permeability materials such as CFRM, this is problematic as the fill time is of the order of minutes. To some extent, this problem can be solved by employing a coarse mesh. In contrast, it was observed in many experiments that in any single control-step, different injection schemes led to similar parameters for the gate scheme selection criteria. It is possible that for the same number of control-steps, a different level of mesh refinement could have led to a completely different selection of injection scheme. Ideally, the mesh size should be fine enough such that successive mesh refinements should not lead to any alterations in the chosen injection scheme. However, this will increase the computation time beyond reasonable limits. Hence, a judicious choice had to be made regarding the mesh refinement level. In many experiments, the time lapse observed between determination of initial conditions for the flow simulations and implementation of a corresponding corrective control action was considerable compared to the mould fill-times. During this time, the flow front continued to progress reducing the window of opportunity for the corrective action to be reflected in process improvements.

In addition, even though the heterogeneity of CFRM is high (Endruweit et al., 2006), the flow front velocity is a strong function of the pressure gradient. Hence, the flow movement is relatively more uniform compared to a hypothetical material with the same level of heterogeneity, but with a lower permeability. This leads to lower level of resin wastage, and hence lower scope for any improvements.

4.4.3 Infusion Experiments: Lay-up # 2 (Plain Weave)

The results from uncontrolled infusion experiments for plain weave also show uneven and irregular flow patterns (Figure 4.14). It is important to note that

in the case of woven materials, nesting is also a contributing factor for the reinforcement heterogeneity. Figure 4.15 shows the unfilled region when resin reached the vent in the uncontrolled experiments. It is clear that a significant amount of resin will need to be bled through the vent for complete infusion of the mould (Table 4.5). In this case also, controlled infusion experiments did not show any clear improvements in the flow patterns or a reduction in the amount of resin bled through the vent (Figure 4.16, Table 4.5). As the flow progression did not show any improvements, the amount of resin bled through the vent was not calculated in this case.

(a) Experiment # 1

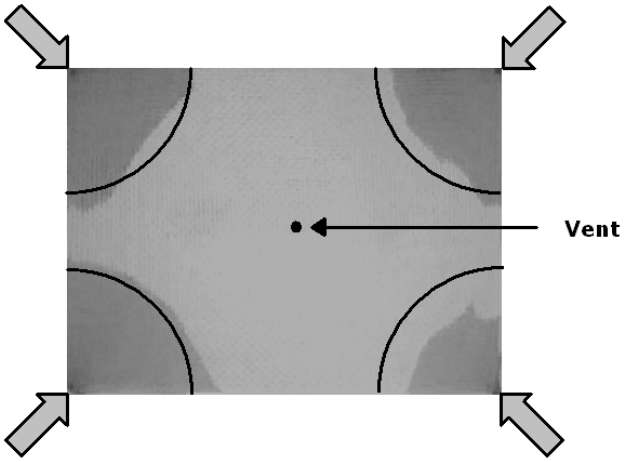

(b) Experiment # 2

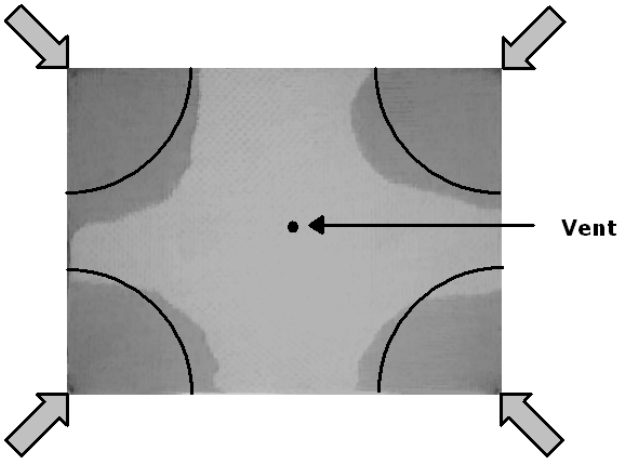

Figure 4.14: Variation in the flow progression due to the reinforcement heterogeneity in uncontrolled infusion experiments. Injection is from four corner injection ports. The circular lines show the expected flow patterns for a homogeneous reinforcement (Reinforcement: Plain Weave).

(a) Experiment # 1

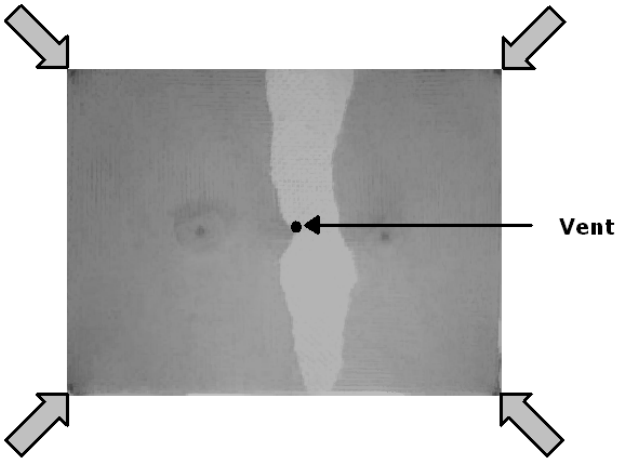

(b) Experiment # 2

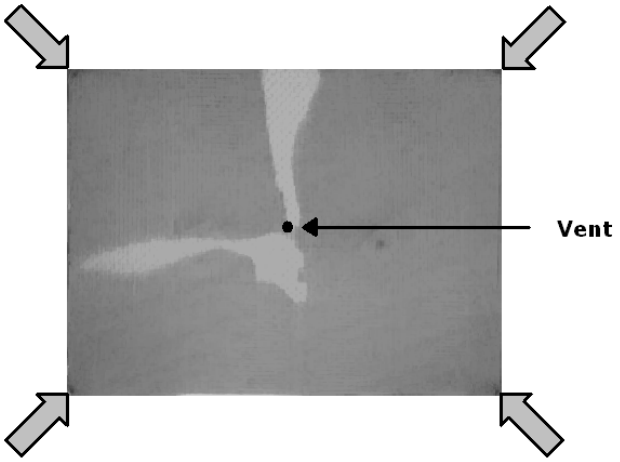

Figure 4.15: Flow front positions and unfilled region, when resin reached the vent, in uncontrolled infusion experiments. The infusion is from all the four corner injection ports. Uneven flow patterns necessitate resin bleeding through the vent for complete infusion of the mould (Reinforcement: Plain Weave).

(a) Experiment # 1

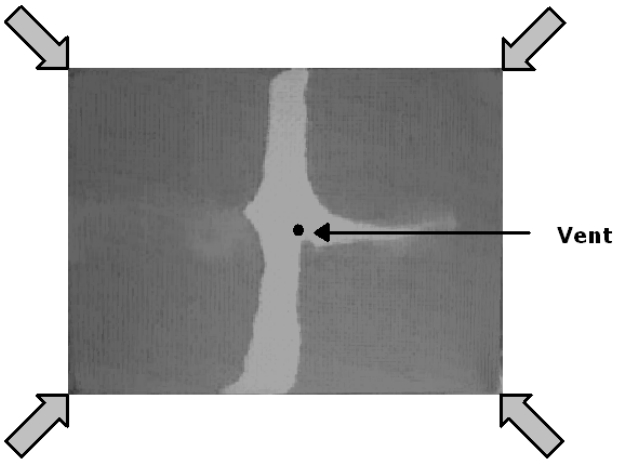

(b) Experiment # 2

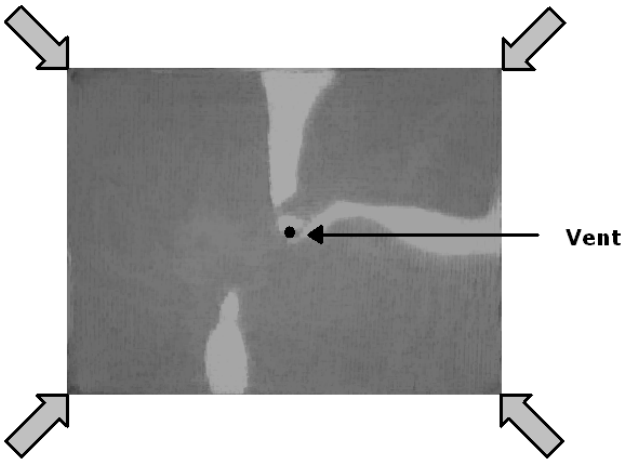

Figure 4.16: Flow front positions and unfilled region, when resin reached the vent, in controlled infusion experiments. All the injection ports are computer controlled and can be in an open or closed configuration. The significant loss of flow velocity, due to low reinforcement permeability and driving pressure, leads to a loss of the gate effectiveness and hence, the process controllability. As a result, the injection system is not able to steer the flow as required to minimise the resin wastage (Reinforcement: Plain Weave).

Table 4.5: Final values of the parameters characterising the efficiency of the infusion experiments. Controlled experiments do not show any major improvements in the infusion efficiency as compared to uncontrolled experiments (Reinforcement: Plain Weave).

Plain Weave (RT 600)							
Uncontrolled Experiments				*Controlled Experiments*			
	Distance (m)	**Area (%)**	**Resin Wastage (%)**		**Distance (m)**	**Area (%)**	**Resin Wastage (%)**
I	0.0102	13.5417	50	I	0.00508	11.7917	
II	0.0458	4.5833	26.31	II	0.0054	23.4583	
III	0.01763	11.0417	66.66	III	0.03985	9.04167	
IV	0.0556	9.125	58.33				

Various researchers (Demirci and Coulter, 1995; Nielsen and Pitchumani, 2002b) have noted the loss of controllability in LCM processes. For a given set of injection conditions and process parameters, the ability of the injection system to steer the flow in a required fashion is linked with a parameter called "gate effectiveness". Demirci and Coulter (Demirci and Coulter, 1995) used a streamline method to analyse the controllability of the injection moulding process, and concluded that the gate influence on flow progression is lost when the flow front reaches a distance greater than half of the mould width. Berker et al. (Berker et al., 1998) analysed the gate effectiveness in the constant flow rate and the constant pressure injection RTM processes and showed that it remains constant in the constant flow rate injection process, but decreases for constant pressure injection process. Extending the same analysis, one can also argue that the gate effectiveness depends on the type of flow i.e. 1D, 2D or 3D. Gokce and Advani (Gokce and Advani, 2003) argued that when the flow front velocity becomes a major function of the permeability, the controllability of the process, using a given set of parameters, is lost. In other words, when the pressure gradient at the flow front becomes negligible or comparable with the capillary pressure, the controllability is lost. The low permeability values of the plain weave led to a faster reduction in the flow front velocities, and hence a reduction or a complete loss of the gate effectiveness. This shows the importance of knowledge about gate effectiveness during the design stage of the control system.

4.4.4 Infusion Experiments: Lay-up # 3 (Stitched Bi-directional + CFRM)

The results from uncontrolled experiments for this lay-up show a delayed flow front in the thick region (region 2) of the reinforcement, which involves a low permeability reinforcement covered with random mat. This leads to a

considerably larger unfilled area than for CFRM when resin reaches the vent, and larger resin wastage due to bleeding (Figure 4.17, Table 4.6). One can argue that readjustment of the vent position could lead to a reduction in resin wastage. However, as shown in Figure 4.17, the last point to be filled varies between experiments and it is difficult to predict a suitable vent position. In addition, a number of design factors can influence the selection of suitable vent locations (Minaie et al., 2002). Relocating vents may also involve increased costs for mould reworking and may not be always feasible due to design and tooling restrictions.

Controlled experiments show a considerable improvement in the flow front progression and a smaller unfilled area, when resin reaches the vent. This reduces the requirement for resin bleeding as well as resin wastage (Figure 4.18, Table 4.6). In addition, the control actions implemented by the system are different from experiment to experiment, which highlight the process variability (Table 4.7). This demonstration of variability also supports the use of an active control system, as opposed to a passive (off-line) approach.

Figure 4.19 shows the location of the centroid of an unfilled region in one of the uncontrolled and controlled infusion experiments. In an uncontrolled infusion, deviating flow patterns move the centroid away from the vent. On the other hand, in an actively controlled infusion, the control system identifies the flow deviations in early stages. Then, using flow advancement predictions from numerical simulations, it identifies and takes an appropriate corrective action such that the centroid moves towards and remains as close to the vent as possible.

(a) Experiment # 1

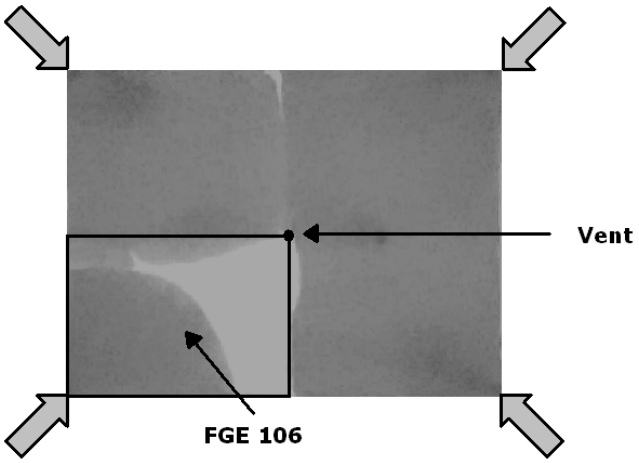

(b) Experiment # 2

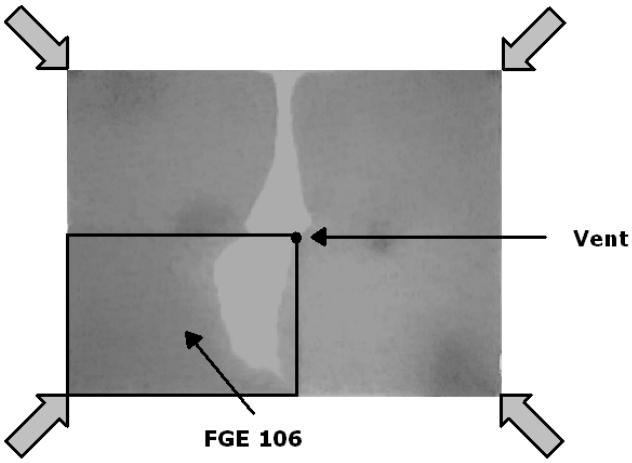

Figure 4.17: Flow front positions and unfilled region, when resin reached the vent, in uncontrolled infusion experiments. The infusion is from all the four corner injection ports. (Reinforcement: CFRM + FGE 106).

(a) Experiment # 1

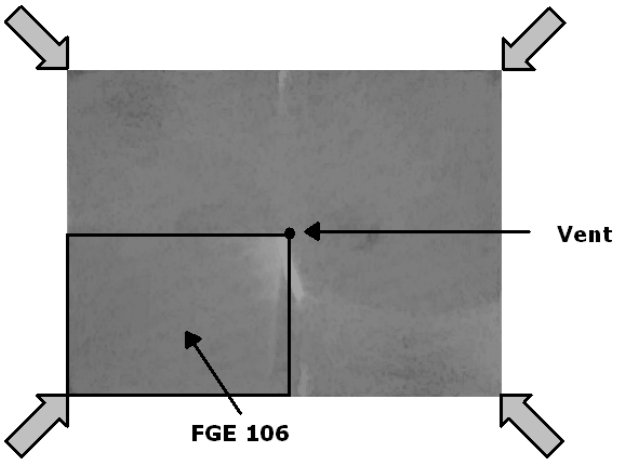

(b) Experiment # 2

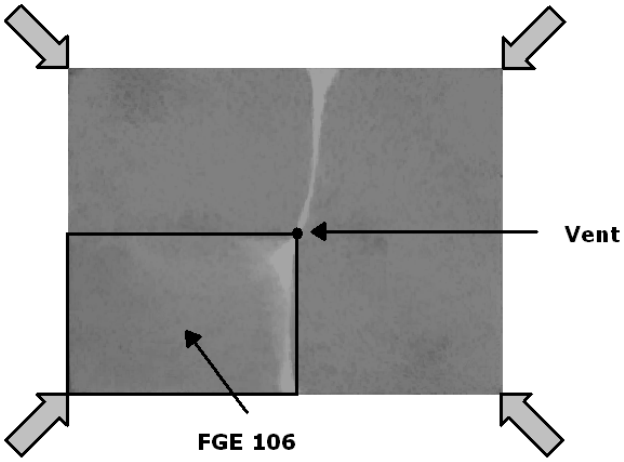

Figure 4.18: Flow front positions and unfilled region, when resin reached the vent, in controlled infusion experiments. All the injection ports are computer controlled and can be in open or closed configuration. The control system successfully identifies the flow deviations and implements an appropriate corrective action, reducing the resin waste through vent bleeding and improving the infusion efficiency (Reinforcement: CFRM + FGE 106).

(a) Uncontrolled experiment

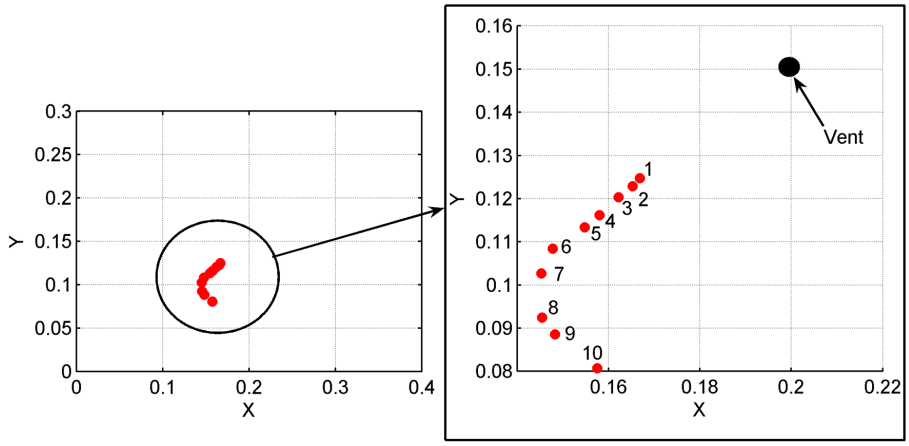

(b) Controlled experiment

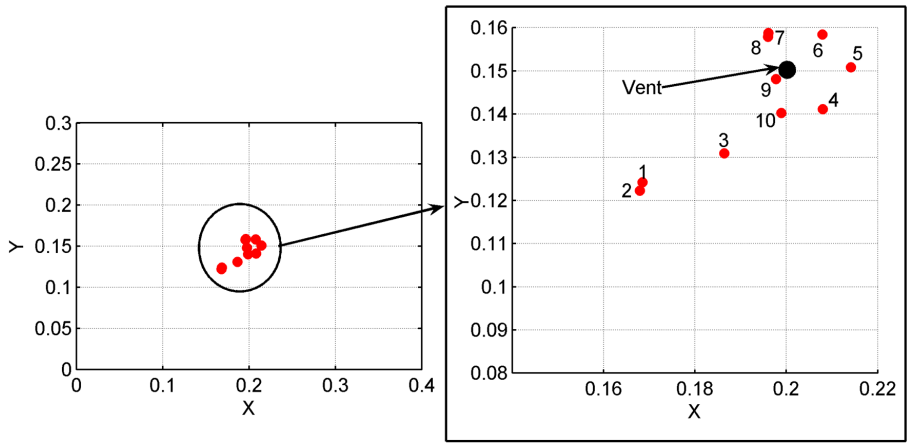

Figure 4.19: Location of the centroid of an unfilled region, at the end of each control step, in one of the uncontrolled and controlled experiments.

Table 4.6: Final values of the parameters characterising the efficiency of the infusion experiments. Actively controlled experiments show significant improvements in the infusion efficiency as compared to uncontrolled experiments (Reinforcement: CFRM + FGE 106).

CFRM + FGE 106							
Uncontrolled Experiments				*Controlled Experiments*			
	Distance (m)	**Area (%)**	**Resin Wastage (%)**		**Distance (m)**	**Area (%)**	**Resin Wastage (%)**
I	0.07034	9.04448	13.30	I	0.00672	4.07568	4.4
II	0.06872	14.2305	13.5	II	0.02771	5.03741	6.6
III	0.05343	13.9149	11.7	III	0.02943	1.85298	5.3
IV	0.08136	16.171	20.5	IV	0.03564	3.40555	6.7

Table 4.7: Open injection ports during controlled infusion experiments for the third lay-up. Control system selects appropriate injection ports to be opened based on the flow information collected by the imaging system and the simulation results of flow advancement.

Control step #	**Experiment #**			
	1	**2**	**3**	**4**
2	1	1	1	1
3	1	1	1	1
4	1, 2	1, 2	1	1
5	1, 2, 4	2, 4	1, 2	1, 2
6	2, 4	1, 2, 3	1, 2, 3	2, 3
7	1, 2, 3	1, 2, 3	1, 2, 4	2, 3, 4
8	2, 3	1, 2, 3, 4	1, 4	1, 3, 4
9	2, 3, 4	2, 4	1, 2, 4	2, 4
10	1, 2, 3, 4	1, 2, 3	1, 2, 4	2, 4
11	1, 2, 4	1, 2, 3	1, 2, 3, 4	1, 2, 3, 4

4.5 Discussion

The extension of the present system for generic VI moulds or variants of the VI process, such as SCRIMP^{TM}, is possible. For this, additional challenges need to be addressed such as control of line injection gates, flow monitoring in moulds with flow-enhancing layers or with three-dimensional geometries etc.

Often, the simple design and ease of implementation of a line injection gate makes it preferrable over a point injection gate. However, there is a considerable loss of controllability with a line injection gate. This is because fill-time restrictions in the VI process make control of the injection pressure impractical, leaving only "on-off" type controllability. Then, switching "off" a line injection gate can stop the flow advancement for all practical purposes. Recently, an approach to regain the controllability by segmenting or compartmentalising a line injection gate (Nalla et al., 2007), has been reported. However, further developments are needed in this direction.

The imaging system reported here can also be used in the SCRIMP^{TM} process to monitor flow progression on the top side of the mould. Additional information regarding the flow beneath the top surface can be gathered by placing any of the previously reported intrusive sensors. The amalgamation of the information collected by multiple sensors and/or different sensor systems and its use in the flow simulation tool will require additional developments. In addition, by using multiple cameras, the present system can also be employed for large two and three-dimensional VI moulds.

4.6 Conclusions

Fibrous reinforcements, used in the manufacture of the composites, can have inherent heterogeneity, which can influence the infusion process in an unpredictable manner. The resulting flow patterns can deviate significantly from

the ideal flow patterns in a homogeneous material. Hence, for full infusion of a part, it is necessary to allow some resin to bleed through the vent, which results in resin wastage and longer fill-times. In extreme cases, resin gelation might occur before the mould is completely filled.

A possible solution to address this issue is to actively control the infusion process. A new control system, complete with a flow monitoring and analysis system as well as computer controlled injection ports, was developed. A low cost web-camera was used to capture images of flow progression, which were analyzed to identify flow disturbances. Using an infusion process simulation tool, flow advancement was simulated to identify the optimum corrective action, which was implemented through computer controlled injection ports. All the steps of this control system were performed and implemented in real-time and were repeated a number of times during the infusion stage. The advantages of the system include low-cost, high SNR, high spatial resolution, no intrusiveness and ease of real-time interfacing.

The system was validated using virtual experiments as well as actual infusion experiments. The results highlight the capabilities as well as limitations of the control system. One can think of the first two cases studied as two extremes. For reinforcements with high permeability values such as CFRM, high flow velocity reduces the chances of improvements in the infusion efficiency. In addition, it is difficult to match the simulation times with the fill-times. For such cases, passive control may be a suitable option. Flow velocity is significantly reduced in reinforcements with low permeability values such as the plain weave. In such cases, the flow is mainly driven by capillary pressure (Dungan and Shastri, 2002) and no control action is possible. Lay-ups that are in the central region of the permeability scale and have non-uniform permeability field offer the best chances of improvement. For such lay-ups (e.g. lay-up # 3), the control system is able to identify flow deviations and take corrective actions, resulting in reduced resin waste and improved infusion efficiency.

Chapter 5

Summary, Conclusions and Future Work

5.1 Summary and Conclusions

Vacuum Infusion is a low-cost manufacturing process, especially suitable for producing high aspect ratio (i.e. width or length to thickness) polymer composite parts. At present, development of accurate, reliable numerial simulation tools or creation of efficient mould designs is not possible due to the limited understanding of the process physics. Therefore, a costlier trial-and-error approach is employed for process optimisation.

The present work was aimed at enhancing this fundamental understanding of the VI process physics. It is hoped that by first analysing the mould set-up with only a single type of reinforcement, greater understanding will be developed, which will then facilitate investigation of more complex processes such as SCRIMP^{TM} that use different types of reinforcements.

In the first part of this work (chapter 2), new formulations for the rectilinear and the radial flow VI processes were developed. Unlike previous efforts, these formulations were derived without any assumptions regarding the changes in

the mould thickness. The coupled formulations were solved using an iterative numerical method for initial value problems. The issue of accuracy and convergence of these solutions was also investigated.

The numerical results showed that the fluid pressure in the filled region of the mould remains higher in VI than in RTM. Although results from numerical flow simulations showed a similar behaviour, they were found to be erroneous due to the technique used by the FE/CV method to track the flow front. Also, it was observed that as the reinforcement compliance increases, the pressure profile in VI diverges more from RTM. From this, it was concluded that for many reinforcements, the pressure profile at the flow front is almost identical in VI and RTM. This facilitated the adaption of the RTM pressure solution for VI to estimate fill-times in the rectilinear and the radial flow VI processes. The RTM and VI fill-time ratio, for both the rectilinear and the radial flow processes, was predicted to remain constant with flow progression.

In the second part of the work (chapter 3), an experimental programme was conducted to investigate the validity of the analytical formulations. New moulds were prepared to accomodate a large number of pressure transducers that increased the accuracy of pressure profile measurements. Continuous pressure measurements were taken during unsaturated flow VI experiments that facilitated collating of the pressure profile evolution with flow progression. In addition, fill-times were monitored as a function of flow progression.

The experimental results showed that in the rectilinear flow VI process, the full injection pressure is not realised immidiately. Also, the unsaturated flow pressure profile is initially lower than the RTM pressure profile. However, with flow progression, it rises to be level with and then above the RTM pressure profile. In addition, it was found that, in contrast to the analytical formulation, fill-time is not proportional to the square of the infused length. A similar trend was observed in the radial flow VI process, where despite realisation of the full injection pressure at the start of the injection, the pressure profile starts from

below and rises towards the RTM pressure profile. Correspondingly, the fill-time is also much higher than the RTM process.

This process phenomenon has not been observed previously. Subsequently, it was observed that the current experimental set-up for the reinforcement compliance characterisation does not reflect the actual events taking place in the VI process. It was hypothesised that the influence of the fluid pressure as well as the stretching and relaxation of the flexible plastic bag may have a significant influence on the compliance behaviour of reinforcements. As the current experimental set-up and the empirical model derived from it do not take into account the influence of these parameters, it leads to a mis-match between the experimental and numerical results. To investigate the validity of this hypothesis, a new experimental set-up should be designed that closely mimics the events in the VI process.

The third part of the work (chapter 4) was focused on a conceptual validation of an automated flow control system for the VI process. It was argued that fibrous reinforcements used in the manufacture of the composites are inherently heterogeneous, which can influence the infusion process in an unpredictable manner. The resulting flow patterns can deviate significantly from the ideal flow patterns in a homogeneous material. Hence, for complete infusion of a part, it is necessary to allow some resin to bleed through the vent, which results in resin wastage and longer fill-times. In extreme cases, resin gelation might occur before the mould is completely filled.

A possible solution to address this issue is to actively control the infusion process. The limitations of present-day control and sensing systems were identified and a novel real-time flow control system was designed and developed for the VI process. As part of this system, a new online flow sensing system was also developed that used non-intrusive image acquisition and analysis technology. In addition, this system performed online flow simulations to optimise the process control. The advantages of this control system were low-cost, high

signal-to-noise ratio (SNR), high spatial resolution, no intrusiveness and ease of real-time interfacing.

The potential of the flow control system to improve the efficiency, reliability and repeatability of the VI process was investigated through actual infusion experiments for three different reinforcement lay-ups. One can think of the first two cases studied as two extremes. For reinforcements with high permeability values such as CFRM, high flow velocity reduces the chances of improvements in infusion. In addition, it is difficult to match the simulation times with the fill-times. For such cases, passive control may be a suitable option. Flow velocity is significantly reduced in reinforcements with low permeability values such as the plain weave. In such cases, the flow is mainly driven by capillary pressure (Amico and Lekakau, 2001; Dungan and Shastri, 2002) and no control action is possible. Reinforcements or lay-ups in the central region of the permeability scale offer the best chances of improvement. For such lay-ups (e.g. lay-up # 3, FGE 106 + CFRM), the control system is able to identify flow deviations and take corrective actions, resulting in reduced resin waste and improved infusion efficiency. Thus, this study also revisited the issue of process controllability and showed the importance of its consideration in designing an effective control system.

5.2 Future Work

5.2.1 Analysis of the VI process

The current study has identified a number of possible avenues for future research. Starting with the analytical formulations, it can be seen that the reinforcement compliance behaviour is the most important factor in understanding the VI process in detail and identifying important process parameters. It was also pointed out that wet expansion behaviour is more relevant for the VI

process. In addition, an effort was made to explain the difference between the numerical and experimental results by, (i) observing that the events in the compliance characterisation experiments are different from the actual events in the VI process, and (ii) hypothesising that the fluid pressure and the stretching and relaxation of the flexible plastic bag may have a significant influence on the reinforcement compliance behaviour i.e. the current methodology of wet expansion characterisation may be of less relevance. However, at present the knowledge of reinforcement wet expansion is marginal. This lack of knowledge, which prevents one from examining the validity of this hypothesis, is identified as the first crucial area for future research.

The entire study can be divided into three separate parts. In the first part of the study, one can investigate the validity of the formed hypothesis by comparing the compliance results from the current characterisation set-up and a modified set-up that will mimic the VI process as closely as possible. Such a modified set-up could include pressure transducers and sensors for thickness measurement (e.g. LVDT) similar to William's (1998) set-up. If the hypothesis were found to be true, it will validate the analytical formulation and open up possibilities for adapting faster, efficient RTM simulation tools for VI, without major modifications. On the other hand, an invalid hypothesis will require further investigation of the subject.

The second set of experiments relate to characterisation of wet expansion behaviour of as many reinforcements as possible. The actual set-up to be used for these experiments will need to be determined from the outcome of the previous study. Note that these results are crucial for the VI process where, unlike the RTM process, one needs to calculate an individual pressure profile for each reinforcement.

Experimental investigation of the pressure profile and fill-times with better equipment (e.g. pressure transducers with full vacuum range) and for variety of reinforcements forms the third part of the study. This will be helpful in

validating the analytical solution more rigorously.

In addition, the extension of the radial formulation for anisotropic flow case and modelling of the SCRIMP^{TM} process need to be investigated. Sun et al. (1998), Han et al. (2000), Hsiao et al. (2000), Andersson et al. (2002) have attempted to model fluid flow in the SCRIMP^{TM} process. However, most of them either neglect the reinforcement thickness variation or use numerical methods such as the FE/CV method that do not ensure conservation of mass. Thus, at best, these are crude approximations of the actual physics. Inclusion of dynamic thickness variation in the model will make the problem impossible to treat analytically and a numerical treatment is required. However, a detailed and a thorough investigation, including experimental validation, needs to be done to establish the validity of any numerical method. Furthermore, availability of appropriate reinforcement property data, mainly permeability, fibre volume fraction and compliance behaviour, is also crucial. As reported previously for compliance behaviour, the currently available methods and data may not be suitable. In addition, any experimental programme for validation purposes will have to include measurement of pressure profile, flow progression on both the sides of the mould as well as thickness distribution. In the past, very few (Mathur et al., 2001) experimental efforts have been reported. The main challenges here are in avoiding or limiting the process intrusiveness due to these sensors as well as ensuring sufficient repetativeness and reliability in experimental results.

5.2.2 Control of the VI/SCRIMP^{TM} Process

As shown in previous chapters, the physics of the VI process are very complex. Also, numerous other sources such as reinforcement and process heterogeneity add random disturbances that are very difficult to characterise. The solution to this problem, i.e. active flow control, is also time-consuming, costly and its success highly depends on one's knowledge of process controllability. However,

very little research work has been done on this subject. Hence, to advance the field of flow control, the first and most critical area that needs investigation is process controllability.

The second area that can be investigated in future is related to the flow control in the SCRIMP^{TM} process. Development of a flow control system for SCRIMP^{TM} will require measuring flow progression, as well as advancements in the injection hardware and optimisation algorithms.

The issue of flow sensing, mainly fluid pressure or flow progression on both the sides of the mould, is in itself a critical area that requires further developments. As listed in Chapter 4, the main requirements for any sensor to be employed for flow sensing in VI / SCRIMP^{TM} are varied, for example speed, accuracy, reliability, cost, intrusiveness and interfacability. Although numerous sensors have already been used, their drawbacks such as higher process intrusiveness make them unsuitable for a generic VI mould. With advancements in microelectronics, it will be interesting to see if any of the new generation of sensors have key features of speed, accuracy, reliability, reduced cost, minimum intrusiveness and an ability to interface with control hardware. One example might be the radio frequency (RF) based sensor such as RFID. Bogdanovich and Wigent (2003) have also reported an effort to weave the fibre optic sensor into the reinforcement. Experimentating with such novel ideas is crucial for developing solutions for such demanding applications as VI and SCRIMP^{TM}.

Also, SCRIMP^{TM} sometimes uses line injection. As discussed previously, the controllability of such an injection system is limited. Hence, improvements in the injection hardware, for example a segmented injection line (Nalla et al., 2007), are necessary.

References

Abdelwahab, K., 2006. An Introduction to Numerical Methods: A MATLAB Approach. Chapman and Hall, London, UK.

Advani, S., Sozer, M., 2003. Process Modeling in Composite Manufacturing. Marcel-Dekker, New York, USA.

Ahn, S., Lee, W., Springer, G., 1995. Measurement of the three-dimensional permeability of fiber preforms using embedded fiber optic sensors. Journal of Composite Materials 29 (6), 714–733.

Amico, S., Lekakau, C., 2001. An experimental study of the permeability and capillary pressure in resin-transfer molding. Composites Science and Technology 61 (13), 1945–1959.

Andersson, H., Lundstorm, T., Gebart, B., 2003a. Numerical model for vacuum infusion manufacturing of polymer composites. International Journal of Numerical Methods for Heat & Fluid Flow 13 (3), 383–394.

Andersson, H., Lundstorm, T., Gebart, B., Langstorm, R., 2002. Flow-enhancing layers in the vacuum infusion process. Polymer Composites 23 (5), 895–901.

Andersson, H., Lundstorm, T., Gebart, B., Synnergren, P., 2003b. Application of digital speckle photography to measure thickness variations in the vacuum infusion process. Polymer Composites 24 (3), 448–455.

Berker, B., Barooah, P., Yoon, M., Sun, J., 1998. Sensor based modeling and control of fluid flow in resin transfer molding. Journal of Materials Processing and Manufaturing Science 7 (2), 195–214.

Bernstein, J., Wagner, J., 1997. Fiber optic sensors for use in monitoring flow front in vacuum resin transfer molding processes. Review of Scientific Instruments 68 (5), 2156–2157.

Bickerton, S., Advani, S., Mohan, R., Shires, D., 2000. Experimental analysis and numerical modeling of flow channel effects in resin transfer molding. Polymer Composites 21 (1), 134–153.

Bickerton, S., Stadefld, H., Steiner, K., Advani, S., 2001. Design and application of actively controlled injection schemes for resin-transfer molding. Composites Science and Technology 61 (11), 1625–1637.

Boccard, A., Lee, W., Springer, G., 1995. Model for determining the vent locations and the fill time of resin transfer molds. Journal of Composite Materials 29 (3), 306–333.

Bogdanovich, A., Wigent, D., 2003. Fabrication of 3-d woven preforms and composites with integrated fiber optic sensors. SAMPE Journal 39 (4), 6–15.

Breard, J., Henzel, Y., Trochu, F., Gauvin, R., 2003. Analysis of dynamic flows through porous media. part ii: Deformation of a double-scale fibrous reinforcements. Polymer Composites 24 (3), 409–421.

Bruschke, M., Advani, S., 1990. A finite element/control volume approach to mold filling in anisotropic porous media. Polymer Composites 11 (6), 398–405.

Burden, R., Faires, J., 2000. Numerical Analysis, 7th Edition. Brooks Cole, Pacific Grove, USA.

Cai, Z., Gutowski, T., 1992. The 3-d deformation behavior of a lubricated fiber bundle. Journal of Composite Materials 26 (8), 1207–1237.

Chan, A., Morgan, R., 1992. Sequential multiple port injection for resin transfer molding of polymer composites. SAMPE Quarterly 24 (1), 45–49.

Chen, B., Cheng, A., Chou, T., 2001. A nonlinear compaction model for fibrous preforms. Composites Part A 32 (5), 701–707.

Chen, Y., Stelson, K., Voller, V., 1997. Prediction of filling time and vent locations for resin transfer molds. Journal of Composite Materials 31 (11), 1141–1161.

Correia, N., 2004. Analysis of the vacuum infusion moulding process. Ph.d. thesis, University of Nottingham, Nottingham, UK.

Dave, R., 1990. A unified approach to modeling resin flow during composite processing. Journal of Composite Materials 24 (1), 22–41.

Delleur, J., 1998. The Handbook of Groundwater Engineering. CRC Press, Florida, USA.

Demirci, H., Coulter, J., 1995. Control of flow progression during molding processes. Journal of Materials Processing and Manufaturing Science 3 (4), 409–425.

DeParseval, Y., Pillai, K., Advani, S., 1997. A simple model for the variation of permeability due to partial saturation in dual scale porous media. Transport in Porous Media 27 (3), 243–264.

DeParseval, Y., Roy, V., Advani, S., 1995. Effect of local variations of preform permeability on the average permeability during resin transfer molding of composites. In: ANTEC 95 - Proceedings of the conference of the Society of Plastics Engineers. Boston, USA, pp. 3040–3044.

Dominauskas, A., Heider, D., Gillespie, J., 2003. Electric time-domain reflectometry sensor for on-line flow sensing in liquid composite molding processing. Composites Part A 34 (1), 67–74.

Dungan, F., Shastri, A., 2002. Saturated and unsaturated polymer flows: Microphenomena and modeling. Journal of Composite Materials 36 (13), 1581–1603.

Endruweit, A., McGregor, P., Long, A., Johnson, M., 2006. Influence of the fabric architecture on the variations in experimentally determined in-plane permeability values. Composites Science and Technology 66 (11-12), 1778–1792.

Fracchia, C., Castro, J., Tucker, C., 1989. A finite element/control volume simulation of resin transfer molding. In: Proceedings of the 4th Technical Conference of American Society of Composites. Blacksburg, Virginia, pp. 157–166.

Gebart, B., 1992. Permeability of unidirectional reinforcements for rtm. Journal of Composite Materials 26 (8), 1100–1133.

Ghanem, R., Dham, S., 1998. Stochastic finite element analysis for multiphase flow in heterogeneous porous media. Transport in Porous Media 32 (3), 239–262.

Gokce, A., Advani, S., 2003. Gate effectiveness in controlling resin advance in liquid composite moulding processes. Journal of Manufacturing Science and Engineering - Transactions of the ASME 125 (3), 548–555.

Gokce, A., Advani, S., 2004. Vent location optimization using map-based exhaustive search in liquid composite molding processes. Materials and Manufacturing Processes 19 (3), 523–548.

Gokce, A., Hsiao, K., Advani, S., 2002. Branch and bound search to optimize

injection gate locations in liquid composite molding processes. Composites Part A 33 (9), 1263–1272.

Green, W., Walsh, S., Shires, D., 2003. Surveillant Concurrent Engineering Process Tool for Environment Rendering for Resin Flow Monitoring in Composites. Patent No: US 6577958 B1.

Grimsley, B., Hubert, P., Song, X., Cano, R., Loos, A., Pipes, R., 2001. Flow and compaction during the vacuum assisted resin transfer molding process. In: Proceedings of the 33rd International SAMPE Conference on Advancing Affordable Materials Technology. Vol. 33. Seattle, USA, pp. 143–153.

Gutowski, T., 1997. Advanced Composites Manufacturing. John Wiley, New York, USA.

Hammami, A., Gebart, B., 1998. A model for the vacuum infusion molding process. Plastics, Rubber and Composites 27 (4), 185–189.

Hammami, A., Gebart, B., 2000. Analysis of the vacuum infusion molding process. Polymer Composites 21 (1), 28–40.

Han, K., Jiang, S., Zhang, C., Wang, B., 2000. Flow modeling and simulation of scrimp for composites manufacturing. Composites Part A 31 (1), 79–86.

Hoes, S., Dinescu, D., Sol, H., Parnas, R., Lomov, S., 2004. Study of nesting induced scatter of permeability values in layered reinforcement fabrics. Composites Part A 35 (12), 1407–1418.

HSE, 2002a. The Control of Substances Hazardous to Health Regulations (4th Ed.) - Approved Code of Practise and Guidance. HSE Books, London, UK, 30-46.

HSE, 2002b. Occupational Exposure Limits. HSE Books, London, UK, 10.

Hsiao, K., Mathur, R., Advani, S., Gillespie, J., Fink, B., 2000. A closed form solution for flow during the vacuum assisted resin transfer molding process. Journal of Manufacturing Science and Engineering 122 (3), 463–475.

Hubert, P., Poursartip, A., 1998. A review of flow and compaction modelling relevant to thermoset matrix laminate processing. Journal of Reinforced Plastics and Composites 17 (4), 286–318.

Jacob, A., 2006. Large aircraft tail structure by rtm. Reinforced Plasitcs 50 (1), 18.

Kang, M., Jung, J., Lee, W., 2000. Analysis of resin transfer molding process with controlled multiple gates resin injection. Composites Part A 31 (5), 407–422.

Kang, M., Lee, W., Hahn, H., 2001. Analysis of vacuum bag resin transfer molding process. Composites Part A 32 (11), 1553–1560.

Kelly, P., Umer, R., Bickerton, S., 2006. Viscoelastic response of dry and wet fibrous materials during infusion process. Composites Part A 37 (6), 868–873.

Kim, Y., McCarthy, S., Fanucci, J., 1991. Compressibility and relaxation of fiber reinforcements during composite processing. Polymer Composites 12 (1), 13–19.

Kuan, Y., Gizawy, A., 2000. Numerical characterisation of mold injeciton in resin transfer molding process. Advances in Polymer Technology 19 (3), 173–179.

Kueh, S., Advani, S., Parnas, R., 2002. A methodology for using long-period gratings and mold-filling simulations to minimize the intrusiveness of flow sensors in liquid composite molding. Composites Science and Technology 62 (2), 311–327.

Kueh, S., Dunkers, J., Advani, S., Parnas, R., Furrows, P., Jones, M., 2000. Long-period gratings as flow sensors for liquid composite molding. In: Proceedings of 4th International Symposium on Nondestructive Evaluation of Aging Materials and Composites, Society of Photo-Optical Instrumentation Engineers (SPIE). Vol. 3993. California, USA, pp. 240–250.

Lai, Y., Khomani, B., Kardos, J., 1997. Accurate permeability characterization of preforms used in polymer matrix composite fabrication processes. Polymer Composites 18 (3), 368–377.

Lang, E., Rydin, R., 2002. Composite Molding Method and Apparatus. Patent No: US 6406659 B1.

Lang, E., Rydin, R., 2005. Channel Assisted Resin Transfer Molding. Patent No: US 6919039 B2.

Lawrence, J., Fried, P., Advani, S., 2005. Automated manufacturing environment to address bulk permeability variations and race-tracking in resin transfer molding by redirecting flow with auxiliary gates. Composites Part A 36 (8), 1128–1141.

Lawrence, J., Hsiao, K., Don, R., Simacek, P., Estrada, G., Sozer, M., Stadfeld, H., Advani, S., 2002. An approach to couple mould design and on-line control to manufacture complex composite parts by resin transfer molding. Composites Part A 33 (7), 981–990.

Lee, C., Rice, B., Buczek, M., Mason, D., 1998. Resin transfer molding process monitoring and control. In: Proceedings of 43rd International SAMPE Symposium and Exhibition on Materials and Process Affordability - Keys to the Future. Vol. 43 (1). California, USA, pp. 231–242.

Lin, M., Hahn, H., Huh, H., 1998. A finite element simulation of resin transfer molding based on partial nodal asaturation and implicit time integration. Composites Part A 29 (5-6), 541–550.

Lin, M., Murphy, M., Hahn, H., 2000. Resin transfer molding process optimization. Composites Part A 31 (4), 361–371.

Liu, X., Falzon, P., Sweeting, R., Paton, R., 2004. Effective compressibility and permeability of multi-layer non-crimp fiberglass reinforcements. Journal of Reinforced Plastics and Composites 23 (8), 861–879.

Lundstorm, T., Frishfelds, V., Jacovics, A., 2004. A statistical approach to permeability of clustered fiber reinforcements. Journal of Composite Materials 38 (13), 1137–1149.

Lundstorm, T., Stenberg, R., Bergstorm, R., Partanen, H., Birkeland, P., 2000. In-plane permeability measurements: A nordic round-robin study. Composites Part A 31 (1), 29–43.

Lynch, K., Hubert, P., Poursartip, A., 1999. Use of a simple inexpensive pressure sensor to measure hydrostatic resin pressure during processing of composite laminates. Polymer Composites 20 (4), 581–593.

Mathur, R., Heider, D., Hoffman, C., Gillespie, J., Fink, B., 2001. Flow front measaurements and model validation in the vacuum assisted resin transfer molding process. Polymer Composites 22 (4), 477–490.

Minaie, B., Chen, Y., Mescher, A., 2002. A methodology to obtain a desired filling pattern during resin transfer molding. Journal of Composite Materials 36 (14), 1677–1692.

Mogavero, J., Sun, J., Advani, S., 1997. A nonlinear control method for resin transfer molding. Polymer Composites 18 (3), 412–417.

Mohan, R., Ngo, N., Tamma, K., 1999. On a pure finite element based methodology for resin transfer mold filling simulations. Polymer Engineering and Science 39 (1), 26–43.

Mychajluk, G., Manoochehri, S., 1994. An integrated process model and cycle time optimization for resin transfer molding. In: Proceedings of the International Engineering Congress and Exposition- Advances in Computer Aided Engineering (CAE) of Polymer Processing. Vol. 49. Chicago, USA, pp. 225–237.

Nalla, A., Fuqua, M., Glancey, J., Lelievre, B., 2007. A multi-segment injection line and real-time adaptive, model-based controller for vacuum assisted resin transfer molding. Composites: Part A 38 (3), 1058–1069.

Nedanov, P., Advani, S., 2002. A method to determine 3-d permeability of fibrous preforms. Journal of Composite Materials 36 (2), 241–254.

Nielsen, D., Pitchumani, R., 2001. Intelligent model-based control of preform permeation in liquid composite molding processes, with on-line optimization. Composites Part A 32 (12), 1789–1803.

Nielsen, D., Pitchumani, R., 2002a. Closed-loop flow control in resin transfer molding using real-time numerical process simulations. Composites Science and Technology 62 (2), 283–298.

Nielsen, D., Pitchumani, R., 2002b. Control of flow in resin transfer molding with real-time preform permeability estimation. Polymer Composites 23 (6), 1087–1110.

Pan, R., Liang, Z., Zhang, C., Wang, P., 2000. Statistical characterization of fiber permeability for composite manufacturing. Polymer Composites 21 (6), 996–1006.

Phelan, F., Wise, G., 1996. Analysis of transverse flow in aligned fibrous porous media. Composites Part A 27 (1), 25–34.

Pillai, K., 1997. Flow modeling in dual scale porous media. Ph.d. thesis, University of Delaware, Delaware, USA.

Ragondet, A., 2005. Experimental characterisation of the vacuum infusion process. Ph.d. thesis, University of Nottingham, Nottingham, UK.

Robitaille, F., Gauvin, R., 1998a. Compaction of textile reinforcements for composites manufacturing. i: Review of experimental results. Polymer Composites 19 (2), 198–216.

Robitaille, F., Gauvin, R., 1998b. Compaction of textile reinforcements for composites manufacturing. ii: Compaction and relaxation of dry and h2o-saturated woven reinforements. Polymer Composites 19 (5), 543–557.

Rudd, C., Bulmer, L., Morris, D., Kendall, K., 1996. Compaction and in-plane permeability characteristics of quasi unidirectional and continuous reinforcements. Materials Science and Manufacturing 12 (5), 436–444.

Rudd, C., Long, A., Kendall, K., Mangin, C., 1997. Liquid Moulding Technologies. Woodhead, Cambridge, UK.

Russ, J., 2002. The image processing handbook. Vol. 4. CRC Press, Boca Raton, USA.

Saunders, R., Lekakou, C., Bader, M., 1999. Compression in the processing of polymer composites 1. a mechanical and microstructural study for different glass fabrics and resins. Composites Science and Technology 59 (7), 983–993.

Sayre, J., Loos, A., 2003. Resin infusion of triaxially braided preforms with through-the-thickness reinforcements. Polymer Composites 24 (2), 229–236.

Scheidegger, A., 1974. The Physics of Flow Through Porous Media. University of Toronto Press, Toronto, Canada.

Seamann, W., 1990. Plastic Transfer Molding Techniques for the Production of Fiber Reinforced Plastic Structures. Patent No: US 4902215.

Simacek, P., Advani, S., 2004. Desirable features in mold filling simulations for liquid composite molding processes. Polymer Composites 25 (4), 355–367.

Skordos, A., Karkanas, P., Partridge, I., 2000. A dielectric sensor for measuring flow in resin transfer molding. Measurement Science and Technology 11 (1), 25–31.

Sun, X., Li, S., Lee, L., 1998. Mold filling analysis in vacuum-assisted resin transfer molding. part i: Scrimp based on a high-permeable medium. Polymer Composites 19 (6), 807–817.

Toll, S., 1998. Packing mechanics of fiber reinforcements. Polymer Engineering and Science 38 (8), 1337–1350.

Vaidya, U., Jadhav, N., Hosur, M., Gillespie, J., Fink, B., 2000. Assessment of flow and cure monitoring using direct current and alternating current sensing in vacuum assisted resin transfer molding. Smart Materials and Structures 9 (6), 727–736.

Walsh, S., 1993. In-situ sensor method and device (1993) Patent No: US 5210499.

Weitzenbock, J., Shenoi, R., Wilson, P., 2002. A unified approach to determine principal permeability of fibrous porous media. Polymer Composites 23 (6), 1132–1150.

WHO, 2000. Air Quality Guidelines for Europe. Vol. 91. World Health Organisation Regional Publications - European Series, 106-108.

Williams, C., Grove, S., Summerscales, J., 1998. The compression response of fibre-reinforced plastic plates during manufacture by the resin infusion under flexible tooling method. Composites Part A 29 (1-2), 111–114.

Williams, C., Summerscales, J., Grove, S., 1996. Resin infusion under flexible tooling (rift): A review. Composites Part A 27 (7), 517–524.

Appendices

Appendix 1.A Journal publications

1. Modi, D., Correia, N., Johnson, M., Long, A., Rudd, C., Robitaille, F., "Active Control of the Vacuum Infusion Process", *Composites Part A*, 38, 5, 1271-1287, 2007.

2. Modi, D., Johnson, M., Long, A., Rudd, C., "Investigation of Pressure Profile and Flow Progression in the Vacuum Infusion Process", *Plastics, Rubber and Composites: Macromolecular Engineering*, 36, 3, 1-10, 2007.

Appendix 1.B Conference publications

1. Long, A., Modi, D., Endruweit, A., Johnson, M., Rudd, C., "Flow Process Control for Liquid Composite Moulding using real-time Process Modelling", Proceedings of the 26^{th} SAMPE-Europe International Conference, Paris (France), 86-91, 2005.

2. Modi, D., Johnson, M., Long, A., Rudd, C., Robitaille, F., "Controlled Vacuum Infusion of Heterogeneous Fibrous Preforms", Proceedings of the 15^{th} International Conference on Composite Materials (ICCM-15), Durban (South Africa), 2005.

3. Modi, D., Johnson, M., Long, A., Rudd, C., "Active Control of Vacuum Infusion Process", Proceedings of the 8^{th} International Conference on Flow Processes for Composite Materials (FPCM-8), Douai (France), 355-362, 2006.

4. Modi, D., Johnson, M., Long, A., Rudd, C., "Comparison of Pressure Profile and Flow Progression between a Radial Flow VI and RTM Processes", Proceedings of the 12^{th} European Conference on Composite Materials (ECCM-12), Biarritz (France), 2006.

Appendix 2.A Correia's analytical formulation for VI

Hammami and Gebart (2000) modified the continuity equation (eq. 2.A.1) to account for the variable thickness in the VI process, resulting in eq. (2.A.2):

$$\oint_S \rho\, u\, \hat{n}\, dS + \frac{\partial}{\partial t} \int_V \rho\, \phi\, dV \;=\; 0 \tag{2.A.1}$$

$$\frac{\partial h}{\partial t} = -\frac{\partial}{\partial x}\,(uh) \tag{2.A.2}$$

Correia (2004) replaced the velocity term in this continuity equation with Darcy's law to get:

$$\frac{\partial h}{\partial t} = \frac{\partial}{\partial x}\left(\frac{Kh}{\mu}\,\nabla P\right) \tag{2.A.3}$$

then,

$$\frac{\partial h}{\partial t} = \frac{1}{\mu}\left[\left(K\,\frac{\partial h}{\partial P} + h\,\frac{\partial K}{\partial P}\right)\left(\frac{\partial P}{\partial x}\right)^2 + hK\,\frac{\partial^2 P}{\partial x^2}\right] \tag{2.A.4}$$

which, after normalising with $\alpha = x/L$, resulted in

$$\frac{\partial h}{\partial t} = \frac{1}{\mu L^2}\left[\left(K\,\frac{\partial h}{\partial P} + h\,\frac{\partial K}{\partial P}\right)\left(\frac{\partial P}{\partial \alpha}\right)^2 + hK\,\frac{\partial^2 P}{\partial \alpha^2}\right] \tag{2.A.5}$$

The left-side was re-cast as:

$$\frac{\partial h}{\partial t} = \frac{\partial h}{\partial \alpha}\,\frac{\partial \alpha}{\partial L}\,\frac{\partial L}{\partial t} \tag{2.A.6}$$

The author argued that the flow rate remains constant in the rectilinear flow process. Hence, the flow front velocity ($\frac{\partial L}{\partial t}$) can be written as:

$$\frac{\partial L}{\partial t}\,[h]_{\alpha=1} = u\,h \tag{2.A.7}$$

where, $[h]_{\alpha=1}$ is the thickness at the flow front. Then,

$$\frac{\partial L}{\partial t} = \frac{u\,h}{[h]_{\alpha=1}} = u\,h^* \tag{2.A.8}$$

Here, h^* is the normalised thickness with the thickness at the flow front. Substituting the Darcy velocity in eq. (2.A.8) gives,

$$\frac{\partial L}{\partial t} = -\frac{K}{\mu\phi}\, h\, \nabla P\, h^* \tag{2.A.9}$$

In addition, $\frac{\partial \alpha}{\partial L} = -\frac{\alpha}{L}$. Substituting in eq. (2.A.6),

$$\frac{\partial h}{\partial t} = -\frac{h^* \alpha K}{\mu L^2}\, \frac{\partial h}{\partial P} \left(\frac{\partial P}{\partial \alpha}\right)^2 \tag{2.A.10}$$

Therefore, eq. (2.A.5) can be written as

$$\frac{d^2 P}{d\alpha^2} + \left[\frac{1}{K}\, \frac{dK}{dP} + \left(\frac{1 - h^* \alpha}{h}\right) \frac{\partial h}{\partial P}\right] \left(\frac{dP}{d\alpha}\right)^2 = 0 \tag{2.A.11}$$

Appendix 2.B Euler method algorithm for solving initial value problems

To find an approximate solution (w) of the initial-value problem

$$y' = f(t,\, y),\ a \leq t \leq b,\ y(a) = \alpha$$

at $(N+1)$ equally spaced nodes in the interval $[a,\ b]$:

Step 1: Set

$$\begin{aligned} h &= (b-a)/N; \\ w &= \beta; \\ t &= a; \end{aligned}$$

Step 2: For $i = 1,\, 2,\, ...,\, N$, do steps 3-4.

Step-3: Set

$$\begin{aligned} w &= w + h\, f(t,\, w); \\ t &= a + i\, h; \end{aligned}$$

Step-4: Output $(t,\, w)$

Appendix 2.C Runge-Kutta method algorithm for solving initial value problems

To find an approximate solution (w) of the initial-value problem

$$y^{'} = f(t,\, y),\ a \leq t \leq b,\ y(a) = \alpha$$

at $(N+1)$ equally spaced nodes in the interval $[a,\ b]$:

Step 1: Set

$$\begin{aligned} h &= (b-a)/N; \\ w &= \beta; \\ t &= a; \end{aligned}$$

Step 2: For $i = 1,\, 2,\, ...,\, N$, do steps 3-5.

Step-3: Set

$$\begin{aligned} K_1 &= h\, f(t,\, w); \\ K_2 &= h\, f(t + h/2,\, w + K_1/2); \\ K_3 &= h\, f(t + h/2,\, w + K_2/2); \\ K_4 &= h\, f(t + h/2,\, w + K_3/2); \end{aligned}$$

Step-4: Set

$$\begin{aligned} w &= w + (K_1 + 2K_2 + 2K_3 + K_4)/6; \\ t &= a + i\, h; \end{aligned}$$

Step-5: Output $(t,\, w)$

Appendix 2.D Euler equations for the radial flow VI process

The pressure formulation for radial flow VI is:

$$\frac{\partial^2 P}{\partial \alpha^2} + \left[\frac{1}{K}\frac{\partial K}{\partial P} + \left(\frac{\phi + \alpha^2}{h\phi}\right)\frac{\partial h}{\partial P}\right]\left(\frac{\partial P}{\partial \alpha}\right)^2 + \left[\frac{(R - r_{inj})}{r_{inj} + \alpha\ (R - r_{inj})}\right]\frac{\partial P}{\partial \alpha} = 0$$

Setting $I = \frac{dP}{d\alpha}$:

$$\frac{dI}{d\alpha} + \left[\frac{1}{K}\frac{dK}{dP} + \left(\frac{\phi + \alpha^2}{h\phi}\right)\frac{dh}{dP}\right](I^2) + \left[\frac{(R - r_{inj})}{r_{inj} + \alpha\ (R - r_{inj})}\right] I = 0$$

$$\text{and, } \frac{dP}{d\alpha} = I$$

Assuming that the approximate solution needs to be found at m nodes, its value at node i can be written as:

$$\frac{I_i - I_{i-1}}{\alpha_i - \alpha_{i-1}} + \left[\frac{1}{K}\frac{dK}{dP} + \left(\frac{\phi + \alpha^2}{h\phi}\right)\frac{dh}{dP}\right]_{i-1}(I_{i-1}^2) + \left[\frac{(R - r_{inj})}{r_{inj} + \alpha_{i-1}\ (R - r_{inj})}\right] I_{i-1} = 0;\ \ i = 2, ..., m$$

$$\text{and, } P_i = P_{i-1} + I_{i-1}\,(\alpha_i - \alpha_{i-1})\,;\ i = 2, ..., m$$

Appendix 2.E Runge-Kutta equations for the rectilinear flow VI process

The pressure formulation for rectilinear flow VI is

$$\frac{\partial^2 P}{\partial \alpha^2} + \left[\frac{1}{K}\frac{\partial K}{\partial P} + \left(\frac{\phi + \alpha^2}{h\phi}\right)\frac{\partial h}{\partial P}\right]\left(\frac{\partial P}{\partial \alpha}\right)^2 = 0$$

Setting $I = \frac{dP}{d\alpha}$:

$$\frac{dI}{d\alpha} + \left[\frac{1}{K}\frac{dK}{dP} + \left(\frac{\phi + \alpha^2}{h\phi}\right)\frac{dh}{dP}\right]\left(I^2\right) = 0 \tag{2.E.1}$$

$$\frac{dP}{d\alpha} = I \tag{2.E.2}$$

Assuming that the solution is to be found at m nodes, let

$$h = \left(\alpha_m - \alpha_1\right)/m;$$

$$\begin{aligned}
K_1 &= -h\left[\frac{1}{K}\frac{dK}{dP} + \left(\frac{\phi + \alpha^2}{h\phi}\right)\frac{dh}{dP}\right]\left(I_{i-1}^2\right); \\
K_2 &= -h\left[\frac{1}{K}\frac{dK}{dP} + \left(\frac{\phi + \left(\alpha + \frac{h}{2}\right)^2}{h\phi}\right)\frac{dh}{dP}\right]\left(I_{i-1} + \frac{K_1}{2}\right)^2; \\
K_3 &= -h\left[\frac{1}{K}\frac{dK}{dP} + \left(\frac{\phi + \left(\alpha + \frac{h}{2}\right)^2}{h\phi}\right)\frac{dh}{dP}\right]\left(I_{i-1} + \frac{K_2}{2}\right)^2; \\
K_4 &= -h\left[\frac{1}{K}\frac{dK}{dP} + \left(\frac{\phi + \left(\alpha + \frac{h}{2}\right)^2}{h\phi}\right)\frac{dh}{dP}\right]\left(I_{i-1} + K_3\right)^2;
\end{aligned}$$

then, the approximate solution of eq. 2.E.1 at node i, can be written as:

$$I_i = I_{i-1} + \left(K_1 + 2K_2 + 2K_3 + K_4\right)/6$$

Also,

$$\begin{aligned} K_1^{'} &= h\, P_{i-1}; \\ K_2^{'} &= h\left(P_{i-1} + \frac{K_1^{'}}{2}\right); \\ K_3^{'} &= h\left(P_{i-1} + \frac{K_2^{'}}{2}\right); \\ K_4^{'} &= h\left(P_{i-1} + K_3^{'}\right); \end{aligned}$$

and the approximate solution of eq. 2.E.2 at node i, can be written as:

$$P_i = P_{i-1} + \left(K_1^{'} + 2K_2^{'} + 2K_3^{'} + K_4^{'}\right)/6$$

Appendix 2.F Runge-Kutta equations for the radial flow VI process

The pressure formulation for radial flow VI is

$$\frac{\partial^2 P}{\partial \alpha^2} + \left[\frac{1}{K}\frac{\partial K}{\partial P} + \left(\frac{\phi + \alpha^2}{h\phi}\right)\frac{\partial h}{\partial P}\right]\left(\frac{\partial P}{\partial \alpha}\right)^2 + \left[\frac{(R - r_{inj})}{r_{inj} + \alpha\ (R - r_{inj})}\right]\frac{\partial P}{\partial \alpha} = 0$$

Setting $I = \frac{dP}{d\alpha}$:

$$\frac{dI}{d\alpha} + \left[\frac{1}{K}\frac{dK}{dP} + \left(\frac{\phi + \alpha^2}{h\phi}\right)\frac{dh}{dP}\right]\left(I^2\right) + \left[\frac{(R - r_{inj})}{r_{inj} + \alpha\ (R - r_{inj})}\right] I = 0 \quad \text{(2.F.1)}$$

$$\text{and, } \frac{dP}{d\alpha} = I \quad \text{(2.F.2)}$$

Assuming that the solution is to be found at m nodes, let

$$h = (\alpha_m - \alpha_1)/m;$$

$$\begin{aligned} K_1 \;=\; & -h\left[\left[\frac{1}{K}\frac{dK}{dP} + \left(\frac{\phi + \alpha^2}{h\phi}\right)\frac{dh}{dP}\right]\left(I_{i-1}^2\right)\right. \\ & \left. + \left[\frac{(R - r_{inj})}{r_{inj} + \alpha_{i-1}\ (R - r_{inj})}\right] I_{i-1}\right]; \end{aligned}$$

$$\begin{aligned} K_2 \;=\; & -h\left[\left[\frac{1}{K}\frac{dK}{dP} + \left(\frac{\phi + \left(\alpha + \frac{h}{2}\right)^2}{h\phi}\right)\frac{dh}{dP}\right]\left(I_{i-1} + \frac{K_1}{2}\right)^2 + \right. \\ & \left. \left[\frac{(R - r_{inj})}{r_{inj} + \left(\alpha_{i-1} + \frac{h}{2}\right)\ (R - r_{inj})}\right]\left(I_{i-1} + \frac{K_1}{2}\right)\right]; \end{aligned}$$

$$K_3 = -h \left[\left[\frac{1}{K} \frac{dK}{dP} + \left(\frac{\phi + \left(\alpha + \frac{h}{2}\right)^2}{h\phi} \right) \frac{dh}{dP} \right] \left(I_{i-1} + \frac{K_2}{2} \right)^2 + \left[\frac{(R - r_{inj})}{r_{inj} + \left(\alpha_{i-1} + \frac{h}{2}\right)(R - r_{inj})} \right] \left(I_{i-1} + \frac{K_2}{2} \right) \right];$$

$$K_4 = -h \left[\left[\frac{1}{K} \frac{dK}{dP} + \left(\frac{\phi + \left(\alpha + \frac{h}{2}\right)^2}{h\phi} \right) \frac{dh}{dP} \right] (I_{i-1} + K_3)^2 + \left[\frac{(R - r_{inj})}{r_{inj} + (\alpha_{i-1} + h)(R - r_{inj})} \right] (I_{i-1} + K_3) \right];$$

then, the approximate solution of eq. 2.F.1 at node i, can be written as:

$$I_i = I_{i-1} + (K_1 + 2K_2 + 2K_3 + K_4)/6$$

Also,

$$\begin{aligned} K_1^{'} &= -h\, P_{i-1}; \\ K_2^{'} &= -h \left(P_{i-1} + \frac{K_1^{'}}{2} \right); \\ K_3^{'} &= -h \left(P_{i-1} + \frac{K_2^{'}}{2} \right); \\ K_4^{'} &= -h \left(P_{i-1} + K_3^{'} \right); \end{aligned}$$

and the approximate solution of eq. 2.F.2 at node i, can be written as:

$$P_i = P_{i-1} + \left(K_1^{'} + 2K_2^{'} + 2K_3^{'} + K_4^{'} \right)/6$$

Appendix 4.A Matlab program for active control system

```
function [] = AREA_MOMENT()
% This is the main function. Calls all other functions %
fid = fopen('records.txt','w');                                    % Open a records file %
% 1. READ RELEVANT INPUTS FROM CONSOLE TO PREPARE THE ALGORITHM %
% ========================================================== %
% Start camera calibration %
NO_OF_CAMERAS = input('Number of CAMERAS =');                      % Get an input %
CAMERA_ROWS = input('Number of CAMERAS ROWS =');                   % Get an input %
CALIBRATE(NO_OF_CAMERAS,CAMERA_ROWS);
% Dmp file creation %
FILENAME = input('Meshed Model Filename =','s');                   % Get the name of the model file %
FILENAME1 = [FILENAME,'.dmp'];
% Get the number of control steps from user %
No_OF_CONTROL_PHASES = input('No_OF_CONTROL_PHASES =\n i.e. ...    % Get the number of control phases %
```

```
                                    the number of times a control ...
                                   action is intended to be taken ...
                                                        during infusion');
% Read the number of nodes from the header line %
HEADER = input('Number of header lines in the dmp file =\n ...     % Get the number of header lines in the dmp %
                                     [The default value is three!]');  % file. Give the default value as a suggestion %
FILENAME2 = [FILENAME,'G','.zon'];
GATE_NODE_NUMBERS = GATE_REGION(FILENAME2);
GATES(1,:) = [1:1:size(GATE_NODE_NUMBERS)];
FILENAME2 = [FILENAME,'V','.zon'];
VENT_NODE_NUMBER = VENT_REGION(FILENAME2);
% Read the number of elements from the header line %
[A,A,A,A,A] = textread(FILENAME1,'%s %s %s %s %d',1, ...
                        'delimiter',' ','headerlines',(HEADER-3));
D = HEADER+A;
[B,B,B,B,B] = textread(FILENAME1,'%s %s %s %s %d',1, ...
                                   'delimiter',' ','headerlines',D);
```

```
No_OF_NODES = A;
No_OF_ELEMENTS = B;
SCHEMES = GATE_SCHEMES;
INTERVAL = round((No_OF_NODES)/(No_OF_CONTROL_PHASES+1));          % Round this number %
% ========================================================== %
% 2. PRINT ALL THE INPUTS ON THE SCREEN.
% ========================================================== %
No_OF_NODES
No_OF_ELEMENTS
GATE_NODE_NUMBERS
VENT_NODE_NUMBER
No_OF_CONTROL_PHASES
GATES
% ========================================================== %
% 3. PRINT ALL THE INPUTS IN THE RECORDS FILE.
% ========================================================== %
fprintf(fid,'Model File = %s.\n',FILENAME1);
```

```
fprintf(fid,‘Number of Nodes = %d.\n’,No_OF_NODES);
fprintf(fid,‘Number of Elements = %d.\n’,No_OF_ELEMENTS);
fprintf(fid,‘Gate Node Numbers = %d %d %d %d.\n’,...
                                          GATE_NODE_NUMBERS);
fprintf(fid,‘Vent Node Number = %d.\n’,VENT_NODE_NUMBER);
fprintf(fid,‘Number of Control Phases = %d.\n’,...
                                       No_OF_CONTROL_PHASES);
fprintf(fid,‘================================================\n’)
% ========================================================== %
% 4. CONTROL CYCLE
% ========================================================== %
GATE_SEQUENCE(1,1:2) = [1 1];
GATE_SEQUENCE(1,3:1:6) = 1-(SCHEMES(1,:)/100000);
DAQ(GATE_SEQUENCE(1,3:1:6));                                  % Open all the injection gates initially %
load backup_file s_f xi yi LALimits mask_cam avg_filter points    % Load the calibration data %
FILLED_NODES = GATE_NODE_NUMBERS;                             % Set injection gate nodes as initially %
                                                              % filled nodes %
```

```
A = length(FILLED_NODES);
CONTROL_PHASE_COUNTER = 1;
B = CONTROL_PHASE_COUNTER*INTERVAL;
while (A<B)
    FILLED_NODES = PIXS_TO_NODES(NO_OF_CAMERAS,CAMERA_ROWS, ...    % Capture an image, analyse it and find the %
                                 s_f,xi,yi,LALimits,mask_cam, ...  % number of filled nodes %
                                           avg_filter,points, ...
                                          CONTROL_PHASE_COUNTER);
    A = length(FILLED_NODES);
end
GATE_SEQUENCE = [1 1 1 1];                                         % Close all injection gates while corrective %
DAQ([1 1 1 1]);                                                    % action is being chosen %
cd('\Figures')                                                     % Go to the folder where all the captured %
                                                                   % images are being stored %
F_N = ['C_S',num2str(CONTROL_PHASE_COUNTER),'.bmp'];               % Create a backup copy of the image file %
copyfile ('1.bmp',F_N);                                            % showing the end of a control step %
cd('\')                                                            % Go back to the working folder %
```

```
for CONTROL_PHASE_COUNTER = 2:1:(No_OF_CONTROL_PHASES+1)
    for GATE_CYCLE_COUNTER = 1:1:max(size(SCHEMES))
        FILE_NAME = [‘Phase’,num2str(CONTROL_PHASE_COUNTER), ...   % Define the filename for the simulation %
                     ‘SCHM#’,num2str(GATE_CYCLE_COUNTER),‘T#’, ...  % results file %
                                                          ‘.tec’];
        No_OF_NODES_TO_BE_LEFT_EMPTY = (No_OF_NODES-(INTERVAL ...  % Calculate the number of nodes to be left %
                                       *CONTROL_PHASE_COUNTER));  % empty at the end of the next control cycle %
        if No_OF_NODES_TO_BE_LEFT_EMPTY < 0
            No_OF_NODES_TO_BE_LEFT_EMPTY = 0                       % Only useful for the last control cycle %
        end
        LIMS_AUTO_FILE(FILENAME1,No_OF_NODES_TO_BE_LEFT_EMPTY,...  % Generate an "auto" file for performing %
                       GATE_CYCLE_COUNTER,GATE_NODE_NUMBERS, ...   % online flow simulations and calculate %
                                          VENT_NODE_NUMBER, ...    % the centroid of the empty region %
                          SCHEMES(GATE_CYCLE_COUNTER,GATES), ...
                                          FILLED_NODES,FILE_NAME);
        !lims                                                      % Call LIMS to perform flow simulations %
        FILE = [FILENAME,‘CV’,‘.txt’];
```

```
    [B,C] = textread(FILE, '%d %f','headerlines',0);          % Read the results %
    P1(:,1) = B;
    P1(:,2) = C;
    REAL_RESULTS(GATE_CYCLE_COUNTER,:) = P1;
end
GATE_CYCLE_COUNTER = GATE_CYCLE_COUNTER+1;
REAL_RESULT_NEW = sortrows(REAL_RESULTS,2);
GATE_SEQUENCE(CONTROL_PHASE_COUNTER,1) = ...
                                    (CONTROL_PHASE_COUNTER);
GATE_SEQUENCE(CONTROL_PHASE_COUNTER,2) = ...
                                     (REAL_RESULT_NEW(1,1));
GATE_SEQUENCE(CONTROL_PHASE_COUNTER,3:1:6) = ...
                    1-SCHEMES(REAL_RESULT_NEW(1,1),:)/100000;
DAQ(GATE_SEQUENCE(CONTROL_PHASE_COUNTER,3:1:6));              % Relay the new control action to solenoid %
                                                              % injection valves %
% Print the control action details in the records file %
fprintf(fid,'=========================================\n');
```

```
fprintf(fid,‘Controls Cycle = %d. \n’,CONTROL_PHASE_COUNTER);
fprintf(fid,‘Results = %d\t %f\n’,REAL_RESULT_NEW’);
fprintf(fid,‘========================================\n’);
fprintf(fid,‘GATE SEQUENCE = %d\n’, ...
                  GATE_SEQUENCE(CONTROL_PHASE_COUNTER,2:1:6));
fprintf(fid,‘++++++++++++++++++++++++++++++++++++\n\n\n’);
% Set-up to perform a flow simulation for the chosen %
% control action and save the results file for records %
FILE_NAME = [‘Phase#’,num2str(CONTROL_PHASE_COUNTER), ...
                                          ‘Sample#’,‘.tec’];
LIMS_AUTO_FILE (FILENAME1,No_OF_NODES_TO_BE_LEFT_EMPTY, ...
                    GATE_CYCLE_COUNTER,GATE_NODE_NUMBERS, ...
                                       VENT_NODE_NUMBER,...
                     SCHEMES(REAL_RESULT_NEW(1,1),GATES), ...
                                    FILLED_NODES, FILE_NAME);
!lims
FILLED_NODES = GATE_NODE_NUMBERS;
```

```
A = length(FILLED_NODES);
B = CONTROL_PHASE_COUNTER*INTERVAL;
if CONTROL_PHASE_COUNTER < (No_OF_CONTROL_PHASES+1)
    while (A<B)
        FILLED_NODES = PIXS_TO_NODES(NO_OF_CAMERAS, ...        % Capture an image, analyse it and find the %
                                     CAMERA_ROWS,s_f,xi, ...   % number of filled nodes %
                                    yi,LALimits,mask_cam, ...
                                      avg_filter,points, ...
                                     CONTROL_PHASE_COUNTER);
        A = length(FILLED_NODES);
    end
    DAQ([1 1 1 1]);
    if CONTROL_PHASE_COUNTER == No_OF_CONTROL_PHASES
        pause
    end
    cd('\Figures')
    F_N = ['C_S',num2str(CONTROL_PHASE_COUNTER),'.bmp'];
```

```
        copyfile ('1.bmp',F_N);
        cd('\')
    end
end
% Print the chosen control action in the records file %
fprintf(fid,'+++++++++++++++++++++++++++++++++++++++++++++++\n');
fprintf(fid,'GATE SEQUENCE = %d\n', GATE_SEQUENCE);
fprintf(fid,'+++++++++++++++++++++++++++++++++++++++++++++++\n');
fclose(fid);
% ========================================================== %
% ================================================================================================================== %
function []= CALIBRATE (no_of_cameras,camera_rows)
% This file calibrates the image acquisition and analysis %
% algorithm for speedy automation during on-line control. %
coordinates=[0 1; .5 1; 1 1; 1 0.5 ; 1 0 ; 0.5 0; 0 0; 0 0.5];
% Creation of various calibration variables
old_cam = cell(no_of_cameras,1);
```

```
LALimits = cell(no_of_cameras,1);
s_f = cell(no_of_cameras,2);
mask_cam = cell(no_of_cameras,1);
for i=1:1:no_of_cameras
    cd('\Figures')
    !DET_DELETE
    pause (1)
    !DET_RENAME
    filename = [num2str(i),'.bmp'];
    copyfile (filename,'cali_image.bmp');
    img_rgb=double(imread(filename));                              % Read the calibration image %
    cd('\')
    img_rgb=imresize(img_rgb,0.5);
    img_gray=(img_rgb(:,:,1)+img_rgb(:,:,2)+img_rgb(:,:,3))/768;   % Convert the image scale from RGB to Gray %
    j=menu('Define region of interest using:','New points?', ...
                                              'Saved points?');
    if j==1
```

```
    [laLimits,x,y] = roipoly(img_gray);                    % Get the masking region and the points defining %
                                                           % the region of interest %
    points(:,1) = y(1:8,:);
    points(:,2) = x(1:8,:);
else
    load backup_file.mat
    laLimits = LALimits{i,1};
    y(1:8,:) = points(:,1);
    x(1:8,:) = points(:,2);
end
ok=2;
while ok==2
    ok=menu('Is the selection satisfactory?','Yes','No');  % Defining the regions of interest %
end
close all
% Preperation of variables for calculating shape functions %
LALimits{i,1} = laLimits;                                  % Masking region %
```

```
img_gray = img_gray.*LALimits{i,1};                          % Image masking %
[i2,j2] = find(img_gray);                                    % Row and column indices of the non-zero %
                                                             % pixels in the masking region %
h = find(img_gray);                                          % Indices of the non-zero pixels in the %
                                                             % the masking region %
a = 201;                                                     % No of pixel columns in the processed image %
b = 151;                                                     % No of pixel rows in the processed image %
% calculation of shape functions. %
[i1, j1] = SHAPE_FUNCTIONS(i2,j2,points,a,b,coordinates);
img_gray = img_gray (h);
% Preparation of a new, planar surface (with no perspective)%
% for projecting the original image with persepctive %
[xi,yi] = meshgrid(1:1:a,1:1:b);                             % 'a' gives columns, while 'b' gives rows %
                                                             % i.e. matrix size = bxa or image size=axb) %
% Projecting the original image onto a new, planar surface %
% to remove the perspective in the image %
Ai = griddata(i1,j1,img_gray,xi,yi,'nearest');               % Interplotes img_gray as a function of shape %
```

```
    old_cam{i,1} = Ai;

    mask_cam{i,1} = h;



    s_f{i,1} = i1;
    s_f{i,2} = j1;
end
master_old = old_cam;
threshold=0.0003;
%Preparation of the filter
iNumberOfpoints=3;
Standard_Deviation=0.4;
avg_filter=fspecial('average',iNumberOfpoints);
% Image processing - filtering
master_old = imhmax(master_old,0.1);
```

```
% functions at xi,yi points %
 % Storing the newly plotted surface into an %
 % individual image cell array %
 % Storing the indices of the non-zero pixels %
 % in the masking region into an individual %
 % cell array %
 % Storing shape functions into an individual %
 % cell array %
```

```
master_old = imfilter(master_old,avg_filter,'same','corr');
% Convert the image to a binary image
c=0.5;
img_bw=master_old>(c);
close all
save backup_file s_f xi yi LALimits mask_cam avg_filter points
% ========================================================================================================== %
function [I,J]=SHAPE_FUNCTIONS(Ii,Ji,Points,n,m,Coordinates)
% This function calculates shape functions for perspective removal %
%Preparation of the shape functions
invX=[[1;1;1;1;1;1;1;1],Points,Points(:,1).*Points(:,1),...
            Points(:,1).*Points(:,2),Points(:,2).*Points(:,2),...
           Points(:,1).*Points(:,1).*Points(:,1).*Points(:,2),...
          Points(:,2).*Points(:,2).*Points(:,2).*Points(:,1)]^-1;
Values=[ones(size(Ii)), Ii, Ji];
I=n*[Values,Values(:,2).*Values(:,2),Values(:,2).*Values(:,3),...
                                     Values(:,3).*Values(:,3),...
```

```
            Values(:,2).*Values(:,2).*Values(:,2).*Values(:,3),...
            Values(:,3).*Values(:,3).*Values(:,3).*Values(:,2)]...
                                        *(invX*Coordinates(:,1));
J=m*[Values,Values(:,2).*Values(:,2),Values(:,2).*Values(:,3),...
                                      Values(:,3).*Values(:,3),...
            Values(:,2).*Values(:,2).*Values(:,2).*Values(:,3),...
            Values(:,3).*Values(:,3).*Values(:,2).*Values(:,3)]...
                                         *invX*Coordinates(:,2);
% ========================================================================================================== %
function [FILLED_NODES]= PIXS_TO_NODES (no_of_cameras,...
                                      camera_rows,s_f,xi,yi, ...
                                LALimits,mask_cam,avg_filter, ...
                                         points,control_step)
% Acquire an image, Analyze it and Calculate the nodal fill %
% factors %
% Calls MODEL_DATA %
coordinates=[0 1;.5 1;1 1;1 0.5;1 0;0.5 0;0 0;0 0.5];              % Example co-ordinates %
```

```
% Creation of various calibration variables %
old_cam = cell(no_of_cameras,1);
c_step = control_step;
for i=1:1:no_of_cameras
    cd('\Figures')
    !DET_DELETE
    pause (1.1)
    !DET_RENAME
    filename = [num2str(1),'.bmp'];
    img_rgb=double(imread(filename));                                  % Read the calibration image %
    cd('\')
    img_rgb=imresize(img_rgb,0.5);
    img_gray=(img_rgb(:,:,1)+img_rgb(:,:,2)+img_rgb(:,:,3))/768;       % Convert the image scale from RGB to Gray %
    img_gray = img_gray.*LALimits{i,1};                                % Image masking %
    [i2,j2] = find(img_gray);                                          % Row and column indices of the non-zero %
                                                                       % pixels in the masking region %
    h = find(img_gray);                                                % Indices of the non-zero pixels in the masking %
```

```
    img_gray = img_gray (h);
    a=201;
    b=151;
    [i1, j1] = SHAPE_FUNCTIONS(i2,j2,points,a,b,coordinates);
    Ai = griddata(i1,j1,img_gray,xi,yi,'nearest');
    old_cam{i,1} = Ai;
end
master_old = old_cam;
% Image processing - filtering %
iNumberOfpoints=3;
% region %
% Projecting the original image onto a new, %
% planar, surface (to remove the perspective %
% in the image) %
% Interplotes img_gray as a function of shape %
% functions at xi, yi points %
% i.e. img_gray = f(I1,J1) Where, I1, J1, %
% img_gray, xi, yi are vectors %
% Storing the newly plotted surface into an %
% individual image cell array %
```

```
avg_filter=fspecial('average',iNumberOfpoints);
master_old = imhmax(master_old,0.1);
master_old=imfilter(master_old,avg_filter,'same','corr');
c=0.5;
img_bw=master_old>(c);
FILENAME = ['img_bw',num2str(control_step),'.bmp'];
cd('\Figures')
imwrite (img_bw,FILENAME,'bmp');
cd('\')
% Calculate the nodal fill-factors %
A=MODEL_DATA';
```

```
% MODEL_DATA is a *.dmp file for LIMS. %
% Not printed due to size limitation. %
% Refer the backup CD. %
```

```
FILLED_NODES=zeros(max(size(A)),1);
counter=0;
count=1;
for i=1:max(size(A));
```

```
    counter=counter+1;
    j(counter,1)=(1000000.*A(i,2).*A(i,3));
end;
for i=1:max(size(A));
    if (j(i,1)>0);
        M=(500.*A(i,2)-49);
        N=(201-500.*A(i,3));
        if (M==1)
            K = ((img_bw(N,M)<1) & (img_bw(N,M+1)<1));
        elseif (N==1)
            K = ((img_bw(N,M)<1) & (img_bw(N+1,M)<1));
        elseif (M==201)
            K = ((img_bw(N,M)<1) & (img_bw(N,M-1)<1));
        elseif (N==151)
            K = ((img_bw(N,M)<1) & (img_bw(N-1,M)<1));
        else
            K = img_bw(N,M)<1;
```

```
        end
        if K==1;
            FILLED_NODES(count,1)=[A(i,1)];
            count=count+1;
            K==0;
        end;
    end;
end;
FILLED_NODES;
H = find(1.*FILLED_NODES>0);
FILLED_NODES = FILLED_NODES(H,1);
% ================================================================================================== %
function [GATE_NODE_NUMBERS] = GATE_REGION(ZON_FILE)
% Column matrix of gate node numbers
A = dlmread(ZON_FILE,' ',3,0);                                  % Read the zon file for gate node numbers %
% 1 Calculate the column matrix of gate node numbers %
% ================================================== %
```

```
count = 0;
for i = 1
    for j = 1:length(A)
        if A(i,j)>0
            count = count+1;
            GATE_NODE_NUMBERS(count,1) = A(i,j);
        end;
    end;
end;
% ================================================================================================================== %
function [VENT_NODE_NUMBERS] = VENT_REGION(ZON_FILE)
% Column matrix of vent node numbers
A = dlmread(ZON_FILE,' ',3,0);                                    % Read the zon file for vent node numbers %
% 1 Calculate the column matrix of vent node numbers %
% ================================================== %
count = 0;
for i = 1
```

```
    for j = 1:length(A)
        if A(i,j)>0
            count=count+1;
            VENT_NODE_NUMBERS(count,1) = A(i,j);
        end;
    end;
end;
% ================================================================================================================== %
function [SCHEMES] = GATE_SCHEMES(  )
SCHEMES = [ 100000  100000  100000  100000  %1%
            100000  100000  100000  0       %2%
            100000  100000  0       100000  %3%
            100000  100000  0       0       %4%
            100000  0       100000  100000  %5%
            100000  0       100000  0       %6%
            100000  0       0       100000  %7%
            100000  0       0       0       %8%
```

```
            0       100000  100000  100000  %9%
            0       100000  100000  0       %10%
            0       100000  0       100000  %11%
            0       100000  0       0       %12%
            0       0       100000  100000  %13%
            0       0       100000  0       %14%
            0       0       0       100000  %15%
            0       0       0       0       %16% ];
% ========================================================================================================== %
% Gate Region File %
Model1G                                                         % Region name %
NODES                                                           % Type of members in the region %
4                                                               % Number of members in the region %
1 2 3 4                                                         % Member numbers %
% ========================================================================================================== %
% Vent Region File %
Model1v                                                         % Region name %
```

```
NODES                                                                    % Type of members in the region %
1                                                                        % Number of members in the region %
706                                                                      % Member numbers %
% ================================================================================================================== %
function [] = DAQ(GATE_SEQUENCE)
% ========================================================== %
% This function creates the DIO object, adds I/O Lines, starts  %
% the lines and sends the signals to the controls hardware to   %
% control the injection gates                                   %
dio = digitalio ('nidaq',1)                                         % Create the DIO object %
hwlines1 = addline(dio,8:11,'out',{'OutLine1','OutLine2',...        % Add the first four hardware lines as output
                                    'OutLine3', 'OutLine4'});       % lines %
putvalue(dio.Line(1:4),GATE_SEQUENCE);                              % Put the control values %
```